Develop~~ing~~ment of the DO3SE-crop model to assess ozone effects on crop phenology, biomass and yield. ~~for Xiaoji, China~~

Pritha Pande[1]; Sam Bland[1]; Nathan Booth [2]; Jo Cook[2]; Zhaozhong Feng[3]; Lisa Emberson[2].

[1] Stockholm Environment Institute at York, Environment & Geography Dept., University of York, YO10 5DD, UK

[2] Environment & Geography Dept., University of York, YO10 5DD, UK

[3] Key Laboratory of Agrometeorology of Jiangsu Province, School of Ecology and Applied Meteorology, Nanjing University of Information Science & Technology, Nanjing, China.

Correspondence to: Pritha Pande (pritha.pande@york.ac.uk)

Abstract

A substantial body of empirical evidence exists to suggest that elevated O_3 levels are causing significant impacts on wheat yields at sites representative of highly productive arable regions around the World. Here we extend the DO_3SE model (designed to estimate total- and stomatal-O_3 deposition ~~of~~ for risk assessment) to incorporate a coupled A_{net}-g_{sto} model to estimate O_3 uptake, an O_3 damage module (that impacts instantaneous A_{net} and the timing and rate of senescence), and a crop phenology, carbon allocation, and growth model based on the JULES-Crop model. The model structure allows scaling from the leaf to the canopy to allow for multiple leaf populations and canopy layers. ~~-~~The DO_3SE-crop model is calibrated and ~~parametrised using O_3 fumigation data from Xiaoji, China~~parametrised using O_3 fumigation data from Xiaoji, China, for the year 2008 and for an O_3 tolerant and sensitive cultivar. The calibrated model was tested on data for different years (2007 and 2009) and for two additional cultivars and was found to ~~can~~ simulate key physiological variables, crop development, and yield with a good level of accuracy ~~compared to experimental observations~~. The DO_3SE-crop model simulated ~~accurately evaluated~~~~depicted~~ the phenological stages~~difference~~ of crop development ~~in yield reductions~~ under ambient and elevated O_3 treatments for the test datasets ~~wheat cultivars Y16 (tolerant) and Y2 (sensitive) with regressions of modelled and observed absolute yields resulting in~~with an R^2 of 0.9~~59~~ and an RMSE of 2.~~59.27~~ days~~g/m²~~. ~~Further, when evaluated for the years 2008 (Y15 and Y19 cultivars), 2007 and 2009 for all cultivars, t~~The DO_3SE-crop model was also able to simulate~~d~~ O_3-induced yield losses of ~11.~~44~~ 19 .~~364~~ ~~25~~% compared to observed yield losses of 12-34 %, with an R^2 of 0.68~~73~~ (n=20) and an RMSE of 76~~58.41~~ g/m². Additionally, our results indicate that the variance in yield reduction is primarily attributed to the premature decrease in carbon assimilation to the grains ~~under elevated O_3 exposure. This is linked to~~caused by ~~-~~accelerated leaf senescence, which ~~brings leaf senescence~~is brought forward by 3-5 days under elevated O_3 treatments.

Introduction

Ground-level ozone (O_3) is considered the most critical air pollutant causing global damage to agricultural crops. Elevated O_3 concentrations are particularly problematic in Asia, where decades of rapid economic growth, industrialisation, and urbanisation have seen sharp rises in pollutant emissions associated with burning fossil fuels (Lin et al., 2017) causing substantial O_3-induced crop yield losses across the region (Feng et al., 2022). At the same time, climate change is considered a substantial threat to arable productivity through changes in average and extreme temperature and precipitation profiles across the region (IPCC, 2021). Reductions in precipitation are considered responsible for poor harvests in recent years (Liu et al., 2010), and rising temperatures that reduce the length of the crop growing season are thought to have caused losses in crop yield -(Malhi et al., 2021)~~, Kaur and Kaushik, 2021)~~. There is now substantial evidence showing that stresses from ~~ozone~~ O_3 pollution and climate variability interact, causing either additive, synergistic, or antagonistic responses in crop development, growth, and yield (Sillmann et al., 2021). The threat posed by these stresses is a particular cause for concern in Asia since the continent contributes approximately 43% of the global wheat production, with China contributing the highest production levels at 17% of the global wheat supply (Feng et al., 2021). O_3 levels are rising substantially in important wheat-growing areas in China such as the North China Plain and the Yangtze River Delta (Li et al., 2020; Zhang et al., 2023). ~~This~~ Concern over O_3 impacts led to the implementation in 2013 of a range of policies to try to reduce O_3 precursor emissions across China. These included ~~e.g.~~ a comprehensive management plan to control volatile organic compounds (VOCs) from key industries, an atmospheric pollution prevention and control law of the People's Republic of China and, ~~the~~ a 2020 VOCs Management Plan (Li et al.,~~, Zhou and Xu,~~ 2021). As a result, nitrogen oxide (NOx) emissions, an important O_3 precursor, have decreased by 21% ~~significantly~~ from 2013 to 2017 ~~by 21%~~ (Li et al., ~~, Zhou and Xu,~~ 2021). By contrast, VOCs have only slightly decreased by 2% over the same ~~time period~~period. Since China has a VOC limited O_3 regime, the reductions in NOx lead to rather insignificant changes in O_3 concentration (Li et al.,~~, Zhou and Xu,~~ 2021) though evidence suggests that reductions in O_3 may be higher in rural than urban areas (Lee et al., 2020). This implies future policies to tackle ground level O_3 pollution in China need to increase their focus on reducing VOCs along with NOx (Lee et al., 2020) and also emphasise the importance of being able to make assessments of O_3 damage to key receptors such as staple crops. ~~,~~

At present, methods to assess the risk to crop productivity from changes in O_3 and climate variables ~~have used~~use a variety of different O_3 risk assessment methods ~~(Ronan et al., 2020)~~(Ronan et al., 2020) and crop models as discussed in depth in Emberson et al. (2018). In the past, ~~Such~~O_3 risk assessment -methods ~~in the past~~ relied heavily on dose-response relationships, empirically derived relationships that assess changes in a response variable (most commonly yield) against an ~~ozone~~ O_3 exposure metric (concentration or, more recently, flux-based indices) (Pleijel et al., 2022). By contrast, methods to assess the impact of climate variables (most commonly changes in temperature, precipitation~~,~~ and CO_2 concentration) tend to use crop models since these allow the integration of the combined effect of a number of different variables acting simultaneously to affect crop development, growth~~,~~ and yield (Schauberger et al., 2019). A new generation of crop models that include O_3 damage are now being developed and applied and have the potential to estimate the combined effect of O_3 and climate variables on crop development, biomass and yield. Such models can arguably be classified into two types of crop model. Firstly, those that rely on O_3 metrics (e.g. AOT40 or M7) to modify crop growth determined by radiation use efficiency (Guarin et al., 2019; 2024) or evapotranspiration (Droustas et al., 2020). Secondly, those that estimate stomatal O_3 uptake to modify crop growth determined by photosynthesis and subsequent carbon assimilation (Tao et al., 2017; Schauberger et al., 2019; Nguyen et al., 2024). The DO_3SE-Crop model falls into the latter category of photosynthetic-based crop models and was developed to bridge the gap between O_3 risk assessment modelling methods and crop models.

~~Recent advances have highlighted the importance of incorporating dynamic ozone stress modules into these crop models to adjust crop growth parameters in real-time based on fluctuating ozone levels (Emberson et al., 2018). Additionally, there is a growing awareness of the need to integrate genotype-specific responses (Feng et al., 2022) and multi-stressor models that account for the combined effects of ozone and other environmental factors (Feng et al., 2022). This holistic approach provides a more comprehensive assessment of the combined impacts of various stressors on crops (Tao et al., 2017; Emberson et al., 2018; Schauberger et al., 2019). However, significant challenges remain, such as the need for extensive data on ozone concentrations and crop responses, and the necessity for interdisciplinary collaboration to develop robust and integrated models. Addressing these challenges will enable more accurate predictions and informed decision-making in agricultural management and policy development.~~

The DO_3SE model is an ~~ozone~~ O_3 deposition model that can be embedded within atmospheric chemistry transport models (e.g. Simpson et al., 2012) and uses either a multiplicative~~-~~ or coupled A_{net}-g_{sto} model to estimate stomatal ~~ozone~~ O_3 flux (Pande et al., ~~sub~~2024). Accumulated stomatal ~~ozone~~ O_3 flux has been successfully used as a damage metric (PODy - Phytotoxic Ozone Dose over a threshold y (LRTAP, 2017)) to predict ~~ozone~~O_3-induced yield loss (Pande et al., ~~sub~~2024). The ability of the DO_3SE model to simulate A_{net}, and the inclusion of a process-based ~~ozone~~ O_3 damage module for both instantaneous A_{net} and early and enhanced senescence (after ~~(~~Ewert and Porter~~,~~ (2000)) lends itself to the development of the DO_3SE model as a process-based crop model. The inclusion of resistance algorithms that can assess the transport of O_3 concentrations from a reference height above a canopy down to the canopy top, means the model can ~~easily~~ be embedded within existing atmospheric chemistry transport schemes and hence applied for regional or global scale O_3 risk assessment whilst also ~~accurately~~ modelling O_3 deposition. A comparison of the coupled stomatal ~~conductance-photosynthesis (~~A_{net}-g_{sto}~~)~~ model with the multiplicative g_{sto} model within the DO_3SE framework has been made in Pande et al. (~~sub~~2024) and showed that the A_{net}-g_{sto} model performed equally well, if not better, when used to develop ~~ozone~~ O_3 dose-response relationships for European wheat. This provides evidence of the suitability of the new photosynthetic based g_{sto} model in DO_3SE.

In this study, we describe the development of a new ~~'~~DO_3SE-Crop~~'~~ model which builds on the modified stomatal deposition component of the DO_3SE model (Pande et al. ~~(sub~~2024~~)~~) so that both CO_2 uptake for carbon assimilation as well as ~~ozone~~ O_3 uptake via the stomata can be modelled consistently. Further, we have incorporated the UK JULES crop model (Osborne et al., 2015) to allocate assimilated carbon to plant components (roots, leaves, stems and harvest organs) according to crop development stage. We also take account of the modifying effect of ~~ozone~~ O_3 on instantaneous A_{net} as well as accumulated A_{net} via O_3 effects on the onset and rate of leaf senescence and timing of crop maturity through incorporation of algorithms developed by ~~(~~Ewert and Porter~~,~~ (2000). The UK JULES crop model is used since this is the UK land surface exchange scheme in the UK Earth System Model (UKESM) (Osborne et al., 2015) which has recently been developed to include exchange and impact of trace gases (including O_3) along with other biogeochemical cycling between the atmosphere and the land surface (Leung et al., 2020). This would in the future allow comparison ~~of~~ of the UK JULES Crop model, which ~~are based on~~uses O_3 mechanisms that modify instantaneous A_{net} to mimic changes in yield consistent with flux-response relationships (Sitch et al., 2007), with the alternative O_3 damage mechanisms used within DO_3SE-crop.

Here, we calibrate and evaluate the DO_3SE-crop model using an experimental FACE dataset collected in Xiaoji, China. This allows us to investigate the ability of the model to simulate O_3 damage for a global region where crop productivity is severely threatened by both ~~ozone~~ O_3 pollution and climate

change. The key objectives of the paper are ~~to:~~to assess the ability of DO_3SE-Crop to simulate i). ~~assess the ability of DO_3SE-Crop to simulate~~ key phenological stages, ii) the relationship between ~~and~~ leaf-level physiological variables~~physiological variables,~~ and within canopy ~~stomatal~~ O_3 ~~profile~~concentrations, iii) C allocation to different parts of the crop and iv) ~~crop development, biomass, and yield; ii). the ability of DO_3SE-crop to estimate the difference in~~ O_3 induced yield losses for tolerant and sensitive cultivars ~~caused due to instantaneous versus long-term senescence effects on photosynthesis. , and iii). the applicability of the prescribed UK JULES crop parameters for Chinese conditions.~~

Methods ~~: DO$_3$SE-Crop Model development, calibration and evaluation~~

1. DO$_3$SE-Crop Model

~~We~~Here we describe the development ~~and calibration~~ of the ~~'~~DO$_3$SE-Crop~~'~~ model (version 4 (V4.39.19)) ~~, an ozone deposition model (Emberson *et al.*, 2000; Simpson *et al.*, 2012)that has been modified to simulate stomatal conductance from a coupled photosynthesis-stomatal conductance model (Leuning, 1995). Photosynthesis is simulated using a biochemical model (Farquhar, Caemmerer and Berry, 1980; Sharkey *et al.*, 2007). The DO$_3$SE model has also been extended to include a photosynthetic-based crop model based on the UK JULES land surface crop model (Osborne *et al.*, 2015) with ozone damage functions incorporated after (Ewert and Porter, 2000). DO$_3$SE-Crop is designed to simulate ozone deposition and stomatal uptake and the effects of ozone and climate related variables on crop development, biomass and yield. The DO3SE-Crop model has been developed to simulate~~for ~~wheat (*Triticum aestivum*) which is widely considered to be one of the most sensitive staple crops to ~~ozone~~ O_3 (Feng et al., 2018).

The key components of DO$_3$SE Crop are illustrated in Fig.1. The model ~~integrates meteorological data, crop parameters, and site characteristics to simulate the impact of O_3 ~~of ozone (O_3)~~ on crop yield. ~~The m~~Model ~~uses~~ inputs ~~such as~~are irradiance, temperature, relative humidity, precipitation, air pressure, wind speed, and ~~ozone~~O_3 concentration at a reference height ($C_{~~hz~~}$) to calculate atmospheric resistances (R_a) and boundary layer resistances (R_b) for O_3 ~~ozone~~ deposition ~~on~~to the crop canopy. It further incorporates crop-specific parameters ~~including~~related to leaf physiology, phenology~~,~~ and carbon coefficients, alongside site-specific data ~~like~~(latitude, longitude~~,~~ and elevation)~~,~~ to ~~accurately~~ simulate crop growth at stages from sowing to maturity, denoted by the Development Vegetative Index (DVI~~); where -1 depicts sowing, 0 as emergence, 1 as anthesis, and 2 as maturity~~. ~~Further, t~~The canopy is divided into four vertical layers, each characterised by sunlit (LAI_{sun}) and shaded (LAI_{sh}) leaf area index, which influence the photosynthetic capacity (V_{cmax}) and ~~ozone~~O_3 uptake in each layer. The model accounts for in-canopy resistance (R_{inc}) and external resistance (R_{ext}) in each layer, affecting the ~~ozone~~O_3 flux ($accf_{~~o3~~st}$) and its impact on net photosynthesis (A_{net}) and stomatal conductance (g_{sto}).The $A_{net}g_{sto}$ relationship is modeled using the Leuning model (1995). Damage from O_3 is estimated after ~~, which describes the coupling between A_{net} and g_{sto}. The~~ Ewert & Porter (2000) ~~model is employed to estimate ozone damage by calculating these effects across the~~for different canopy layers ~~canopy~~, which are ~~then~~ aggregated to ~~assess~~ give the overall O_3 impact on ~~the crop's~~canopy A_{net} ~~and yield. This model is~~ which is integrated ~~with~~according to the JULES Crop model (Osborne et al., 2015), which uses the daily accumulated canopy A_{net} to calculate the net primary productivity (NPP). The NPP is then distributed as carbon to various parts of the crop~~, such as~~(roots (C_{root}), stems (C_{stem}), leaves (C_{leaf}), harvestable organs (C_{harv})). The C_{harv} provides~~calculated~~ the yield and grain dry matter; C_{leaf} ~~calculate~~ the LAI and C_{stem} ~~calculated~~ the ~~stem~~crop height.

~~and can be defined as i). crop phenology to ensure the correct length and timing of crop growth for carbon assimilation and ozone exposure; ii). leaf scale processes to ensure leaf level estimates of photosynthesis and stomatal conductance for sunlit and shaded leaves are able to accurately model carbon assimilation and stomatal ozone flux and associated damage over the leaf life span; iii). leaf-to-canopy upscaling that incorporates a within canopy irradiance and ozone concentration gradient and iv). carbon allocation processes to ensure carbon is allocated correctly to different crop compartments (roots, leaves, stem, grain) throughout the growing season.~~

Fig. 1 Schematic of the DO$_3$SE-Crop model.

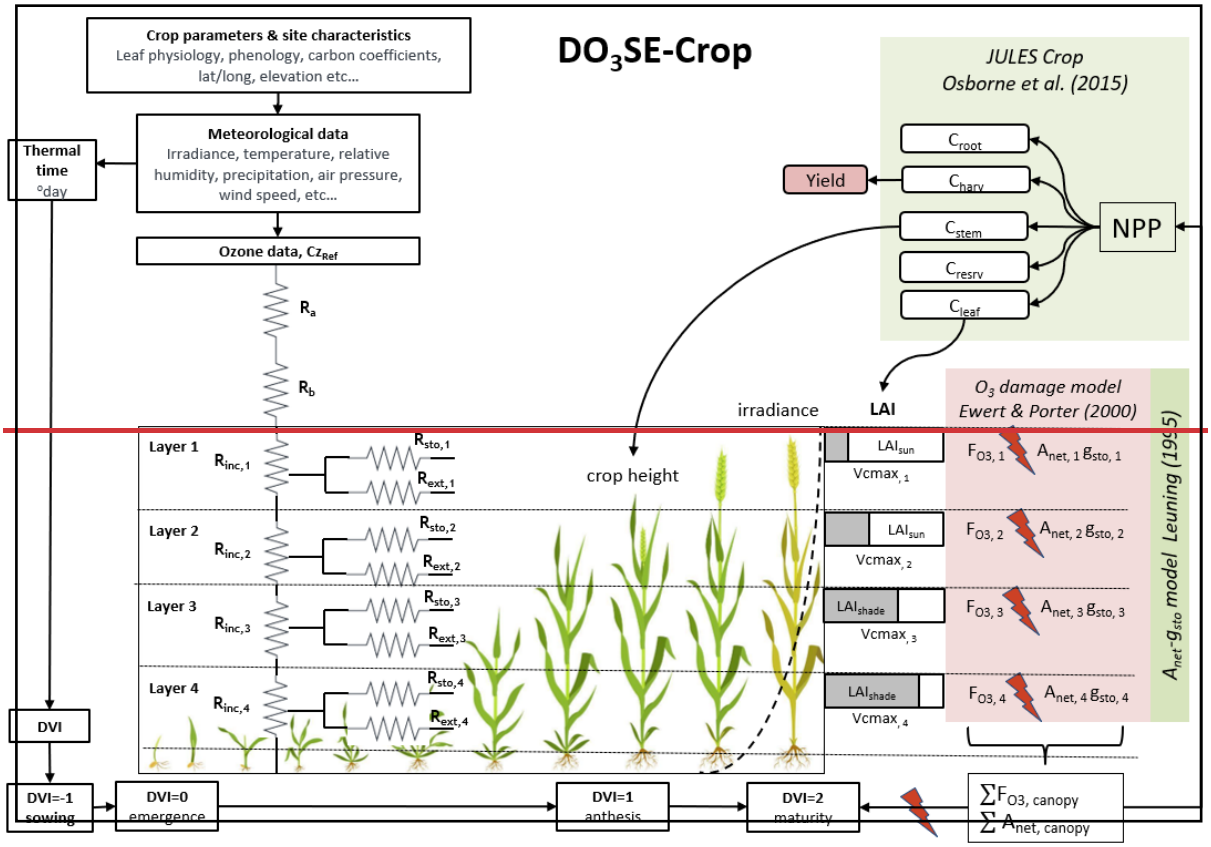

185

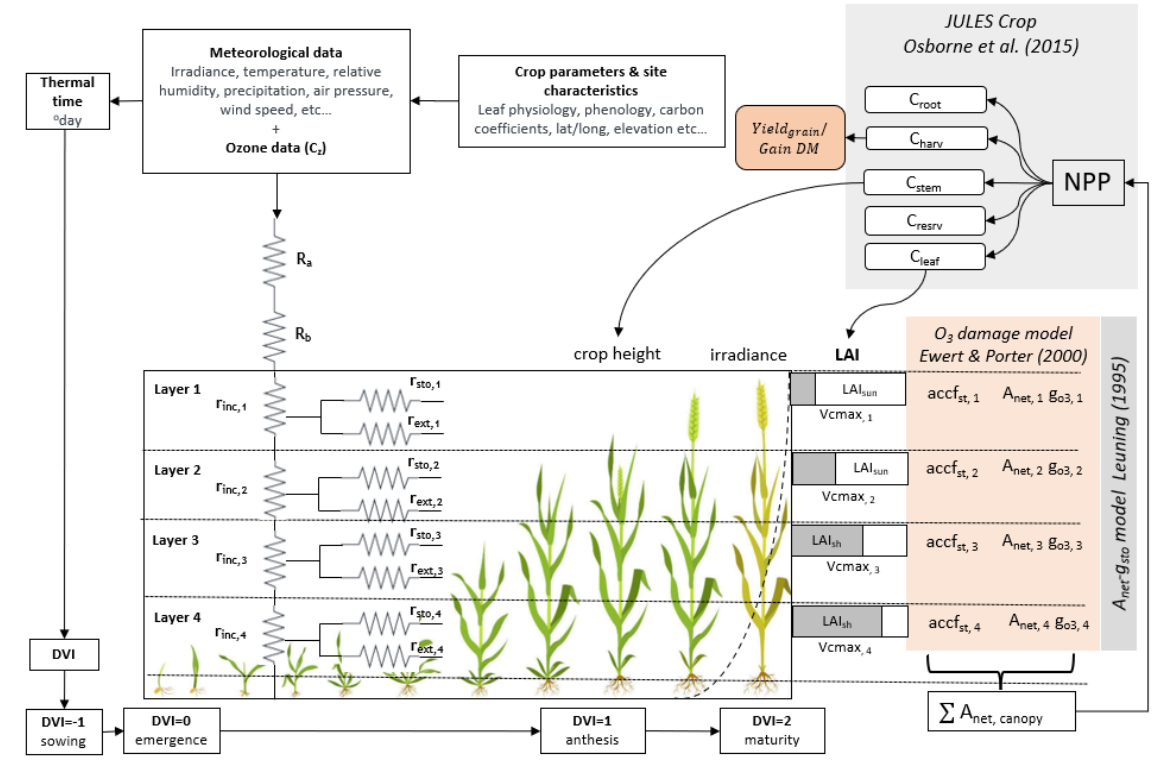

186

187 1.1 DO₃SE–Crop Phenology

188 The DO₃SE-Crop model uses thermal time to define the rate of crop development in relation to the
189 timing of three key developmental stages, TT_{emr} (the period from sowing to emergence), TT_{veg} (the

period of emergence to start of grain filling) and TT_{rep} (the period from the start of grain filling to maturity) based on the method of (Osborne et al., (2015). ~~TT~~ Thermal time is calculated by ~~estimating~~ accumulating an effective temperature (T_{eff}) using base (T_b), optimum (T_o) and maximum (T_m) cardinal temperatures as shown in eq. [1].

$$T_{eff} = \begin{cases} 0 & for\ T_{air} < T_b \\ T_{air} - T_b & for\ T_b \leq T_{air} \leq T_0 \\ (T_0 - T_b)\left(1 - \frac{T_{air} - T_0}{T_m - T_0}\right) & for\ T_0 < T_{air} < T_m \\ 0 & for\ T_{air} \geq T_m \end{cases} \quad [1]$$

Where, T_{air} is the surface air temperature in °C, T_{eff} is at a maximum when $T_{air} = T_o$, this point denotes the highest developmental rate. T_{eff} declines as the temperature falls or rises above T_o, with a linear decrease in crop development. T_{eff} is zero, i.e. no development, when T_{air} falls below or rises above T_b and T_m respectively i.e., $T_m \leq T_{air} < T_b$. During the sowing to emergence phase, development is dependent on T_b, whereas during the vegetative and reproductive phase, development depends on T_m or T_o.

Winter wheat requires vernalisation (a period of exposure to low temperature during germination to accelerate flowering). Vernalisation alters the length of TT_{veg} and hence flowering initiation, with subsequent effects on later growth stages such as heading. Vernalisation occurs when the minimum (VT_{min}) and maximum (VT_{max}) daily temperature is less than 15°C and 30°C respectively (Zheng et al., 2015). Accumulated vernalised days (V_{dd}) are calculated as the sum of vernalised and devernalised days from emergence to the start of anthesis (Zheng et al., 2015) as shown in eq. [2].

$V_{dd} = \sum(V - V_d)$, where [2]

$V = \left(1.4 - 0.778 \times T_{air}, 0.5 + 13.44 \frac{T_{air}}{(Tmax - Tmin + 3)^2}\right)$ ~~for~~ for $VT_{max} < 30°C\ and\ VT_{min} < 15°C$

$V_d = (min(0.5(T_{max} - 30), Vprev)$ ~~for~~ for $VT_{max} > 30°C\ and\ V_{dd} < 10\ days$

The vernalisation factor (VF) decreases from 1 to 0 as (V_{dd}) increases. VF depends on a cultivar-specific vernalisation coefficient (PIV) as described by eq. [3].

$$VF = 1 - (0.0054545 \times PIV + 0.0003) * (50 - V_{dd}) \quad [3]$$

Photoperiod (PP) or day length also affects the occurrence and timing of the flowering stage and is calculated according to latitude using standard solar geometry to estimate daylength (Jones, 1992). The photoperiod factor (PF) represents the sensitivity to PP which decreases from 1 to 0 as the photoperiod shortens and is estimated according to a cultivar-specific photoperiod coefficient (PID) after Tao et al. (2012) as described in eq. [4].

$$PF = 1 - \left[\left(\frac{PID}{10000}\right) \times (20 - PP)^2\right] \quad [4]$$

Crop development is related to the development index (DVI) after (Osborne et al., (2015) which takes values of -1 upon sowing, 0 on emergence, 1 at anthesis and 2 at crop maturity. The DO_3SE-Crop model DVI equations have been modified from (Osborne et al., (2015) to take account of the photoperiod and vernalisation for winter wheat (see eq. [5]); for spring wheat these factors are omitted.

$-1 \leq DVI < 0 \quad for\ TT_{eff}$ ~~$TTtd$~~ $< TT_{emr}$

$$0 \leq DVI < 1 \qquad for\ TT_{emr} \leq TT_{eff} \times VF \times PF < TT_{veg} \quad [5]$$

$$1 \leq DVI \leq 2 \qquad for\ TT_{veg} \leq TT_{eff} \leq TT_{rep}$$

DO_3SE-Crop allows for any number of representative leaf populations (pop) and canopy layers (n) to be defined over the course of the crop growing season. In this study, we used a single leaf population and 4 canopy layers (i.e. $pop = 1;\ n = 4$) for simplicity. The crop sowing is assumed to be at DVI = -1 (start of TT_{emr}) and emergence at DVI = 0 (start of TT_{veg}). The flag leaf is assumed to develop at DVI=1, at the commencement of TT_{rep}, marking the initiation of anthesis (A_{start}, flowering) and flag leaf emergence, which typically occurs 4-5 days prior to the onset of anthesis and is further divided into expanding and senescing leaf periods (i.e. tl_{ep} and tl_{se}) with a default ratio of 0.67 to 0.33 for each of these periods. Maturity is assumed at DVI =2, at the end of TT_{rep}. The model allows estimation of the $PODy$ metric by accumulating stomatal ozone O_3 flux from the start of anthesis to maturity. The total canopy-leaf life span (TT_{leaf}) of the crop is distributed over the DVI between 0 and 2. The relationship between these different variables are described in Fig. 2.

1.2 DO_3SE-Crop leaf-level physiology

Key leaf-level physiological variables of the DO_3SE-Crop model are net photosynthesis (A_{net}) and stomatal conductance (g_{sto}). Net photosynthesis is simulated using the biochemical photosynthesis-based model initially developed by (Farquhar, et al., G.D., von Caemmerer, S., Berry, 1980) and since modified by (Sharkey et al., (2007). The coupled $A_{net}g_{sto}$ model of (Leuning, (1995) is used to estimate g_{sto} from A_{net} which means that g_{sto} is regulated by the demand of CO_2 for A_{net} on consideration of environmental conditions and crop physiology. Ozone stress, causing both instantaneous effects on A_{net} and long-term effects on A_{net} via leaf senescence, is simulated based on algorithms developed by (Ewert and Porter, (2000).

1.2.1 Leaf net photosynthesis (A_{net})

The A_{net} model assumes that photosynthesis is constrained depending on prevailing environmental conditions according to three main mechanisms: Rubisco activity (A_c); ribulose-1,5-bisphosphate (RuBP) regeneration, which is constrained by the speed of electron transport (A_j); and the low rate of transfer of photosynthetic products (most frequently triose phosphate consumption) (A_p) (Sharkey et al., 2007a) and by soil water stress (f_{swPAW}); the algorithm for A_c which is based on (Medlyn et al., (2002) and modified in DO_3SE-crop to include the O_3 damage functions is given in eq. [6].

$$A_c = V_{cmax} \times f_{swPAW} \times \frac{(C_i - \Gamma^*) \times fO_{3,s}(d) \times f_{LS}}{C_i + K_c\left(1 + \frac{O_i}{K_o}\right)} \quad [6]$$

where Vc_{max} (µmol CO_2 $m^{-2}s^{-1}$) is the maximum carboxylation capacity at 25°C, C_i (µmol mol^{-1}) and O_i (mmol mol^{-1}) are the intercellular CO_2 and O_2 partial pressures; K_c (µmol mol^{-1}) and K_0 (mmol mol^{-1}) are the Rubisco Michaelis-Menten constants for CO_2 and O_2; Γ^* (µmol mol^{-1}) is the CO_2 compensation point in the absence of respiration; $fO_{3,s}(d)$ is the factor that accounts for the cumulative stomatal O_3 flux effect on V_{cmax} over the course of a day and; f_{LS} is the factor that accounts for the cumulative stomatal O_3 flux effect over the course of a leaf life span on leaf senescence. Section 1.2.1.1 gives a full description of the methods used to estimate O_3 damage. The f_{PAW} factor is calculated by eq. [7].

$$f_{PAW} = 1 \quad for\ PAW_t \leq PAW \leq 100\%, \qquad [7]$$

$$f_{PAW} = 1 + \{min\{1, max\{f_{min}, f_{min} + (1 - f_{min}) \times \frac{(ASWPAW / PAWASW_{tfc}) \times 100 - ASW_{min}}{PAASW_{tmax} - ASW_{min}}\}$$

$$for\ PAW \leq PAW_t$$

Where PAW is plant available water. PAW is the amont of water in the soil (in % terms) which is available to the plants. At PAW=100% the soil is at field capacity, at PAW=0% the soil is at wilting point. PAW_t is the threshold PAW, above whichwhich it is assumed there is no constraint on A_c, h $gsto$ is at a maximum as described f_{PAW} functiondefined as 50% after {LRTAP, (2017)Where: f_{PAW} is the plant available water factor, influencing stomatal conductance. f_{min} is the minimum stomatal conductance under dry soil conditions. ASW represents the available soil water. ASW_{fc} is the available soil water at field capacity, converted to a percentage. ASW_{max} is the plant available soil water below which stomatal conductance will start to reduce, and ASW_{min} is the plant available soil water at which stomatal conductance will equal f_{min} (Nguyen *et al.*, 2024).

This model scales the stomatal conductance between a minimum value and a value of unity, which represents fully open stomata, based on the available soil water as a percentage of its field capacity. The constraint on A_{net} photosynthesis due to the rate of electron transport A_j is described in eq. [8].

$$A_j = J \times \frac{C_i - \Gamma^*}{a \times C_i + b \times \Gamma^*} \qquad [8]$$

where *J* is the electron transport rate (µmol CO_2 $m^{-2}s^{-1}$), the parameters a and b denote the electron requirements for the formation of NADPH and ATP respectively (Sharkey et al., 2007)

Finally, the photosynthesis l A_{net} limitation due to the low rate of transfer of photosynthetic products A_p (µmol CO_2 $m^{-2}s^{-1}$) is given in eq. [9].

$$A_p = 0.5 \times V_{cmax} \qquad [9]$$

The net leaf net photosynthetic photosynthesis carbon uptake (A_{net}) in µmol CO_2 $m^{-2}s^{-1}$ is calculated by eq. [10]

$$A_{net} = (A_c, A_j, A_p) - R_d \qquad [10]$$

Where leaf dark respiration (R_d) in µmol CO_2 $m^{-2}s^{-1}$ is calculated as $Vc_{max} \times R_{dcoeff}$ where R_{dcoeff} is the leaf dark respiration coefficient initially set equal to 0.015 after Clark et al. (2011), a value provided for C3 grasses.

1.2.1.1 Short- and long-term O_3 damage to A_c

The short-term impact of O_3 on A_c is calculated according to the $fO_{3,s}(d)$ factor (between 0 and 1) which allows for an instantaneous effect of O_3 on photosynthesis when stomatal O_3 flux (f_{st}), in nmol O_3 m^{-2} s^{-1} calculated as described later in section 1.2.3, overwhelms detoxification and repair mechanisms (Betzelberger et al., 2012; Feng et al., 2022), and is estimated following {Ewert and Porter, (2000). Here, $f_{O3,s}(h)$ represents the relationship between f_{st} and a potential decrease in A_c calculated for every hour of the day by eq. [11].

$$f_{O3,s}(h) = 1; \qquad for\ f_{st} \leq \frac{\gamma 1}{\gamma 2}$$

$$f_{O3,s}(h) = 1 + \gamma 1 - \gamma 2 \times f_{st} \qquad for\ \frac{\gamma 1}{\gamma 2} < f_{st} < \frac{1+\gamma 1}{\gamma 2} \qquad [11]$$

$$f_{O3,s}(h) = 0\ ; \qquad for\ f_{st} \geq \frac{1+\gamma 1}{\gamma 2 \gamma 2}$$

where $\gamma 1$ (dimensionless) and $\gamma 2$ (nmol O_3 m^{-2} $s^{-1})^{-1}$ are both short-term O_3 damage coefficients, with $\gamma 1$ representing the O_3 detoxification threshold below which no damage occurs to the photosynthetic system and $\gamma 2$ determines the effect of f_{st} on A_c once this detoxification threshold is exceeded; $fO_{3,s}(d)$ and $fO_{3,s}(d-1)$ (i.e. $fO_{3,s}(d)$ at the end of the previous day), are calculated by eq. [12].

$$f_{O3,s}(d) = f_{O3,s}(h) \times r_{O3,s}\ ; \qquad for\ hour = 0; PAR \leq 50\ W\ m^{-2}$$

$$f_{O3,s}(d) = f_{O3,s}(h) \times f_{O3,s}(d-1) \qquad for\ PAR > 50\ W\ m^{-2}\ for\ hour = 0$$

[12]

where $r_{O3,s}$ (dimensionless) is represents incomplete recovery from O_3 overnight which depends on leaf age according to eq. [13].

$$r_{O3,s} = f_{O3,s}(d-1) + \left(1 - f_{O3,s}(d-1)\right) \times f_{LA} \qquad [13]$$

The long-term impact of O_3 on V_{cmax} represented by the f_{Ls} term represents the longer-term accumulation of stomatal ozone O_3 flux (acc_{fst}) causing degradation to the Rubisco enzyme which triggers early and enhanced senescence of mature leaves (Gelang et al., 2000; Osborne et al., 2019). The acc_{fst} term is accumulated from 200°C days before anthesis until maturity to be consistent with the LRTAP (2017) which defines this as the O_3 sensitive period for wheat. The simulation of f_{Ls} (and f_{LA} used in the short-term O_3 effect) are related to thermal time defined periods over the course of a leaf population life span TT_{leaf} as described in Fig. 2.

Figure 2. The division of thermal time defined periods (TT_{emr} , TT_{veg}, TT_{rep} and TT_{leaf} and the relationship with f_{LA} and f_{Ls}) for the canopy, as represented in this study by a single leaf population.

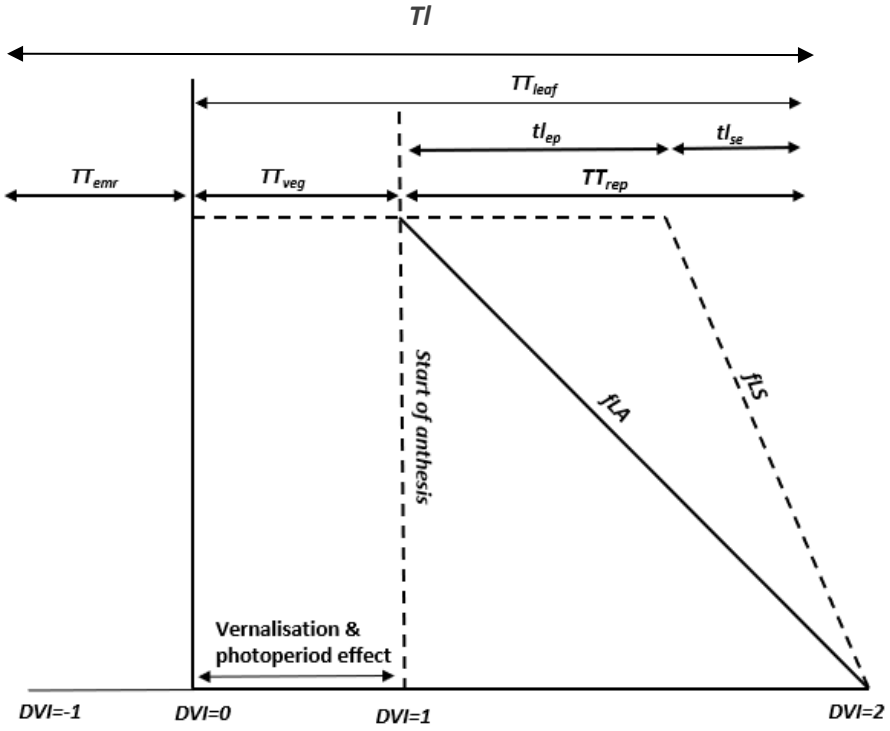

The O_3 effect on f_{Ls} is first simulated by estimating a weighted accumulated fst ($fO3_l$) modified from (Ewert and Porter, 2000) by eq. [14].

$$fO3_l = 1 - max\left(min\left(\gamma 3 \times \left(acc_{fst} - CLsO3\right), 1\right), 0\right) \quad [14]$$

where $\gamma 3$ determines the occurrence of senescence once a critical cumulative stomatal O_3 flux $CLsO3$ (in mmol/m^2) has been exceeded. The rate of senescence is determined by $\gamma 4$, which determines the onset of senescence and $\gamma 5$ which determines maturity as described in eq. [15]

$$tl_{ep_{O3}} = tl_{ep} \times \left(1 - \left((1 - fO3_l) \times \gamma 4\right)\right)$$

$$tl_{se_{O3}} = tl_{se} \times \left(1 - \left((1 - fO3_l) \times \gamma 5\right)\right) + zc \quad [15]$$

$$zc = tl_{ep} - tl_{ep_{O3}}$$

Where tl_{ep} is the ~~effective temperature ($teffT_{eff}$)~~ thermal time accumulated by a leaf (LTT) in °C days between a fully expanded leaf and the start of leaf senescence, $tl_{ep_{O3}}$ is tl_{ep} with an O_3 effect which may bring senescence earlier, tl_{se} is the is the LTT in °C days ~~(T_{eff} teff)~~ between the onset of senescence and maturity and $tl_{se_{O3}}$ is tl_{se} with an O_3 effect which may bring maturity earlier. f_{Ls} is estimated by eq. [16].

$$f_{Ls} = 1; \qquad for\ \ T_{eff}LTTteff \leq TT_{veg} + tl_{ep}$$

$$f_{Ls} = 1 - \frac{TT_{eff}LTT - TT_{veg} - tl_{ep_{O3}}}{tl_{se_{O3}}}; \qquad for\ TT_{veg} + tl,ep < T_{eff}LTTteff < TT_{leaf}$$

$$f_{Ls} = 0; \qquad for\ T_{eff}LTTteff \geq TT_{leaf}$$

[16]

1.2.2 Stomatal conductance (g_{sto})

The coupled photosynthesis-stomatal conductance ($A_{net}g_{sto}$) model based on (Leuning, 1995) and modified for vapour pressure deficit (VPD) is used to estimate g_{CO_2}, stomatal conductance to CO_2 in µmol CO_2 m^{-2} s^{-1} as described in eq. [17].

$$g_{CO2} = [f_{min} + m \times A_{net} \times f_{VPD}/(c_s - \Gamma)] \quad [17]$$

where f_{min} (µmol m^{-2} s^{-1}) is the minimum daytime g_{CO_2} (Leuning, 1990). The parameter m (dimensionless) is the composite sensitivity of g_{CO2} to assimilation rate and vapour pressure deficit (VPD) with the relationship between VPD and relative stomatal conductance (f_{VPD}) estimated by eq. [18]. ~~A_{net} (µmol m-2 s-1) is estimated from eq [10]. f_{VPD} is calculated by eq. [18].~~

$$f_{VPD} = \left(1 + \left(\frac{VPD}{VPDo}\right)^8\right)^{-1} \quad [18]$$

where VPD_0 is an empirical parameter, defined using boundary line analysis, describing the variation in relative stomatal conductance with VPD (Danielsson et al., 2003; Pleijel et al., 2007). c_s (mmol mol^{-1}) is the external CO_2 concentration at the leaf surface and is calculated from the external CO_2 concentration at the upper surface of the leaf boundary layer c_a (mmol mol^{-1}) so that $c_s = c_a - \left(\frac{A_{net}}{g_{bCO2}}\right)$ after (Masutomi, 2023) where g_{bCO2} is the boundary layer conductance to CO_2 (in mol m^{-2} s^{-1}), conversion factors for gases and heat across the boundary layer are given in S1a.

Finally, g_{CO2} is converted to g_{O3} in mmol O_3 m^{-2} s^{-1} by dividing by 1000 and using the conversion factor 0.96 which assumes that the ratio of the diffusivities of gases in air are equal to the inverse of the square root of the ratio of molecular weights (as described in ~~(~~Campbell & ~~, G.S.,~~ Norman ~~(,~~ 1998~~)~~), see also supplementary S1b).

1.2.3 Stomatal ozone flux (f_{st})

Stomatal [O_3] flux (f_{st} in ~~(~~nmol m^{-2} s^{-1}) is calculated after the method described in the UNECE Mapping Manual (~~UNECE~~LRTAP, 2017) described in eq. [19].

$$f_{st} = C_l \times g_{O3m/s} \times \frac{r_c}{r_{b,O3}+r_c} \quad [19]$$

Where C_l is the [O_3] at the upper surface of the laminar layer of a leaf (nmol O_3 m^{-3}). Ozone concentration in ppb can be converted to nmol m^{-3} by multiplying O_3 in ppb by $P/(R \times T_{air,k})$ where P is the atmospheric pressure (1.013 × 10^5 in Pascal)~~in Pascal~~, R is the universal gas constant (8.31447 J/mol/K) and $T_{air,k}$ ~~is surface~~is surface air temperature in degrees Kelvin~~;~~. T~~$g_{O3m/s}$ (m/s) is stomatal conductance to O_3, t~~o convert g_{O3} (mol O_3 m^{-2} s^{-1}) to $g_{O3m/s}$ (m/s) we assume a standard temperature ~~T_{st}~~(20°C) and P, ~~air pressure P_{st} (1.013 × 10^5 in Pascal) and~~ divide by 41 to give the conductance value in m/s. The $r_c/(r_{b,O3}+r_c)$ term represents the O_3 deposition rate to the leaf through resistances r_b (the quasi-laminar resistance (s/m)) and r_c (the leaf surface resistance (s/m)) which allow for both stomatal and non-stomatal deposition to the leaf surface. r_c is 1~~/(~~/($g_{O3m/s}$+g_{ext}) where g_{ext} is 1/2500 (s/m). $r_{b,O3}$~~r_b~~ is estimated by eq. [20].

$$r_{b,O3} = 1.3 \times 150 \times \sqrt{\frac{L}{u_l}} \quad [20]$$

Where the factor 1.3 accounts of the differences in diffusivity between heat and O_3~~.~~ (see S1a) ~~and The value of 150 provides the equivalent conductance leaf layer for O_3 as compared to forced convection of heat (Campbell, G.S., Norman, 1998)~~, L is the cross wind leaf dimension (m) and u_l is the windspeed (m/s) at the top of the leaf laminar boundary layer. The leaf boundary layer resistance to CO_2 is estimated using a value of 1.24 for the difference between heat and CO_2 in place of the 1.3 value for O_3 (Campbell and ~~, G.S.,~~ Norman, 1998).

1.3 DO_3SE-Crop canopy

The DO_3SE crop model uses a multi-layer approach to scale from leaf to the canopy. We assume that wind, irradiance, [O_3] concentration and leaf nitrogen content are the key environmental conditions which change with cumulative canopy leaf area index (LAI) and influence leaf physiology and therefore canopy layer estimates of A_{net}, $g_{~~sto~~O3}$ and g_{ext}; other environmental variables (e.g., $T_{air~~,oC~~}$ and VPD) are assumed to remain constant over the canopy.

1.3.1 Canopy irradiance

Changes in irradiance through the canopy are described as sunlit and shaded canopy fractions and the associated quantity of direct and diffuse photosynthetically active radiation PAR (W/m^2), these are estimated according to increasing levels of cumulative LAI using the methods of (Pury and Farquhar, 1997); full details are given in the supplementary material (see section S2). Application of

this method requires the canopy to be divided into layers of equal LAI (including both green (LAI_G) and brown (LAI_B) LAI.

PAR absorbed per unit leaf area is divided into PAR_{dir}, PAR_{diff} which also includes scattered (re-reflected by the canopy) beam calculated by,

$$PAR_{dir}\ (LAI) = (1 - \rho_{cb}(\beta))\ K_b'\ I_b(0)\ exp(-k_b'LAI) \quad [21]$$

$$PAR_{diff}\ (LAI) = \ (1 - \rho_{cd})\ K_d'\ I_d(0)\ exp(-k_d'LAI) \quad [22]$$

Estimates of the LAI fractions of sunlit (LAI_{sun}) and shaded (LAI_{sh}) parts of each canopy layer (i) are made by eq. 23 and 24.

$$LAI_{sun,i} = \left[1 - exp\ \left(-0.5 \times \frac{LAIi}{sin\beta}\right)\right] \times 2sin\beta \quad [23]$$

Where β is the solar elevation angle (see supplementary section S3)

$$LAI_{sh,i}\ =\ LAI_i - LAI_{sun,i} \quad [24]$$

The DO$_3$SE-Crop model simulates LAI as part of the crop growth model and LAI is assumed to be evenly distributed across all layers (see section 1.5.2 and eq. 43).

Therefore, PAR for the sunlit part of each layer can be described as

$$\int_{LAI_i}^{LAI_n} PA\,R_{sun} = \int_{LAI_i}^{LAI_n}(\,LAI_{sun,i}) \times (PAR_{sh} + PAR_{bsun}\,(\beta))\ \text{dLAI}$$

Where $\int_{LAi_i}^{LAi_n} P\,AR_{dir}$ can be written as $(1 - \rho cb(\beta)) \times Kb' \times Ib(0) \times [exp(-Kb'LAI_i) - exp(-Kb'LAI_n)]$ and $PAR_{bsun}\,(\beta)\ =\ (1 -\ \sigma)I_b(0)\frac{Cos_{\alpha l}}{Sin\beta}$

Similarly, PAR for the shaded part of each layer can be described as

$$\int_{LAI_i}^{LAI_n} PA\,R_{sh} = \int_{LAI_i}^{LAI_n}(\,LAI_{sh,i}) \times (PAR_{diff} + PAR_{bsun})dL\text{AI}$$

Where $\int_{LAi_i}^{LAi_n}(\,PAR_{diff}\ (LAI)$ can be written as $(1 - \rho cd) \times Kb' \times Ib(0) \times [exp(-k_d'LAI_i) - exp(-k_d'LAI_n)]dL$ and $\int_{LAi_i}^{LAi_n} P\,AR_{bs}\ (LAI)$ is $I_b\ (0)\ [\,PAR_{dir} - (1 -\ \sigma)k_b \times\ [exp(-k_bLAI_i) - exp(-k_bLAI_n)]$

1.3.2 Canopy [O$_3$] concentration

O_3 concentration will vary as a function of O_3 loss to the canopy (i.e. deposition via the stomates and external plant parts) and O_3 replacement from ambient air concentrations above the canopy. Limited data have been collected showing how O_3 concentrations vary with canopy depth in semi-natural communities (Jaggi et al., 2006). These data suggest that a minimum, bottom canopy O_3 concentration (C_{zb}), is about 0.2 times that at the top of the canopy (C_{zh}) and that the O_3 concentration difference within the canopy is closely related to the LAI of the canopy layers.

Since each canopy layer can be assumed to be a parallel sink, the O_3 flux to a layer depends on the conductance (inverse of resistance) of that layer and the O_3 concentration at the top of the layer (C_i; with C_0 being C_{zh} (i.e. the O_3 concentration at height C_h, the top of the canopy)); we follow and generalise the work of Waggoner (1971) by separating the canopy into nL leaf layers. We calculate the O_3 concentration for each layer, C_i, from O_3 intake, I_i, by;

$$C_i = r_{c,i} I_i \quad [25]$$

With $r_{c,i}$ the leaf surface resistance to O_3 for layer i. I_i is calculated as the solution to a system of linear equations. Relating r_{ci}, I_i, and resistances of the bulk air among the leaves ~~-(RR_{ii})~~, the in-canopy aerodynamic resistance for layer i. Assuming above the canopy there is a uniform O_3 concentration C_0, we use generalised equations from Waggoner (1971) ~~Waggoner., 1971~~ for the difference in O_3 concentration between the exterior air and leaf interior, which for the top layer is C_0 minus 0, so C_0 and for each lower layer the difference is 0. This O_3 concentration difference is calculated by;

$$C_0 = RR_{i1} \sum_{j=1}^{nL} I_j + r_{c,1} r_1 I_1 \quad [26]$$

~~[26]~~

For the top canopy layer,

$$0 = RR_i \sum_{j=i}^{nL} I_j + r_{c,i} r_i I_i - r_{c,i-1} r_{i-1} I_{i-1}$$

[27]

For each canopy layer i between the top layer and the bottom layer, and;

$$0 = RR_{nL+1} I_{nL+1} - r_{c,nL} I_{nL} \quad [28]$$

For the bottom layer of the canopy, between the lowest leaf layer and the ground. These can also be written into the matrix form;

$$\begin{pmatrix} r_{c,1} + R_1 & R_1 & R_1 & \cdots & R_1 \\ -r_{c,1} & r_{c,2} + R_2 & R_2 & \cdots & R_2 \\ 0 & -r_{c,2} & r_{c,3} + R_3 & \cdots & R_3 \\ \vdots & \vdots & \vdots & \ddots & \vdots \\ 0 & 0 & 0 & \ldots & R_{nL+\_1} \end{pmatrix} \begin{pmatrix} I_1 \\ I_2 \\ I_3 \\ \vdots \\ I_{nL+1} \end{pmatrix} = \begin{pmatrix} C_0 \\ 0 \\ 0 \\ \vdots \\ 0 \end{pmatrix} \quad [29]$$

Which can be numerically solved for I_x when $r_{c,1} \neq 0$ and $R_1 \neq 0$.

Resistances for each layer are calculated as described in the supplementary material (section S54) using standard DO_3SE deposition modelling methods (Emberson et al., ~~, L.D., Ashmore, M.R., Simpson, D., Tuovinen, J.-P. and Cambridge, 2001; Simpson *et al.*,~~ 2012).

1.3.3 Canopy maximum carboxylation capacity (V_{cmax})

We allow for an exponential decrease in leaf N with canopy depth which will influence both the photosynthetic capacity (V_{cmax}) and hence dark respiration (R_{dc}). Photosynthetic capacity at each canopy layer i is calculated by eq. [30].

$$V_{cmax,i} = n_e \times n_0 \times e^{-kN \left(\frac{LAIi}{LAI~~total~~}\right)} \quad [30]$$

Where n_e (mol CO_2 m^{-2} s^{-1} kg C (kg N)$^{-1)}$ is a constant relating leaf nitrogen to Rubisco carboxylation capacity, n_0 (kg N[kg C]-1) is the leaf N concentration at the top of the canopy and kN is a nitrogen profile co-efficient initially set at 0.78 after (Clark et al., 2011).

1.3.4 Canopy Photosynthesis ($Anet_c$)

Net canopy photosynthesis ($Anet_c$) determines the amount of C assimilated by the entire canopy that can subsequently be allocated to different plant parts (i.e. less than the C respired for plant growth and maintenance, see section 1.4.1), the amount of C assimilation will ultimately determine whole plant biomass. The net photosynthesis for each canopy layer ($Anet_i$) is calculated according to the LAI fraction of that layer that is sunlit ($LAI_{sun,i}$) and shaded ($LAI_{sh,i}$) within the layer (i), multiplied by the net photosynthesis of the sunlit ($Anet_{sun,i,j}$) and shaded leaf ($Anet_{sh,i,j}$), respectively described by eq. [31] and [32].

$$Anet_i = LAI_{sun,i} \times Anet_{sun,i} + LAI_{sh,i} \times Anet_{sh,i} \quad [31]$$

with $Anet_c$ calculated by,

$$Anet_c = \sum_{i=1}^{n} Anet_i \quad [32]$$

$Anet_c$ is converted from µmol CO_2 m^{-2} s^{-1} to kg C m^{-2} day^{-1} by multiplying by 3600 (converting from seconds to hours), multiplying by 1.2 (representing the kg of C per mol) and summing each hourly $Anet_c$ over the course of a day. This $Anet_c$ is used in the equation 37.

1.3.5 Canopy Stomatal Conductance ($gO3_c$) (~~g_{sto3_i}~~)

Similarly, canopy layer (i) stomatal conductance to O_3 (g_{O3_i}), which is converted from g_{CO_2} by assuming a diffusivity ratio of 0.96 to convert from CO_2 to O_3 and is calculated by eq. [33] with whole canopy stomatal conductance calculated by eq. [34].

$$gO3_i ~~g_{sto_i}~~ = LAI_{sun,i} \times gO3_{sun,i} ~~g_{sto\,sun,i}~~ + LAI_{sh,i} \times gO3_{sh,i} ~~g_{sto\,sh,i}~~ \quad [33]$$

$$gO3_c ~~g_{sto_c}~~ = \sum_{i=1}^{n} gO3_i ~~g_{sto_i}~~ \quad [34]$$

This is converted from $gO3_i ~~g_{sto_i}~~$ in eq. [33] by dividing the conductance value in mmol m^{-1} s^{-1} by 41000 (assuming standard temperature (20°C) and air pressure (1.013 x 10^5 Pa)) to give conductance in m/s.

1.4 Crop biomass, LAI, height and yield variables

The following section describes how to estimate crop biomass, important canopy characteristics (LAI and crop height (h)) and yield variables from accumulated calculations of $Anet_c$ over the course of the growing season following (Osborne et al., 2015).

1.4.1 Crop biomass (NPP and GPP)

The simulation of crop growth requires an estimate of the net primary productivity (NPP) which is calculated at the end of each day and summed over the growing season. Carbon is assumed to be allocated to five key crop components: root, leaf, stem, harvest, and reserve pools (Osborne et al., 2015). This carbon allocation is ultimately used to simulate leaf area index (LAI), canopy height (h), biomass, harvest index, and yield at the end of each day throughout the growing season.

Net primary productivity NPP (kg C m^{-2} day^{-1}) is accumulated throughout the day using the JULES-crop approach to model crop growth (Osborne et al., 2015) described in eq. [35].

$$NPP = GPP - R_p \quad [35]$$

where GPP is the gross primary productivity (kg C m^{-2} day^{-1}) and R_p is plant respiration divided into maintenance (R_{pm}) and growth (R_{pg}) respiration (kg C m^{-2} day^{-1}) (Clark et al., 2011) where $R_p = R_{pm} + R_{pg}$ and where R_{pg} is assumed to be a fixed fraction of the NPP as shown in eq. [36].

$$R_{pg} = R_{gcoeff}\ (GPP - R_{pm}) \quad [36]$$

Where R_{gcoeff} is the growth respiration co-efficient which was initially set to 0.25 based on the value for all PFTs (i.e. forests and grasses including crops) in (Clark et al., 2011). GPP is calculated by eq. [37].

$$GPP = Anet_c + f_{\sout{swPAW}} R_{dc} \quad [37]$$

where $Anet_c$ is net canopy photosynthesis (see eq. 28) and $f_{PA\sout{sW}w}R_{dc}$ is the soil-moisture modified canopy dark respiration (kg C m^{-2} day^{-1}) where $R_{dc} = V_{cmax,i} \times R_{dcoeff}$ with R_{dcoeff} initially assumed to be 0.015 based on (Clark et al., 2011); $V_{cmax\ ,i}$ is the maximum carboxylation efficiency for each canopy layer i which decreases from the top to bottom of the canopy (see eq. 30) and $f_{\sout{s}PAW\sout{w}}$ is calculated in eq. [7].

Leaf maintenance respiration (R_{pm}) is assumed equivalent to the soil moisture modified canopy dark respiration, while root and stem respiration are assumed to be independent of soil moisture but to have the same dependencies on C content. We assume a fixed relationship between C and N contents of these organs so that R_{pm} can be estimated by eq. [38].

$$R_{pm} = R_{dc} \times (f_{sw} + (\ \tfrac{C_{root} + C_{stem}}{C_{leaf}}\ )] \quad [38]$$

The C accumulating as NPP each day is divided into five carbon pools i.e. root (C_{root}), leaf (C_{leaf}), stem (C_{stem}), reserve (C_{resv}), and harvest (C_{harv}) (kg C m^{-2} day^{-1}) according to partition coefficients (see eq. [39]) allowing for accumulation of C in these pools over the course of the crop growth period.

$$\begin{aligned}
\frac{dC_root}{dt} &= p_{root} NPP, \\
\frac{dC_leaf}{dt} &= p_{leaf} NPP, \\
\tfrac{dC_stem}{dt} &= p_{stem} NPP\ (1 - \tau), \\
\frac{dC_harv}{dt} &= p_{harv} NPP, \\
\tfrac{dC_{resv}}{dt} &= p_{stem} NPP, \tau
\end{aligned} \quad [39]$$

where τ is the fraction of stem C that is partitioned into the reserve pool. p_{root}, p_{leaf}, p_{stem}, $p_{harv} = 1$. The partition coefficients are related to the crop development stage (DVI) and hence effective thermal time (TT_{eff}) since emergence. The partition coefficients are based on Osborne et al. (2015) and provided as a function of DVI using six parameters to continuously describe varying partition coefficients over the duration of the crop growing season. We use the same multinomial logistic as that described in (Osborne et al., 2015) to define this function according to eq. [40].

$$\begin{aligned}
p_{root} &= \frac{e^{\alpha_{root} + (\beta\ root\ DVI)}}{e^{\alpha_{root} + (\beta\ root\ DVI)} + e^{\alpha_{stem} + (\beta\ stem\ DVI)} + e^{\alpha_{leaf} + (\beta\ leaf\ DVI)} + 1}, \\
p_{stem} &= \frac{e^{\alpha_{stem} + (\beta\ stem\ DVI)}}{e^{\alpha_{root} + (\beta\ root\ DVI)} + e^{\alpha_{stem} + (\beta\ stem\ DVI)} + e^{\alpha_{leaf} + (\beta\ leaf\ DVI)} + 1}, \\
p_{leaf} &= \frac{e^{\alpha_{leaf} + (\beta\ leaf\ DVI)}}{e^{\alpha_{root} + (\beta\ root\ DVI)} + e^{\alpha_{stem} + (\beta\ stem\ DVI)} + e^{\alpha_{leaf} + (\beta\ leaf\ DVI)} + 1},
\end{aligned} \quad [40]$$

$$p_{harv} = \frac{1}{e^{\alpha_{root}+(\beta\ root\ DVI)} + e^{\alpha_{stem}+(\beta\ stem\ DVI)} + e^{\alpha_{leaf}+(\beta\ leaf\ DVI)} + 1},$$

Where DVI is the development index; α and β partition parameters. These parameters describe the shape of the thermal time varying partition coefficient for leaves, roots and stems.

Once C is no longer partitioned to stems, C from the stem reserve pool will mobilise to the harvest pool at a rate of 10% per day following (Osborne et al., 2015) described by eq. [41].

$$C_{harv} = C_{harv} + (0.1\ C_{resv})\ C_{resv} = 0.9\ C_{resv}\ \} \quad for\ p_{stem} < 0.01 \qquad [41]$$

Total leaf C is divided between green leaf C ($C_{leaf,green}$), and brown leaf carbon ($C_{leaf,brown}$). Carbon from the $C_{leaf,green}$ will mobilise to the harvest pool at the rate of 5% per day after (Osborne et al., 2015) and to the $C_{leaf,brown}$ at a rate of 24% per day once $f_{LS} > 1$ as described in eq. [42]

$$\{C_{harv} = C_{harv} + \left(0.05\ C_{leaf,green}\right) C_{leaf,green} = 0.86\ C_{leaf}\ \ C_{leaf} = 0.86 C_{leaf,green} + 0.24 C_{leaf,brown}\ \}\ \ for\ f_{LS} > 1 \qquad [42]$$

1.4.2 Leaf area Index (LAI) and stem height (h)

At the end of each day, the C content of the stem and leaf is used to estimate LAI by eqs. [43] and [44].

$$LAI = (C_{leaf}\ /f_c) \times SLA \qquad [43]$$

where $SLA = \Upsilon\ (DVI + 0.06)^{\delta}$ [44]

The values Υ and δ were determined by fitting the values to the paired values of DVI and specific leaf area (SLA). The value of f_c is 0.5 (unitless), denotes carbon fraction of dry matter.

The amount of C in the stem is used to calculate the crop height h in m by eq. [45].

$$h = k\ (C_{stem}\ /f_c\ )^{\lambda} \qquad [45]$$

where k and λ were determined by fitting the value C_{stem} and h.

1.4.3 Yield variables

According to (Osborne et al., 2015) yield can be calculated from the C allocated to the harvest pool (C_{harv}) at the end of the growing season as described in eq. [46]

$$Yield_{grain} = \frac{(C_{harv} \times (1/f_c) \times D_W \times E_g)}{1000} \qquad [46]$$

Where harvested C is converted to total biomass (using the conversion factor f_c=0.5), i.e., by multiplying the harvested C by $1/f_c$, and then by 1/0.84 (D_w) to account for the grain moisture content (Mulvaney and Devkota, 2020). C_{harv} includes both chaff and grain however, O_3 fumigation experimentalists tend to only include grain when calculating total crop yield at the end of the growing season, so we assume 15% of the yield is chaff and include a grain to ear ratio, E_g, of 0.85. Dividing by 1000 converts yield from kg C m^{-2} to g C m^{-2}, the unit most often used to describe experimental yield results.

Evaluation of the DO_3SE-crop model uses a variety of growth 'dry matter (DM)' metrics. Some of the most important metrics and their calculations are: '$Straw\ DM$' which is calculated as the sum of carbon allocated to C_{stem}, C_{leaf}, and C_{resv}; '$Ear\ DM$' is calculated from C_{harv} excluding the moisture content (D_w) conversion; '$Grain\ DM$' is calculated from C_{harv} excluding both the moisture content (D_w) conversion and removing the chaff fraction conversion E_g; '$Above\ ground\ DM$' is the $straw\ DM$ plus the $Ear\ DM$; '$Below\ ground\ DM$' is converted from C_{root}; and '$Harvest\ index$' is the $Gain\ DM$ divided by the $Above\ ground\ DM$. In all cases the f_c conversion factor is used to convert from e.g. g C m^{-2} to g DM m^{-2}.

2. DO_3SE-Crop model calibration

2.1 Xiaoji China experimental dataset

The DO3SE-crop model was used to analyse the O_3-FACE (Free Air Concentration Enrichment) experimental data collected in Xiaoji, Jiangdu, Jiangsu Province, China. The wheat crop was grown in fully open-air field conditions for three consecutive growing seasons from 2007 to 2009. Thies dataset includes four modern cultivars of winter wheat (*Triticum aestivum* L.) grown under ambient (AA) and elevated (E) [O_3], with the elevated treatment being, on average, 25% above the ambient [O_3] concentrations of 45.7 ppb from early March/April to the end of May each year. The four cultivars were Yannong 19 (strong-gluten wheat, hereafter Y19), Yangmai 16 (medium-gluten wheat, hereafter Y16), Yangmai 15 (weak-gluten wheat, hereafter Y15), and Yangfumai 2 (weak-gluten wheat, hereafter Y2) (Zhu et al., 2011).

TheSoil water availability was sufficient for optimum the wheat crop growth, so we assumed there was no soil moisture stress (Feng et al., 2012). Any data gaps were filled following the AgMIP-O3 gap filling protocol (see S4). For large [O_3] data gaps (i.e., greater than 2 weeks) occurring outside the [O_3] fumigation period, we used scaled WFRChem (version 4.2) data for Xiaoji (Conibear et al., 2018) to ensure consistency in model calibration and potential applications across China. The dataset provides grain yield components, including the number of ears per square meter, the number of grains per ear, and the grain dry matter ($Grain\ DM$, in g/-m^{-22}) (Feng et al., 2011; 2016). Additional physiological datasets (i.e., A_{net} *Anet*, V_{cmax} *Vcmax*25, J_{max} *Jmax*25, and g_{H2O} *gH20* (further, converted to g_{O3} *gO3* in this paper to match the model outputas described in S1b)) are also provided, but only for the year 2008 for all cultivars (Y2, Y19, Y15, and Y16) and for the flag leaf. The 2008 data also include measurements of the Chlororophyll (in mg m^{-2}) which can be used to assess the level of senescence experienced by the leaf (Mariën et al., (2019). Since the year 2008 also showed significant differences in $Grain\ DM$*Yield*$_{grain}$ between AA and E O_3 treatments (a mean relative yield difference of 6.73 for all cultivars, see Table S3b) Therefore, thethis year 2008 was used to train the DO_3SE-crop model whereaswith other years (i.e., 2007 and 2009) are used to test the model.

Further experimental details are provided in Feng et al. (2011, 2016). Table 1 describes the average, minimum and maximum values for all measured variables required to run the DO_3SE-Crop model collected at the Xiaoji site for each year. Additionally, the M7 (mean 7-hour O_3 concentration over the exposure period in ppb) is included for both AA and E O_3 treatments. Measurements were taken at a height of 2 metres above the ground surface.

Further experimental details are provided in Feng et al. (2011, 2016). .

~~Additional physiological datasets (i.e., A_net, V_cmax, J_max, and g_O3) are also provided but only for the year 2008 for all cultivars (Y2, Y19, Y15, and Y16) for the flag leaf, which were used to parameterize the DO3SE-crop model's simulations of these variables. The 2008 data also include measurements of Chlorophyll Content Index (CCI), which can be used to assess the level of senescence experienced by the leaf (Mariën et al., 2019).~~

~~The DO3SE-crop model was used to analyse the O3-FACE (Free Air Concentration Enrichment) experimental data collected in Xiaoji, Jiangdu, Jiangsu Province, China. This dataset includes four modern cultivars of winter wheat (Triticum aestivum L.) grown under ambient and elevated [O3] with the elevated treatment being, on average, 25% above the ambient [O3] of 45.7 ppb for the period early March/April to end of May each year. Pants were grown in fully open-air field conditions for three consecutive growing seasons over 2007 to 2009. Table 1 describes the~~ average, minimum, and maximum values for all measured variables required to run the DO_3SE-Crop model ~~collected at the Xiaoji site for each year.~~ Additionally, the M7 ~~(mean 7-hour O_3 concentration over the exposure period in ppb)~~ value for ozone concentration during the exposure period is included ~~for both ambient (AA) and elevated (E) O_3 treatments. Measurements were taken at a height of 2 meteress above the ground surface and at an atmospheric pressure of 101 kPa. hourly meteorological and [O_3] data that are required to run the DO_3SE-Crop modelmodel, and which are provided at the Xiaoji site.~~

Table 1. Summary of ~~H~~hourly ~~M~~meteorological and ~~O~~ozone ~~C~~concentration ([O_3]) ~~D~~data at Xiaoji.

~~This table provides average, minimum, and maximum values for all measured variables required to run the DO3SE-Crop model. Additionally, the M7 value for ozone concentration during the exposure period is included. Measurements were taken at a height of 2 meters and at atmospheric pressure of 101 kPa.~~

Variable	Unit	Description	Year 2007 (~~M~~min~~;~~, ~~A~~avg~~;~~, ~~M~~max)	Year 2008 (~~m~~M~~in;~~, ~~A~~avg~~;~~, ~~M~~max)	Year 2009 (~~M~~min~~;~~ ~~A~~avg~~;~~, m~~M~~ax)
PAR_{total}	W/m^2	Direct and diffuse PAR at the top of the canopy	0~;~, 241.94~;~, 1759	0~;~, 265.15, ~;~1810.48	0~;~, 262.16~;~, 1850.5
T_{air}	°C	Surface air temperature in degrees Celsius	-6.35~;~, 10.07~;~, 34.10	-9.22~;~, 8.24~;~, 32.7	-9.17~;~, 9.62~;~, 33.64
VPD	kPa	Leaf to air vapour pressure deficit	0~;~, 0.34~;~, 3.77	0~;~, 0.3~;~, 3.5	0~;~, 0.38~;~, 3.8
u_z	m/s	Wind speed at a reference height z	0.03~;~, 2.14~;~, 8.19	0.07~;~, 2.11, 8.83	0.05~;~, 2.10~;~ 8.45
~~pa~~	~~Pa~~	~~Surface air pressure~~			
~~$CO3_z$~~ (~~and~~ M7 value) for AA O_3 treatment~~value~~	~~m/s~~ppb	Ozone concentration at a	0~;~, 15.48~;~, 129.95 (47.2)	0~;~, 16.2~;~, 137.07 (49)	0~;~, 15.9~;~, 102.02 (47)

~~during O_3 exposure period)~~		reference height z~~(C_z)z~~			
C_z (and M7 value) for E O_3 treatment~~value during O_3 exposure period)~~	ppb	Ozone concentration at a reference height z~~(C_z)Ozone concentration at a reference height z~~	0~~;~~, 16.83~~;~~, 176.73 (56.1)	0~~;~~, 17.46~~;~~, 171.19 (60.7)	0~~;~~, 17.95~~;~~, 153.40 (58.7)
O_3 exposure period	Days		38	92	92

~~The water availability is sufficient for the wheat crop so we assume there was no soil moisture stress (Feng *et al.*, 2012). Any data gaps were filled following the AgMIP-O_3 gap filling protocol (see S4). For large [O_3] data gaps (i.e. greater than 2 weeks) which occur outside the [O_3] fumigation period we use scaled WRFChem (version 4.2) data for Xiaoji (Conibear et al., 2018a) to ensure consistency in model calibration and potential applications across China. The four cultivars were Yannong 19 (strong-gluten wheat, hereafter Y19), Yangmai 16 (medium-gluten wheat, hereafter Y16), Yangmai 15 (weak-gluten wheat, hereafter Y15) and Yangfumai 2 (weak-gluten wheat, hereafter Y2). The dataset provides measurements of key physiological variables for the Y2 and Y16 cultivars (i.e. A_{net}, V_{cmax}, J_{max} and g_{O3}) for the flag leaf which were used to evaluate the DO_3SE-Crop model's simulations of these variables.~~

~~Additional data also provide measurements of chlorophyll content Index (CCI), which can be used to assess the level of senescence experienced by the leaf (Mariën *et al.*, 2019).The dataset also provides grain yield components, including the number of ears per square meter, the number of grains per ear and the grain dry matter ($Grain\ DM$) (the latter in g m^{-2}) (Feng *et al.*, 2011, 2016). Further experimental details are provided in (Feng *et al.*, 2011, 2016).~~

2.2 DO_3SE-Crop calibration and evaluation

Development and calibration of the DO_3SE-Crop model with the ~~The~~ Xiaoji experimental data set ~~analysis~~ followed three main steps: i). sensitivity analysis to identify key model parameters to calibrate~~,~~; ii). calibration of these key parameters for a single year and both tolerant and sensitive cultivars~~, ~~;and iii). evaluation of key DO_3SE-Crop model outputs for different years and cultivars from those used in model calibration.

~~Initially, a~~To perform the sensitivity analysis we used ~~,~~the SaLIB python library ~~SaLIB was used~~ (Iwanga et al., 2022, , Herman and Usher, 2017). The analysis requires ranges to be specified for the parameters (identified by an initial manual calibration) that are included ~~involved~~ in the sensitivity analysis. For physiological parameters, ~~these~~ranges were determined by considering the range of these parameters in the literature. For carbon allocation parameters, the range was identified by considering the maximum and minimum values of these parameters that would result in realistic plant response. Once the ranges ~~within which to vary the parameters was~~were identified, the sensitivity analysis was run using the extended fourier amplitude sensitivity analysis, which has been commonly used by other crop modellers to improve their calibrations (Silvestro et al., 2017, Vazquez-Cruz et al., 2014) . From the sensitivity analysis outputs, the parameters whose variation contributes the most to variations in selected modelling outputs (in this case

photosynthetic rate and yield) ~~are~~were identified as the key model outputs for calibration. Using this method ~~W~~we ~~Thewas conducted following the approach of Iwanaga et al. (2022) which was [....] and~~ identified the following DO_3SE-crop parameters as those most important to calibrate: (i) leaf photosynthesis parameters (V_{cmax25}, J_{max25}, kN, m, and VPD_0); (ii) C allocation parameters (α_{root}, α_{leaf}, α_{stem}, ~~Υ~~ ~~λ~~, τ ~~θ~~) and related dark respiration coefficients (R_{dcoeff} and R_{gcoeff}), and (iii) O_3 damage module parameters related to senescence (γ_3, γ_4 and γ_5). Phenology parameters were excluded from this sensitivity analysis as earlier studies have shown these are relatively straightforward to calibrate using automated methods for a range of environmental conditions (Nguyen et al., 2024). We note that assessing the probability distribution of these ranges would also be useful but consider this outside the scope of the current paper due largely to data limitations.

The DO_3SE-Crop model was then calibrated using the 2008 dataset for the Y2 and Y16 cultivars. The year 2008 was selected since this showed a substantial difference in yield of 208 and 148 g/m2 between the AA and EO_3 treatments for the Y2 and Y16 cultivars respectively. These cultivars were chosen since they were identified as the most sensitive (Y2) and tolerant (Y16) cultivars according to the experimental analysis conducted by Feng et al. (2016).

~~The DO_3SE-Crop model was then calibrated using the 2008 dataset for the Y2 and Y16 cultivars. The year 2008 was selected since this showed a substantial difference in yield of 208x and 148y g/m2 between the ambient and elevated O_3 treatments for the Y2 and Y16 cultivars respectively. These cultivars were chosen since they were identified as the most sensitive (Y2) and tolerant (Y16) cultivars according to the experimental analysis conducted by Feng et al. (2016).~~

Calibration of the phenology module used only the Y2 cultivar data describing the timing of emergence, anthesis and maturity to calibrate key phenology parameters (T_b, T_0, T_m, VT_{min}, VT_{max}, PIV, and PID, TT_{emr}, TT_{veg} and TT_{rep}). Phenology data are only provided for the AA O_3 treatment. The phenology calibration was automated by computationally applying a genetic algorithm (Wang, 1997), an optimisation technique with gradient decent to find the best parameters. This uses a combination of crossover strategy (selecting parameters randomly from parameter pairings) and mutation strategy (which takes a parameter range and uses incremental step changes) to identify the parameters which give the highest R^2 and lowest root mean square error (RMSE) when compared with observations of the timing (day of year) of emergence, anthesis and maturity.

~~Calibration of the phenology module used Y2 cultivar data describing the timing of emergence, anthesis and maturity to calibrate key phenology parameters (T_b, T_0, T_m, VT_{min}, VT_{max}, PIV, and PID, TT_{emr}, TT_{veg} and TT_{rep}. The phenology calibration was automated by computationally applying a genetic algorithm (Wang, 1997), an optimisation technique with gradient decent to find the best parameters. This uses a combination of crossover strategy (selecting parameters randomly from parameter pairings) and mutation strategy (which takes a parameter range and uses incremental step changes) to identify the parameters which give the highest R^2 and lowest root mean square error (RMSE) when compared with observations of the timing (day of year) of emergence, anthesis and maturity.~~

Calibration of the leaf physiology, canopy C allocation and O_3 damage DO_3SE-Crop modules was performed manually. This required that an initial value and range be defined for each parameter. which were defined from a combination of observations from the Xiaoji experimental dataset as well as values taken from the literature (see Appendix Tables A1 and A2 for details). The model was manually calibrated until certain conditions were satisfied, as explained below.

Calibration of the leaf physiology parameters (V_{cmax}, J_{max}, kN, m, and VPD_0) was performed whilst keeping all other parameters fixed. This calibration aimed to achieve a maximum A_{net} value of 30

µmol CO_2 m^{-2} s^{-1} and a g_{O3} value of 350 mmol O_3 m^{-2}PLA s^{-1}, consistent with the maximum values observed in the Xiaoji dataset (Zhu et al., 2011). We calibrated V_{cmax} and J_{max} as measurements are only provided for Y2 and Y16 cultivars and only for certain points during the growth period and we know that V_{cmax} and J_{max} can vary seasonally.

Calibration of the C allocation parameters (α_{root}, α_{leaf}, α_{stem}, Υ, τ and related dark respiration coefficients (R_{dcoeff} and R_{gcoeff}), was also performed keeping all other parameters fixed. This calibration aimed to achieve the following criteria:- a stem dry matter to leaf dry matter ratio (R_{SL}) of approximately 2:1 (Huang et al., 2022); relative growth of different plant parts (i.e. leaves, stem, roots, grain) consistent with profiles found in the literature (Osborne et al., 2015; de Vries et al., 1989); a modelled $Grain\ DM$ within ± 30% of the observed; an $above\ ground\ DM$ value of between 1200-1600 g m^{-2}; an LAI value between 4-7 m^2 m^{-2}; and an R_d value of between 30 to 60% of A_{net} (Amthor et al., 2019). We calibrated C allocation parameters as in the JULES-crop model calibration has only been performed for broad, global scale application for wheat (Osborne et al., 2016) and therefore requires further calibration for application under Chinese conditions. Further, the observed dataset does not provide any information with regards to the change in carbon allocation parameters due to ozone. The C allocation parameters were only calibrated for ambient ozone conditions, and we only investigate the effect of ozone on C assimilation (not C allocation).

Finally, calibration of the O_3 parameters (γ_3, γ_4 and γ_5) was performed using 2008 data for both the Y2 and Y16 cultivars whilst again keeping the other parameters fixed. Calibration was targeted so that the difference in $Grain\ DM$ between ambient and elevated O_3 treatments as close as possible to ± 10% of the observed.

Evaluation of the DO_3SE-Crop model was conducted using Xiaoji data for 2007 and 2009 for all cultivars, and 2008 data for Y19 and Y16 cultivars. This evaluation tested the ability of the calibrated DO_3SE-Crop model to simulate $Grain\ DM$ using R^2 and RMSE statistical tests.

~~Calibration of the manual (for leaf physiology, canopy C allocation and O_3 damage DO_3SE-Crop modules was performed manually. This required that an initial value and range be defined for each parameter.) calibration methods. Both methods require defining an initial parameter value and a realistic range over which the parameter value may vary. These parameter values arewhich were defined from a combination of observations from the Xiaoji experimental dataset as well as values taken from the literature (see supplementary Tables S4 and S5–2 for details). The model iswas manually calibrated until certain conditions were satisfied, as explained below.~~

~~Firstly, we cCalibrationed of the leaf physiology parameters (V_{cmax25}, J_{max25}, kN, m, and VPD_0) was performed whilest keeping theall other parameters fixed. This step calibration aimed to achieve a maximum Anet A_{net} value of 30 µmol CO_2 m^{-2} s^{-1} and a g_{O3} g_{O3} value of 350 mmol O_3 m^{-2}PLA s^{-1}, consistent with the maximum values observed in the Xiaoji dataset (Zhu et al., 2011). We calibrated V_{cmax25} and J_{max25} as measurements are only provided for Y2 and Y16 cultiuvars and only for certain points during the growth period and we know that Vcmax and Jmax can vary seasonally.~~

~~Secondly, we cCalibrationed of the C allocation parameters (α_{root}, α_{leaf}, α_{stem}, Υ, τ λ, θ and related dark respiration coefficients (R_{dcoeff} and R_{gcoeff}), was also , again performed keeping all other parameters fixed. Theis calibration aimed to achieve the following criteria:- included: a stem dry matter to leaf dry matter ratio (R_{SL}) of approximately 2:1 (Huang et al., 2022); relative growth of different plant parts (i.e. leaves, stem, roots, grain) consistent with profiles found in the literature (Osborne et al., 2015; de Vries et al., 1989); a high R2 value (above 0.70) when a modelled grain DM $Grain\ DM$ is plotted against within ± 30% of the observed grain DM; an $above\ -\ ground\ DM$~~

values of between 1200-1600 g m^{-2}; an LAI value between 4-7 m^2 m^{-2}; and an R_d R_d beingvalue of between 30 to 60% of A_{net} the assimilated A_net (Amthor et al., 2019).

Finally, we calibratedcalibration of the O_3 parameters (γ_3, γ_4 and γ_5), was performed using 2008 data for both the Y2 and Y16 cultivars whilst again keepingkeeping the other parameters fixed. Calibration was targeted so that the difference in $Grain\ DM$ $Yield_{grain}$ between ambient and elevated O_3 treatments as close as possible to was within ± 10% of the observed. . The best-calibrated parameters were those that resulted in an R^2 value above 0.90 when the modeled grain yield difference was compared against the observed grain yield difference for ambient versus elevated O_3 treatments.

Evaluation of the DO$_3$SE-Crop model was conducted using Xiaoji data for 2007 and 2009 for all cultivars, and 2008 data for Y19 and Y16 cultivars. This evaluation tested the ability of the calibrated DO$_3$SE-Crop model to simulate $Grain\ DM$ and $Yield_{grain}$ using R^2 and RMSE statistical tests. to assess the capability of the model to simulate observations.

The Xiaoji experimental data were split into calibration (year 2008, Y2 and Y16 cultivars) and evaluation (year 2007 & 2009, Y15 & Y19 cultivars). The calibration of DO$_3$SE-Crop has two main steps, firstly, to calibrate for crop development and growth (i.e. phenology and C allocation). This calibration was performed using the Y2 cultivar. Secondly, the calibration of the O_3 damage module, this was calibrated for using the Y2 cultivar (representing a sensitive cultivar and Y16 (representing a tolerant cultivar), these cultivar sensitivities followed information provided in (Feng *et al.*, 2016).

Phenology cCalibration

Calibration of the DO$_3$SE-Crop model used a combination of automated (for phenology) and manual (for leaf physiology, canopy C allocation and O_3 damage) calibration methods. Both methods require defining an initial parameter value and a realistic range over which the parameter value may vary. These parameter values are defined from a combination of observations from the Xiaoji experimental dataset as well as values taken from the literature (see supplementary Table 2 for details). The model is calibrated until certain conditions were satisfied, as explained below.

Calibration of the phenology module used the Xiaoji 2008 dataset for the Y2 cultivar. These data were used to determine the key phenological stages (emergence, anthesis and maturity). For this the thermal life span of the canopy from sowing to maturity (TT_{leaf}) and calibrate key phenology parameters (T_b, T_0, T_m, VT_{min}, VT_{max}, PIV, and PID, emergence td, flag leaf emergence td, $A_{start\ td}$, tl_{ep} and tl_{se})harvest td) were calibrated. The phenology calibration was automated by computationally applying a genetic algorithm (Wang, 1997), an optimisation technique with gradient decent to find the best parameters. This uses a combination of crossover strategy (selecting parameters randomly from parameter pairings) and mutation strategy (which takes a parameter range and uses incremental step changes) to identify the parameters which give the highest R^2 and lowest RMSE when compared with observations of the timing (day of year) of emergence, anthesis and maturity. The calibrated phenology parameters were tested for the other years (i.e. 2007 and 2009, including all the cultivars; 2008, Y19 and Y16 cultivars) to assess their ability to represent crop development between years.**Leaf physiology, carbon allocation and O3 damage module sensitivity analysis and calibration**

First, we conducted a sensitivity analysis to identify the leaf physiology, carbon (C) allocation, and ozone (O_3) damage module parameters that were most important to calibrate (Iwanaga et al., 2022). The analysis pinpointed the following DO3SE-crop parameters for calibration: (i) leaf photosynthesis parameters (V_cmax, J_max, kN, m, and VPDo), (ii) C allocation parameters (a_root, a_leaf, a_stem, λ, θ), (iii) dark respiration coefficients (R_dcoeff and R_gcoeff), and (iv) O3 damage module parameters related to senescence (γ3, γ4, and γ5). Calibration was performed manually in steps to find the optimal parameters.

Firstly, we calibrated the leaf physiology parameters while keeping the other parameters fixed. This step aimed to achieve a maximum Anet value of 30 µmol CO_2 m^{-2} s^{-1} and a g_{O3} value of 350 mmol O_3 m^{-2} s^{-1}, consistent with the maximum values observed in the Xiaoji dataset (Zhu et al., 2011).

Secondly, we calibrated the C allocation parameters, again keeping other parameters fixed. The calibration criteria included: a stem dry matter to leaf dry matter ratio of approximately 2:1 (Huang et al., 2022); relative growth of different plant parts consistent with profiles found in the literature (Osborne et al., 2015; de Vries et al., 1989); a high R2 value (above 0.70) when modelled grain DM is plotted against observed grain DM; above-ground DM values between 1200-1600 g m-2; an LAI between 4-7 m2 m-2; and R_d being 30 to 60% of the assimilated A_net (Amthor et al., 2019).

Finally, we calibrated the O_3 parameters, keeping the other parameters fixed. The best-calibrated parameters were those that resulted in an R^2 value above 0.90 when the modeled grain yield difference was compared against the observed grain yield difference for ambient versus elevated O_3 treatments.

We applied a sensitivity analysis to identify the leaf physiology, C allocation and O_3 damage module parameters that were most important to calibrate (Iwanaga et al., 2022). The sensitivity analysis identified the following DO3SE-crop parameters for calibration: i). leaf photosynthesis parameters (V_{cmax}, J_{max}, kN, m and $VPDo$; ii). C allocation parameters (a_{root}, a_{leaf}, a_{stem}, λ,θ); iii). dark respiration coefficients (R_{dcoeff} and R_{gcoeff}), and iv). O_3 damage module parameters related to senescence ($\gamma 3$, $\gamma 4$ and $\gamma 5$). Calibration for these parameters was performed manually and in steps; firstly, the best parameters are found for leaf photosynthesis i.e. parameters which give a maximum A_{net} value of 30 µmol CO_2 m^{-2} s^{-1} and g_{O3} value of 350 mmol O_3 m^{-2} s^{-1} (consistent with maximum values observed in the Xiaoji dataset, Xhu et al., 2011) . Secondly, calibration is then performed for the C allocation parameters, identifying the best parameters which meet each of the following criteria: a stem dry matter: leaf dry matter ratio of approx. 2:1 (after (Huang *et al.*, 2022)); relative growth of different plant parts which are consistent with growth profiles found in the literature ((Osborne *et al.*, 2015)and de Vries et al., 1989); an R^2 value of above 0.90 when modelled $Grain\ DM$ is plotted against observed $Grain\ DM$; $Above\ ground\ DM$ values are between 1200-1600 g m^{-2}; a LAI of between 4-7 m^2 m^{-2} and R_d is 30 to 60% of the assimilated A_{net} (Amthor *et al.*, 2019). Finally, the model is then calibrated for the O_3 parameters, while other parameters remain fixed, the best calibrated parameters are those that give an R^2 value of above 0.90 when modelled $Yield_{grain}$ difference was compared against observed $Yield_{grain}$ difference for ambient versus elevated O_3 treatments.

Full details and description of the DO3SE-crop parameters for wheat and their associated ranges are given in Table S43, S54 and S65.

Validation - Phenology calibration, Leaf physiology, carbon allocation and O3 damage module

The calibrated phenology, leaf physiology, carbon allocation, and O3 damage module parameters were validated/tested for other years in the Xiaoji dataset (i.e., 2007 and 2009 for all cultivars, and

2008 for Y19 and Y16 cultivars) to assess their ability to simulate grain dry matter. A comparison between the modelled test dataset and the observed dataset is presented in Fig. 8.

The calibrated phenology parameters were tested for the other years (i.e. 2007 and 2009, including all the cultivars; 2008, Y19 and Y16 cultivars) to assess their ability to represent crop development between years.

Results

We first examine the model's ability to simulate the key phenological development stages since this is key to simulating the variation in C allocation to different plant parts over the course of the growing season and hence how O_3 exposure will influence growth and yield which is determined by the timing and length of the grain filling period. We also explore how DO_3SE-Crop simulates within canopy [O_3] profiles to understand which layers of the canopy are most important in determining O_3 response. We then examine the ability of the model to simulate leaf-level physiology and C allocation to the different parts of the crop. Lastly, the impact of both instantaneous and long-term O_3 damage on the crop's final $Grain\ DM$ is evaluated for different cultivars and years.

We first examine the model's ability to simulate the key phenological development stages since this is key to simulating the variation in C allocation over the course of the growing season and hence how O_3 exposure will influence growth and yield which is determined by the timing and length of the grain filling period. We also explore how DO_3SE-Crop simulates within canopy [O_3] profiles to understand which layers of the canopy are most important in determining O_3 response. We then examine the ability of the model to simulate leaf-level physiology and C allocation to the different parts of the crop. Lastly, the impact of both instantaneous and long-term O_3 damage on the crop's final grain yield is evaluated.

i) Crop Phenology

The Xiaoji dataset provides sowing and harvest dates for all cultivars for each year but only provides the date of the timing of anthesis for the years 2008 and 2009 for all cultivars. We assume that DVI = 1 is equivalent to the start of anthesis and that this occurs 4-5 days after flag leaf emergence as shown in Fig. 2. We determine the influence of O_3 on the start and end of senescence (SOS and EOS) using the breakpoint method (described in Pande et al., 2024) to assess significant changes in the chlorophyll values that indicate senescence onset and rate of change for the quantification of tl_{ep} and tl_{se}. This method is applied for chlorophyll data collected in 2008 under both AA and E O_3 treatments for the Y2 cultivar. We then assume that these key phenology parameters (i.e., TT_{emr}, TT_{veg}, TT_{rep}, tl_{ep} and tl_{se}) are consistent across cultivars and years. Our results in Fig 3 suggests this is a reasonable assumption however, we appreciate that assuming these phenology parameters will work for a wider variety of cultivar types (e.g., early or late sown and/or maturing) and years with rather different meteorological conditions, needs to be done with caution.

Fig S1 shows the modelled vs observed timing of anthesis and harvest for the training dataset. Fig 3 shows the same for the test dataset. For the test dataset there is a variation of 2 to 4 days and 1 to 6 days for the modelled anthesis and maturity in relation to observed anthesis and maturity respectively, with observed phenology tending to be a little later than modelled. The T_l ranges between 1325 and 1478 °C days for the three years, with crop sowing occurring between 315 and 324 days of year and harvests occurring between 135 and 151 day of year (of the following year). The number of days from the modelled crop sowing to harvest was between 181 and 191 for the three years, compared to 198 and 201 for the observations.

The Xiaoji dataset provides sowing and harvest dates for all cultivars for each year but only provides , however the date of the timing of anthesis is only provided for the year. However, the date of the timing of anthesis is only provided for the years 2008 and 2009 for all the cultivars. We assume that DVI = 1 is equivalent to the start of anthesis (and happens and that this occurs 4-5 days after the flag leaf emergence of the flag leaf) as shown in Fig. 2. We determine the influence of O_3 on the start and end of senescence (SOS and EOS) using the breakpoint method (described in Pande et al., 2024) to assess significant changes in the CCIchlorophyll values that indicate senescence onset and rate of change for the quantification of tl_{ep} and tl_{se}. This method is applied for CCIchlorophyll data collected in 2008 under both AA and E O_3 treatments for the Y2 cultivar. The year 2008, Ambient and elevated dataset is used to determine the start and the end of senescence (SOS and EOS) model is calibrated using the 2008 Y2 data to provide the thermal times for TT_{veg} and TT_{rep} day of the year and the relative uses the CCI data and the associated breakpoint method is used to determine the SOS and the polynomial regression is used to determine the end of senescence (not shown) (Pande et al., 2024) to estimate tl_{ep} and tl_{se}. We then assume that these key phenology parameters (i.e. TT_{emr}, TT_{veg}, TT_{rep}, tl_{ep} and tl_{se}) values are consistent across cultivars and years. Figure 3 suggests this is a reasonable assumption since the phenology module captures the timing of anthesis and maturity for unseen cultivars and years within 2 to 4 days and 1 to 6 days respectively, of the observed timings. However, we appreciate that assuming these phenology parameters will work for a wider variety of cultivar types (e.g. early or late sown and/or maturing) and years with rather different meteorological conditions, needs to be done with caution.

Figure S1 shows the timing of crop emergence, anthesis and harvest in relation to simulated anthesis (i.e. at DVI=1) for the training dataset. Figure 3 shows the timing of anthesis and harvest for the test dataset. ThereThere is a variation of 24 to 410 days and 1-6 days for the modelled anthesis and maturity in in relation to days from crop emergence between yearsobserved anthesis and maturity respectively. The T_t ranges between 1325 and 1478 °C days for the three years with crop emergence occurring between day of year 37-45 and harvest occurring between day of year, with crop sowing occurring between the days of years 315 and 324 and harvests occurring between the days of the years 135-151. The number of days from the modelled crop emergence to harvest was between 100 and 104 for the three years.

Fig. 3 Modelled *vs* observed phenological stages provided as day of year (DOY) for the test dataset (i.e., excluding the year 2008 for the Y2 cultivar).

Fig.3 The Chinese dataset used to plot modelled phenological stages against experimental dataset for the testing set.

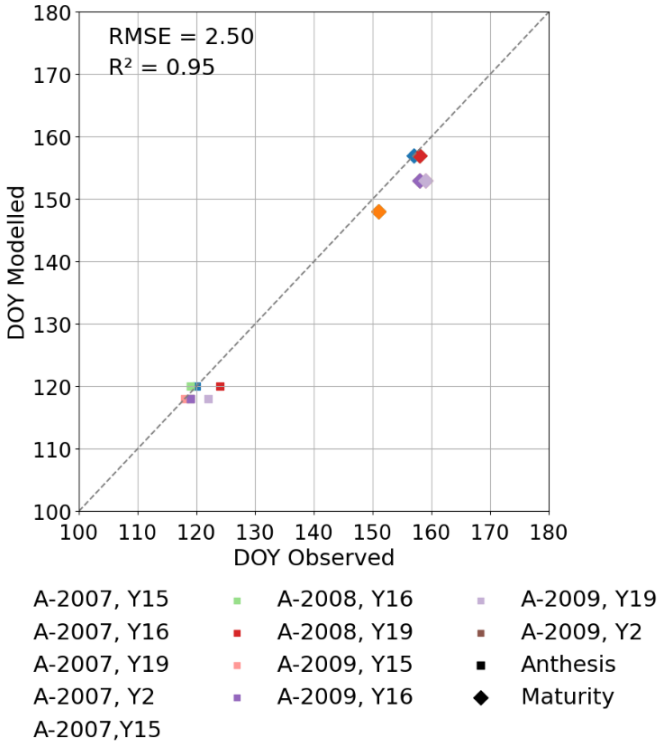

960

961 ~~ii) Within canopy stomatal O_3 profile~~

962 ~~An important determinant of O_3 deposition and damage is stomatal O_3 deposition (or stomatal O_3~~
963 ~~uptake) which is a function of within canopy transfer of O_3 and stomatal and non-stomatal~~
964 ~~deposition. The multi-layer aspect of the DO_3SE-Crop model allows within canopy stomatal and non-~~
965 ~~stomatal O_3 deposition to be simulated. Figure 3 shows the variation in key variables that determine~~
966 ~~total and stomatal O_3 canopy deposition across 4 canopy layers as a mid-day average over the~~
967 ~~course of the tl_{ep} period of the flag leaf, for the year 2008 and the Y2 cultivar.~~

968 ~~Figure 3. Plot showing variation in key O_3 deposition terms as daily maxima by canopy layer (N.B. $i =$~~
969 ~~1 is the top canopy layer, $n = 4$) a). $[O_3]$, b). $rb_{,O3}$, c). PAR_{sun} and d). g_{O3} for the duration of the~~
970 ~~flag leaf period for the Y2 cultivar E-O_3 treatment in 2008.~~

971 ~~a). b).~~

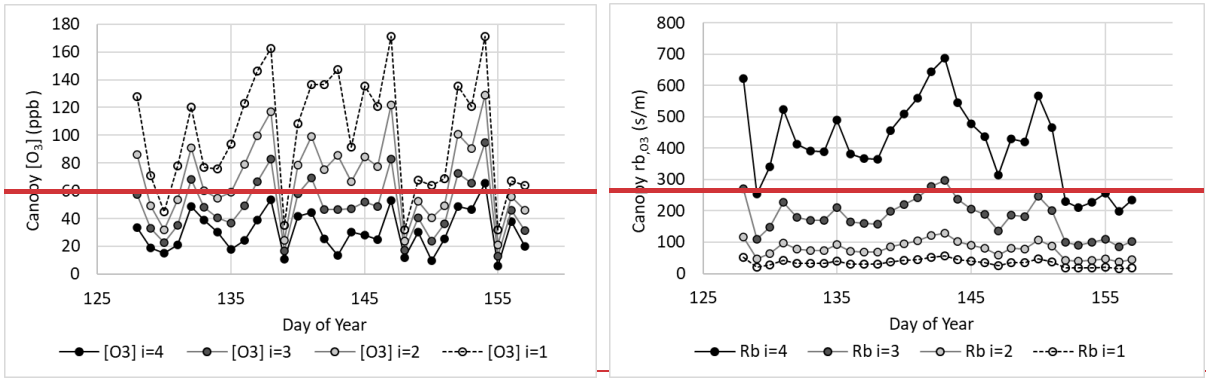

972

973

974 ~~c). d).~~

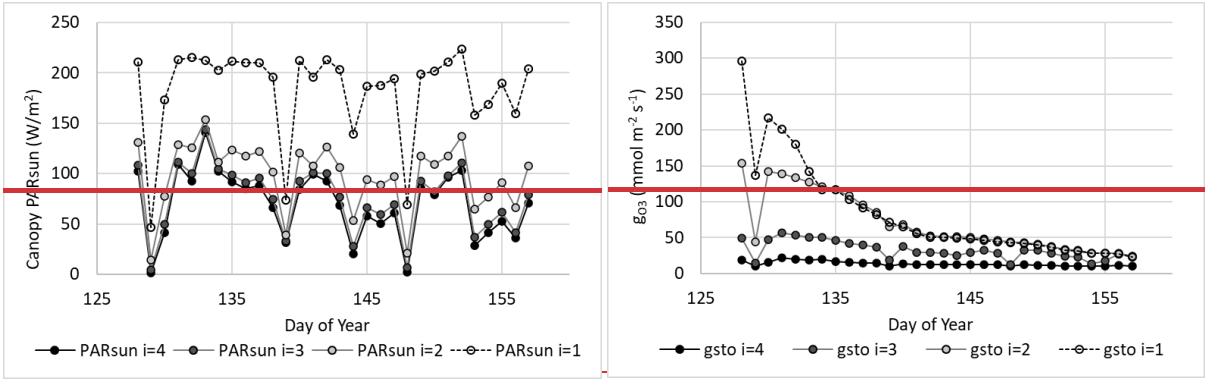

~~Figure 3a. shows a decrease of within canopy [O_3] from highs of around 140ppb to values within the range of 10 to 50 ppb between the topmost and bottom canopy layer. Similarly, PAR_{sun} reduces from maximum values of around 200 W m^{-2} to values of around 100 W m^{-2} on sunny days (see Fig. 3b). The leaf rb_{O3} (Fig. 3c) also increases with canopy depth from resistances in the region of approximately 100 s m^{-1}; and g_{O3} (Fig. 3d) similarly reduces from around 300 to 20 nmol O_3 m^{-2} s^{-1} between canopy layers, these differences reduce with the onset of senescence.~~

ii.a) Leaf physiology variables (A_{net}, g_{O3})

The DO_3SE-Crop model was able to simulate the seasonal A_{net} and g_{O3} with values ranging from 0 to 27 µmol CO_2 m^{-2} s^{-1} and 10 to 351 mmol O_3 m^{-2} s^{-1} for A_{net} and g_{O3} respectively over the course of the growing season (see Fig 4). The simulated daily maximum values of modelled g_{O3}, of 351 mmol O_3 m^{-2} s^{-1} were in the range of the observed value of 340 mmol O_3 m^{-2} s^{-1}. Similarly, the modelled maximum A_{net} is 27 µmol CO_2 m^{-2} s^{-1} compared to observed value of 28 µmol CO_2 m^{-2} s^{-1} for the period between anthesis and 10 days before maturity for the year 2008, for the Y2 cultivar. In Fig. 4a and b, the steep decline in modelled A_{net} and g_{O3} is not seen in the observed dataset. This discrepancy may occur since the simulated A_{net} and g_{O3} values represent sunlit parts of the upper canopy which comprise both green and senesced leaf material. In contrast, observed A_{net} and g_{O3} values are measured specifically on the flag leaf and most likely for only the green parts of the leaf, , since the LI-6400 photosynthesis system mounted with a 6400–40 leaf chamber fluorometer (used to measure A_{net} and g_{O3} in the Xiaoji experiment, Feng et al., 2016) will not provide values for senesced leaf material. See also Figure 4 which combines A_{net} and g_{O3} with observed normalised chlorophyll content and clearly shows the leaf is senescing as predicted by the model. However, the decline in observed chlorophyll values aligns well with the decline in modelled A_{net} and g_{O3} with the timing of the earlier onset of senescence by 0-3 days between the AA and E O3 treatments being captured well by the model. It is useful to note that the calibrated V_{cmax} and J_{max} values match the observed values within ± 2 µmol $CO_2/m^2/s$.

~~The DO_3SE-Crop model was able to simulate the seasonal A_{net} and g_{O3} with values ranging from 0 and to 27 and 10 and to 35110 for A_{net} and g_{O3} respectively over the course of the growing season (see Fig.ure 4). The simulated daily maximum values of modelled g_{O3}, of 35110 mmol O_3 m^{-2} s^{-1} were in the range of the observed value of 340 mmol O_3 m^{-2} s^{-1}. Similarly, the modelled maximum A_{net} is 27 µmol CO_2 m^{-2} s^{-1} compared to observed value of 28 µmol CO_2 m^{-2} s^{-1} for the period between anthesis and 10 days before maturity for the year 2008, for both the Y2 and Y16 cultivar. In Figure. 4a and b,. Athe steep decline in modelled A_{net} and g_{O3} is seen as opposed to thenot seen in the observed dataset. This discrepancy may occurs since because the simulated A_{net} and g_{O3} values represent are for the sunlit parts of the upper canopy which comprise both green and senesced leaf material. In contrast, for the top layer (which also includes some leaves other than the flag leaf as the model divides layer into equal fraction), whereas the observed A_{net} and g_{O3} values are~~

~~measured specifically at the leaf level for on the flag leaf and most likely . In addition to these observed values are often taken only for only the the green parts of the leaf. However, the decline in observed chlorophyll values aligns well with the decline in modelled A_{net} and g_{O3}. It is useful to note that the calibrated V_{cmax} and J_{max} values match the observed values within ± 2z and y µmol $CO_2/m^2/s$. which could lead to error if A_{net} and g_{O3} are only provided for the green part of the leaf.~~

Fig 4. Comparison of daily maxima seasonal profiles of DO_3SE-Crop modelled canopy leaf vs observed flag leaf data for a). AA O_3 treatment A_{net}, and b). AA O_3 treatment g_{O3} and c) E O_3 treatment A_{net}, and d). E O_3 treatment g_{O3} for the period after anthesis for the year 2008 and the Y16 cultivar. The left (solid blue line) and right (solid red line) represent the segment fits to the relative chlorophyll content values for application of the breakpoint method to define the SOS (Start of Senescence) shown as the solid black dashed line. The black scatter solid dots, along with their standard measurement error, represent the relative observed chlorophyll content values (see Fig 7 for further details)~~Figure 4. DO_3SE-Crop modelled diurnal profile of a). A_{net} g_{O3}, and b). A_{net} for a fully expanded flag leaf prior to the start of senescence tl_{ep} for the AA and seasonal profile of daily maxima a). Ambient O_3 treatment A_{net}, and b). g_{O3} ; c) Elevated O_3 treatment A_{net}, and d). g_{O3} c). g_{O3}, and d). A_{net} for the flag leaf for the period between tl_{ep} and tl_{se} after anthesis (i.e. period between flowering and fully senescence leaf (maturity))for the AA treatments for the year 2008 and the ,Y2 cultivar. Black line showing shows the Sstart of ssenescence (SOs)The left (solid blue line) and right (solid red line) segment fits represent the relative chlorophyll values, with the predicted breakpoint (Start of Senescence, SOS) identified using a piecewise linear regression method and shown as a solid black dashed line. The black scatter solid dots, along with the standard error, represent the relative observed chlorophyll values.~~

a). b).

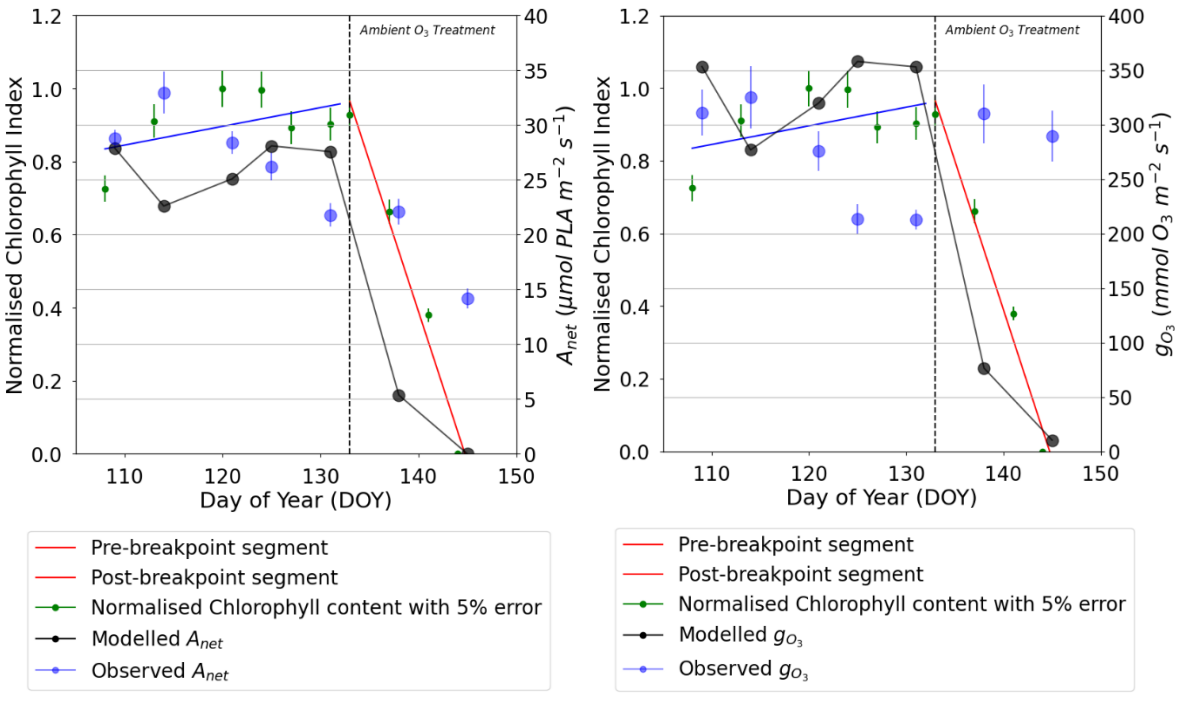

c). d).

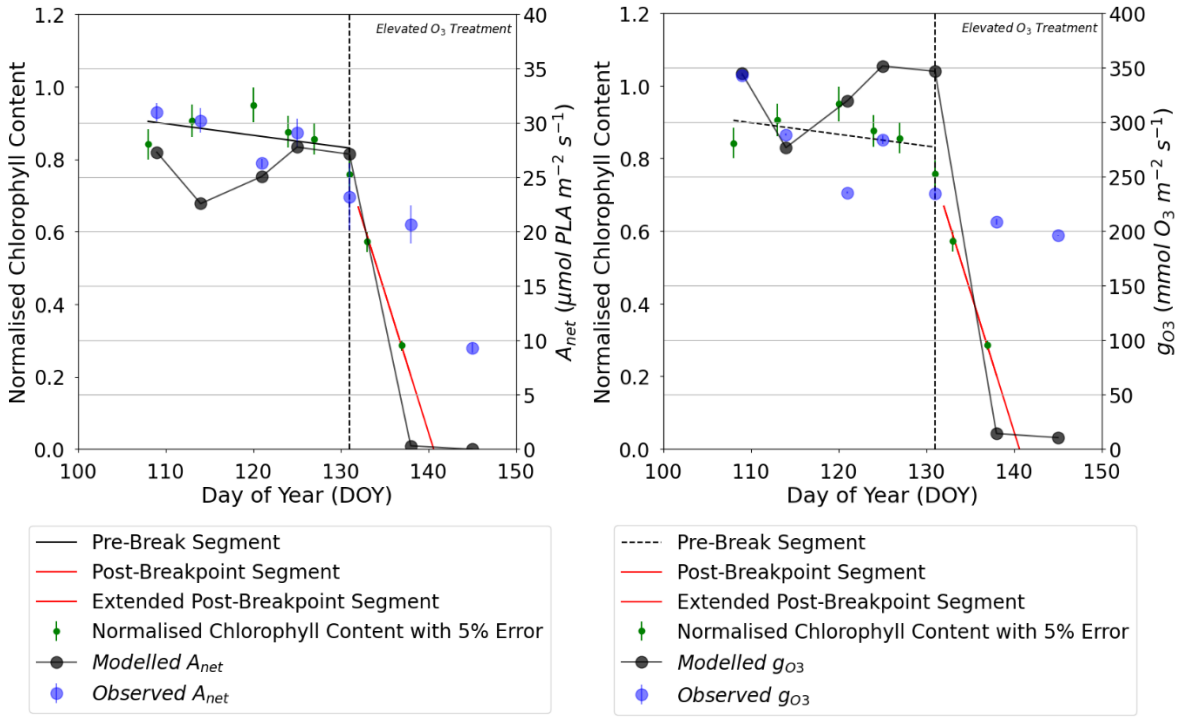

ii.b) Within canopy variation in O_3 and physiology

An important determinant of O_3 deposition and damage is stomatal O_3 deposition (our $gO3_c$) which is a function of within canopy transfer of O_3 and stomatal and non-stomatal deposition. The multi-layer aspect of the DO$_3$SE-Crop model allows within canopy stomatal and non-stomatal O_3 deposition to be simulated. Fig 5 shows the variation in key variables that determine total and stomatal O_3 canopy deposition across 4 canopy layers as a mid-day average over the course of the tl_{ep} period of the flag leaf, for the year 2008 and the Y16 cultivar.

Fig 5. Plot showing variation in key O_3 deposition terms as daily maxima by canopy layer (N.B. $i = 4$ is the top canopy layer, $n = 4$) a). O_3 concentration at the top of each layer, b). leaf boundary layer resistance by canopy layer ($rb_{,O3}$), c). PAR for the sunlit LAI component of each layer (PAR_{sun}) and d). leaf level stomatal conductance to O_3 (g_{O3}) for the period from anthesis (i.e., flowering to maturity) for the Y16 cultivar and for the E O_3 treatment in 2008.

~~Within canopy stomatal O_3 profile~~

~~An important determinant of O_3 deposition and damage is stomatal O_3 deposition (or stomatal O_3 uptake) which is a function of within canopy transfer of O_3 and stomatal and non-stomatal deposition. The multi-layer aspect of the DO$_3$SE-Crop model allows within canopy stomatal and non-stomatal O_3 deposition to be simulated. Figure 5 shows the variation in key variables that determine total and stomatal O_3 canopy deposition across 4 canopy layers as a mid-day average over the course of the tl_{ep} period of the flag leaf, for the year 2008 and the Y2 cultivar.~~

~~Figure 5. Plot showing variation in key O_3 deposition terms as daily maxima by canopy layer (N.B. $i = 14$ is the top canopy layer, $n = 4$) a). [O_3], b). $rb_{,O3,}$ c). PAR_{sun} and d). g_{O3} for the duration of the~~

~~flag leaf period from anthesis (i.e., flowering to end of senescence (maturity)) for the Y2 cultivar E-O_3 treatment in 2008.~~

a). b).

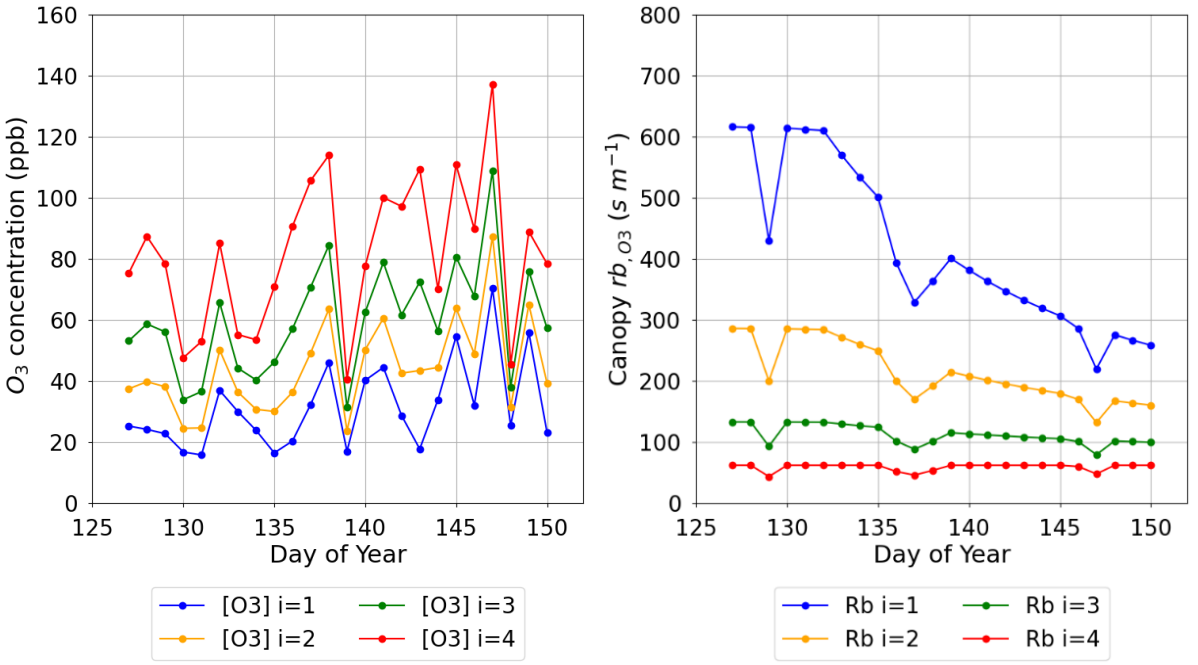

c). d).

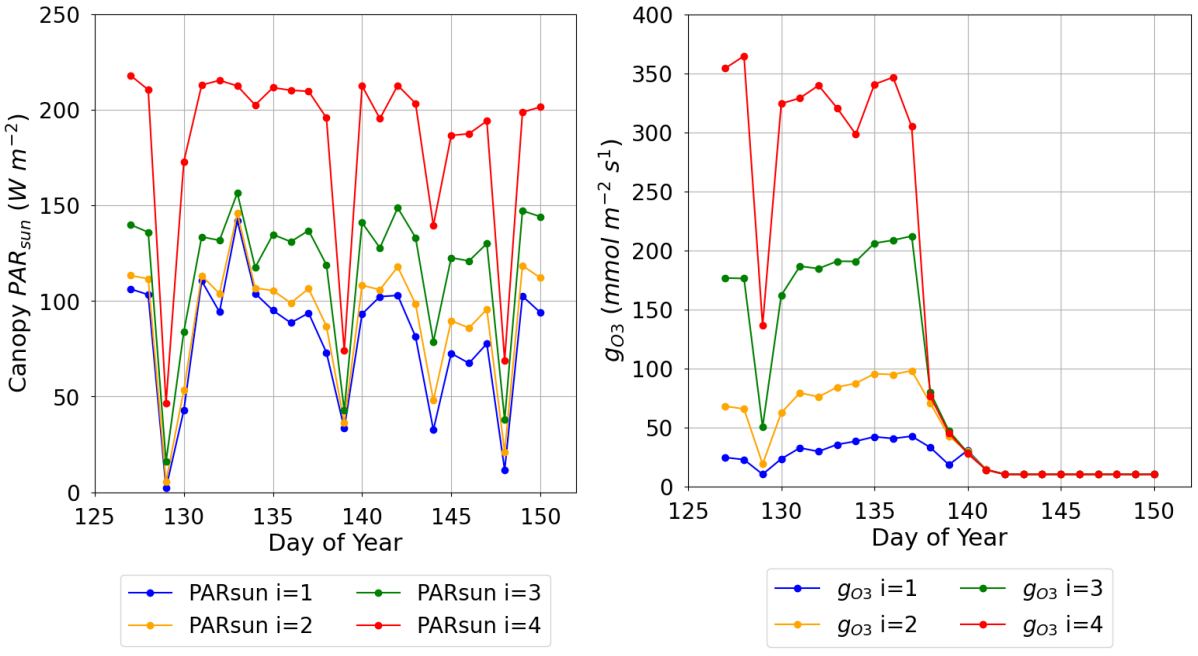

Figure 5a. shows a decrease of within canopy ~~[~~O_3 concentration ~~]~~from highs of around 140 ppb to values within the range of 10 to 50 ppb between the ~~topmost~~top of the canopy and bottom canopy layer, the penetration of O3 into the canopy increases over time as the canopy senescence and O_3 uptake is reduced. Similarly, PAR_{sun} reduces from maximum values of around 200 W m^{-2} at the top of the canopy to values of around 100 W m^{-2} in the lower canopy layers even on sunny days (see Fig.

5c). The leaf rb_{O3} (Fig. 5b) ~~also in~~increases with canopy depth ~~from~~with resistances in the region of approximately ~~100 s m^{-1};~~50 s m^{-1} at the top of the canopy to values of around 600 s m^{-1} at the bottom of the canopy, this will limit stomatal O3 uptake in the lower canopy layers, finally ~~and~~ these factors combine to influence canopy level g_{O3} (Fig. 5d) which ~~similarly~~ reduces from values of around 350 at the top of the canopy to ~~to~~ 20 nmol O_3 m^{-2} s^{-1} ~~between~~ at the bottom of the canopy layer~~s~~, these differences in leaf rb_{O3} and g_{O3} reduce with the onset of senescence. This analysis shows the importance of interplay between these different factors for an accurate whole canopy estimate of O_3 deposition.

~~Figure 5a. shows a decrease of within canopy [O_3] from highs of around 140 ppb to values within the range of 10 to 50 ppb between the topmosttop of the canopy and bottom canopy layer. Similarly, PAR_{sun} reduces from maximum values of around 200 W m^{-2} to values of around 100 W m^{-2} on sunny days (see Fig. 5c). The leaf rb_{O3} (Fig. 5b) also inincreases with canopy depth fromwith resistances in the region of approximately 100 s m^{-1};50 s m^{-1} at the top of the canopy to values of around 600 s m^{-1} at the bottom of the canopy and g_{O3} (Fig. 5d) similarly reduces from values of around 350 to 20 nmol O_3 m^{-2} s^{-1} between the top and bottom canopy layers, these differences in leaf rb_{O3} and g_{O3} reduce with the onset of senescence.~~

~~i)~~ iii) Crop development, biomass~~growth~~ and yield.

The dry matter dynamics of the different parts of the crop are shown in Fig. 6. The modelled $Grain\ DM$ value of 851 g m^{-2} was reasonably close to the observed value of 888 g m^{-2}. The stem to leaf dry matter ration (R_{SL}) is 2.1:1 and therefore in the range provided in the literature (Huang et *al.*, 2022). The above-ground biomass values of 1510 g m^{-2} also match reasonably well against the 1200 to 1600 g m^{-2} range described in the literature (Huang et al., 2022; Liu et al., 2022). Further, the partition fraction profiles are consistent with those of Osborne *et al.* (2015) as shown in Fig. 6a) with the main differences being that the modelled stem and root partition profiles are somewhat higher and lower, respectively.

~~The dry matter dynamics of the different parts of the crop are shown in Fig. 65. The modelled $Grain\ DM$ value of 843 g m^{-2} matched the observed value of 876 g m^{-2}. The R_{SL} stem-to-leaf ratio is 2.1:1, in the range provided in the literature (Huang et al., 2022). Above-ground biomass values of 1510 g m^{-2} also match well against the 1200-1600 g m^{-2} range described in the literature (Huang et al., 2022; Liu et al., 2022). Further, the partition fraction profiles are consistent with those of (Osborne et al., 2015)(see Fig. 6 a5); the main differences are that the modelled stem and root partition profiles are somewhat higher and lower, respectively, as compared to (Osborne et al., 2015).~~

Fig 6. Seasonal profiles (i.e., plotted against DVI) of carbon allocation variables for the Xiaoji calibrated DO_3SE-Crop model (i.e. AA O_3 treatment, year 2008 and Y16 cultivar) with a). showing the partition fractions of the daily accumulated NPP partitioned to roots, stems, leaves, and grains for the Xiaoji calibrated DO_3SE-Crop model (solid lines) *vs* the JULES Crop model (dashed line) calibrated for global application after Osborne *et al.* (2015)) and b). showing the DM (in g/m^2) of daily accumulated NPP partitioned to roots, stems, leaves, and grains with the observed final $GrainDM$ for Y16 cultivar in 2008 also shown (solid dot).

~~Figure 65 a). the partition fractions of the daily accumulated NPP partitioned to roots, stems, leaves, and grains for the Xiaoji calibrated DO_3SE-Crop modelled (solid lines) *vs* the JULES Crop model (dashed line) calibrated for global application after (Osborne et al., (2015)) plotted against~~

~~*DVI* for AA treatment, year 2008 Y2 cultivar, and b). the *DM* of daily accumulated *NPP* partitioned to roots, stems, leaves, and grains plotted against *DVI* for AA O_3 treatment, year 2008 and Y2 cultivar.~~

a). b).

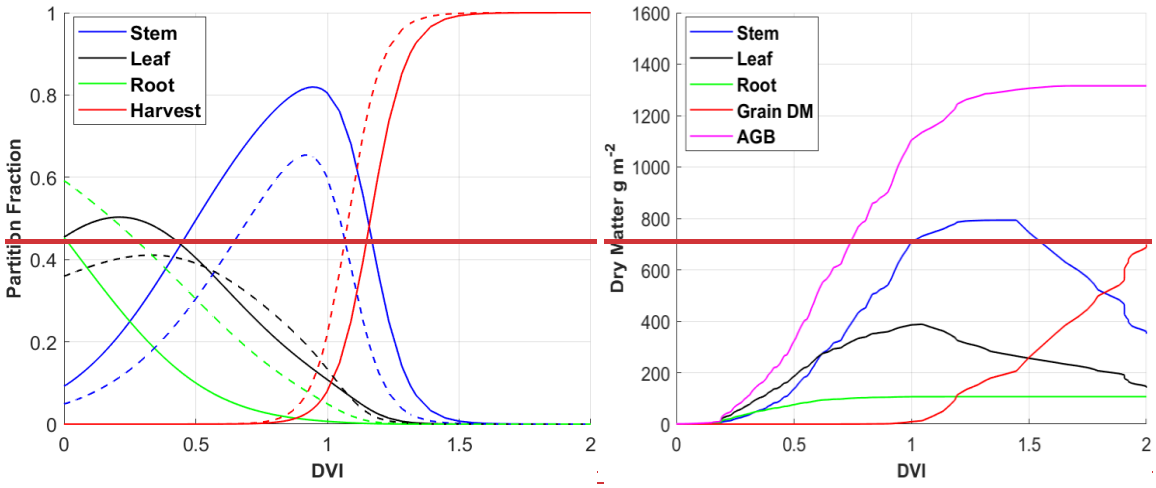

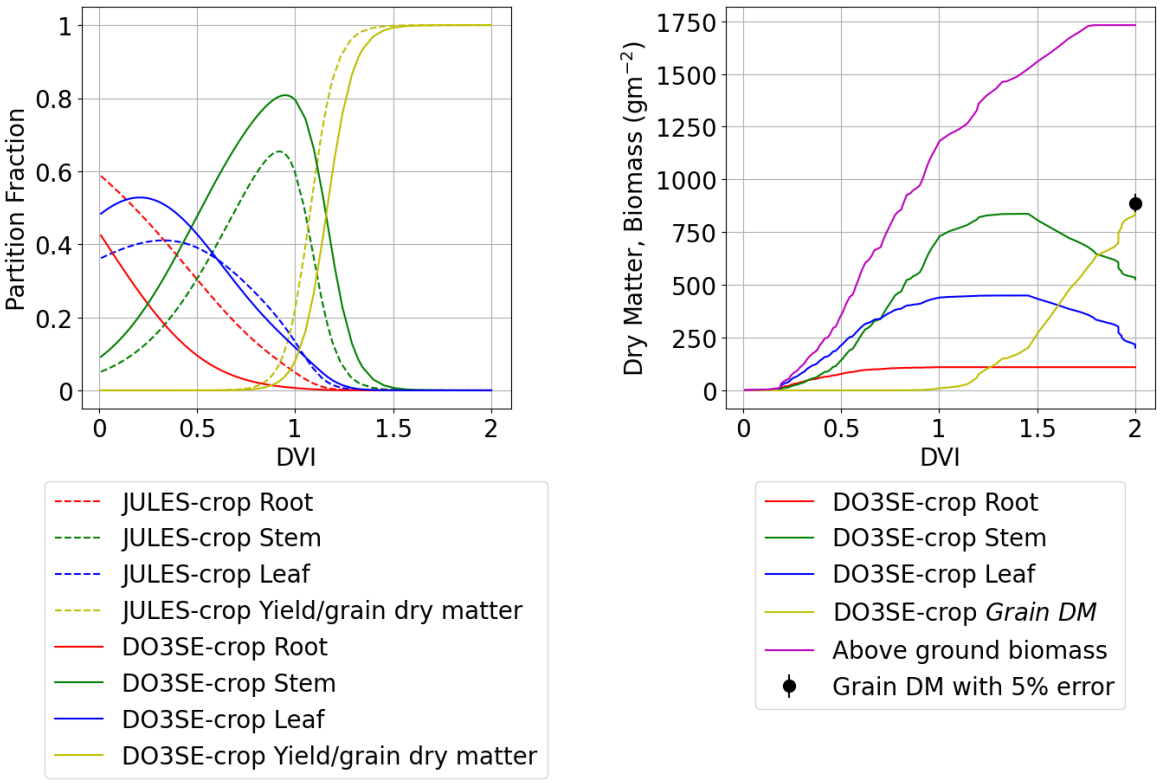

~~ii)~~ iv.a) ~~Instantaneous and long-term~~ O_3 induced yield loss difference between tolerant and sensitive cultivars: Instantaneous and long-term senescence ~~impact~~impact.

The $Grain\ DM$ is assumed to be damaged by both the instantaneous impact of O_3 (Farage et al., 1991) on photosynthesis as well as a longer-term O_3 effect that can lead to enhanced senescence (Feng et al., 2022). To explore which of these damage mechanisms is most important we calculated the difference in the $Grain\ DM$ caused by carbon assimilation for the AA and E O_3 treatments as compared to a simulated very low O_3 treatment representing pre-industrial conditions (for which C_z

O_3 concentration did not exceed 15 ppb) for both the tolerant (Y16) and sensitive (Y2) cultivar for each of the three years (see Table 2). We found a negligible effect of O_3 (0 to 0.2 %) on $Grain\ DM$ due to the instantaneous effect of O_3 on photosynthesis compared to a highly 9.85 to 31.13 %) impact due to the long-term O_3 effect on carbon assimilation *via* the enhancement of senescence on final $Grain\ DM$.

~~The $Yield_{grain}$ is assumed to be damaged by both the instantaneous impact of O_3 (Farage et al., 1991) on photosynthesis as well as the long-term O_3 effect that can lead to enhanced senescence (Feng et al., 2022). To explore which of these damage mechanisms is most important we calculated the difference between the C accumulation that would be partitioned to~~in the ~~the grain$Yield_{grain}$ caused by C assimilation for the AA and E -O_3 treatment as compared to a simulated very low [O_3] treatment representing pre-industrial conditions for both the tolerant (Y16) and sensitive (Y2) cultivar for each of the three years (see Table 21). We found a negligible effect of O_3 (0-0.2 %) on C allocations~~assimilation ~~due to the instantaneous effect of O_3 on photosynthesis compared to a highly significant (2.86-35.85 %) impact due to the long-term O_3 effect on C assimilation *via* the enhancement of senescence on final $Yield_{grain}$.~~

Table 2. The modelled % $Grain\ DM$~~$Yield_{grain}$~~ loss compared to a pre-industrial O_3 scenario divided between that $Grain\ DM$~~$Yield_{grain}$~~ loss caused by the direct and instantaneous effect of [O_3] on photosynthesis and that due to the long-term [O_3] impact on senescence.

Year	**Tolerant: Instantaneous O_3 effect on % $Grain\ DM$**		**Tolerant: Long-term O_3 effect on % $Grain\ DM$**	
	Ambient versus pre-industrial	Elevated versus pre-industrial	Ambient versus pre-industrial	Elevated versus pre-industrial
2007	0.01	0.01	18.43	31.13
2008	0	0	13.43	29.14
2009	0.03	0.03	19.5	28.11
	Sensitive: Instantaneous O_3 effect on % $Grain\ DM$		**Sensitive: Long-term O_3 effect on % $Grain\ DM$**	
	Ambient versus pre-industrial	Elevated versus pre-industrial	Ambient versus pre-industrial	Elevated versus pre-industrial
2007	0	0.2	16.60	29.05
2008	0	0	9.85	24.37
2009	0.01	0.01	17.48	25.87

~~iii)~~ iv.b) Senescence

The breakpoint method (Mariën et al., 2019) was used to determine the onset (SOS) and end (EOS) of senescence and maturity respectively using the chlorophyll data which was available for the year 2008, and the Y2 and Y16 cultivars. Results in Fig. 7 and Fig. S4 show that the E-O_3 treatment for cultivars Y16 and Y2 brought forwards the SOS by 3 and 5 days respectively, and EOS by 6 and 9 days respectively. Fig 7 also shows the f_{LS} profile which denotes the DO$_3$SE-Crop models accumulated stomatal O_3 flux effect on senescence , it is clear that f_{LS} is able to simulate the change in relative chlorophyll content reasonably well. The slope of the ambient f_{LS} is already steep since the ambient treatment already has rather high O3 levels as is now made clear in Table 1 with a value of 47ppb. According to the M7 wheat dose-response relationship this would result in a yield loss of ~ 5%.

~~i)~~ Fig 7. Profiles of O_3 induced leaf senescence for the Y16 cultivar for the a). AA O_3 treatment and b). E O_3 treatment. The timing of the SOS (solid black line) and EOS (dashed black line) were determined by applying the break point method to the chlorophyll data and are shown in relation to the f_{LS} simulations of senescence (yellow solid line). The observed relative chlorophyll content data, shown as filled blue symbols, include error bars representing the standard deviation of the measurements.~~The breakpoint method (Mariën et al., 2019) was used to determine the onset (SOS) and end (EOS) of senescence and maturity respectively using the chlorophyll content index (CCI) data which was available for the year 2008, and the Y2 and Y16 cultivars. Results showed (Fig. 7~~6) that the E-O_3 treatment for cultivars Y2 and Y16 brought forwards the SOS by 9 and 7 days respectively, and EOS by 4 and 2 days respectively.~~

~~Figure 7~~6. Leaf senescence profiles of O_3 induced leaf senescence for the Y2 cultivar for the ~~a).ambient).~~ ambient (AA) and ~~b). elevated (E-O_3) O_3~~. The timing of the SOS (solid ~~solid~~ black line) and EOS (dashed black line) were determined by applying the break point method to the CCI chlorophyll data and are shown in relation to the f_{LS} simulations of senescence (grey ~~yellow solid~~ line). The observed relative chlorophyll data, shown as filled blue symbols, include error bars representing the standard deviation of the measurements.~~The observed relative CCI data are also shown (open symbols)~~

a). b).

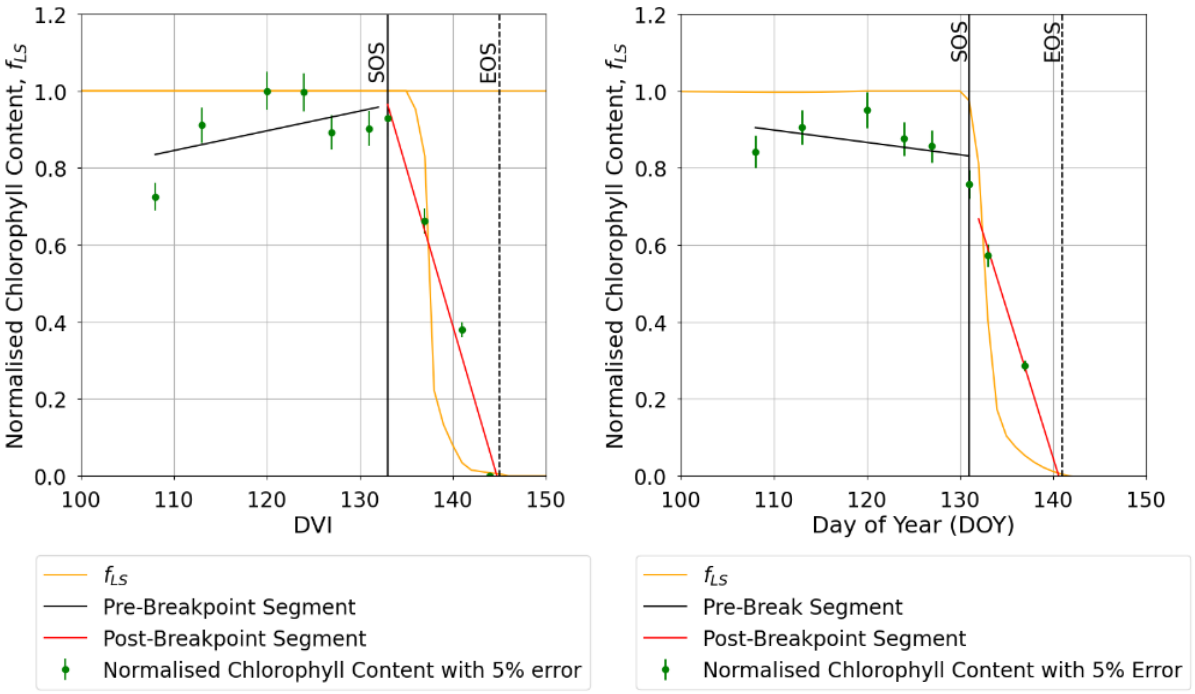

b).

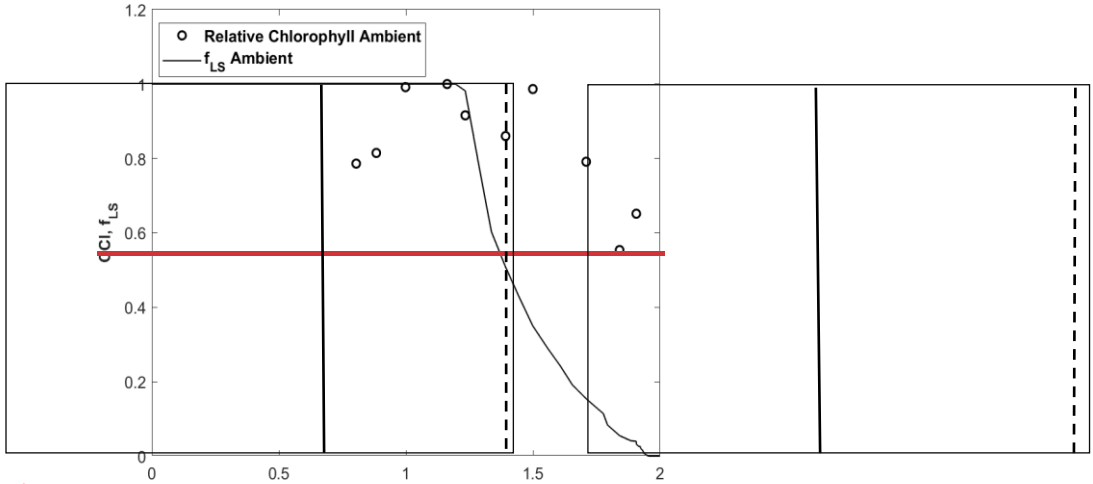

iv)

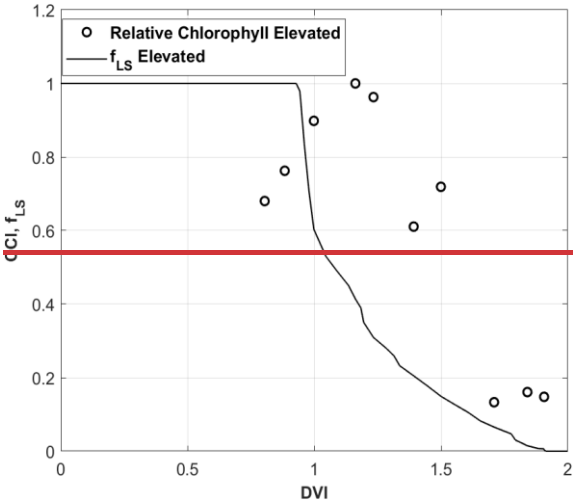

v) iv.c) Grain yield sSimulations across years and between cultivars

Fig. 8 shows a box plot of the modelled *vs* observed $Grain\ DM$ for both the sensitive (Y2, Y19) and tolerant (Y15, Y16) cultivars for each O_3 treatment (AA and E) for the years 2007, 2008 and 2009 (i.e. all data). Given the variability in the experimental data the model simulates the difference in $Grain\ DM$ between the AA and E O_3 treatments reasonably well with a simulated reduction in $Grain\ DM$ of 29 to 131 g m^{-2} compared with observed values of 81 to 165 g m^{-2} for the tolerant; and 49 to 196 g m^{-2} compared with observed values of 54 to 293 g m^{-2} for the sensitive cultivars respectively. The most notable difference is that there is a larger range in the simulated $Grain\ DM$ losses of the modelled sensitive cultivars though the simulated mean value for absolute $Grain\ DM$ suggests a more conservative influence of O_3 with yields at 610 g m^{-2} *vs* observed average yields of 590 g m^{-2}.

~~Figure 87 shows a box plot of the modelled *vs* observed $Yield_{grain}$ for both the sensitive (Y2, Y19) and tolerant (Y15, Y16) cultivars for each O_3 treatment (AA and E-O3), for the years 2007, 2008 and 2009. The model simulates the difference in $Yield_{grain}$ between the AA and E-O_3 reasonably well with a simulated reduction in $Yield_{grain}$ of 29 and 131 g m^{-2} compared with observed 81 and 165 g m^{-2} for the tolerant and as 49 and 196 g m^{-2} compared with observed 54 and 293 g m^{-2}sensitive cultivars respectively. The most notable difference is that there is a larger range in the simulated $Yield_{grain}$:~~

~~Llosses of the modelled sensitive cultivar though the mean value is more conservative at 610 g m^{-2} *vs* an observed value of 590 g m^{-2}.~~

Fig 8. Boxplots (crosses: 0.01 and 0.99 percentiles; box: 0.25 quartile, median and 0.75 quartile; triangle: mean) of simulated and observed wheat $Grain\ DM$ for the tolerant (Y15 and Y16) and sensitive (Y2 and Y19) cultivars under a.) AA and b.) E O_3 treatment for the years 2007, 2008 and 2009; these data include all the dataset.

~~Fig 87. Boxplots (crosses: 0.01 and 0.99 percentiles; box: 0.25 quartile, median and 0.75 quartile; square: mean) of simulated and observed wheat $Yield_{grain}$ for the tolerant (Y15 and Y16) and sensitive (Y2 and Y19) cultivars under a.) AA ambient and b.) E-O_3 elevated O_3 treatment conditions infor the years 2007, 2008 and 2009.~~

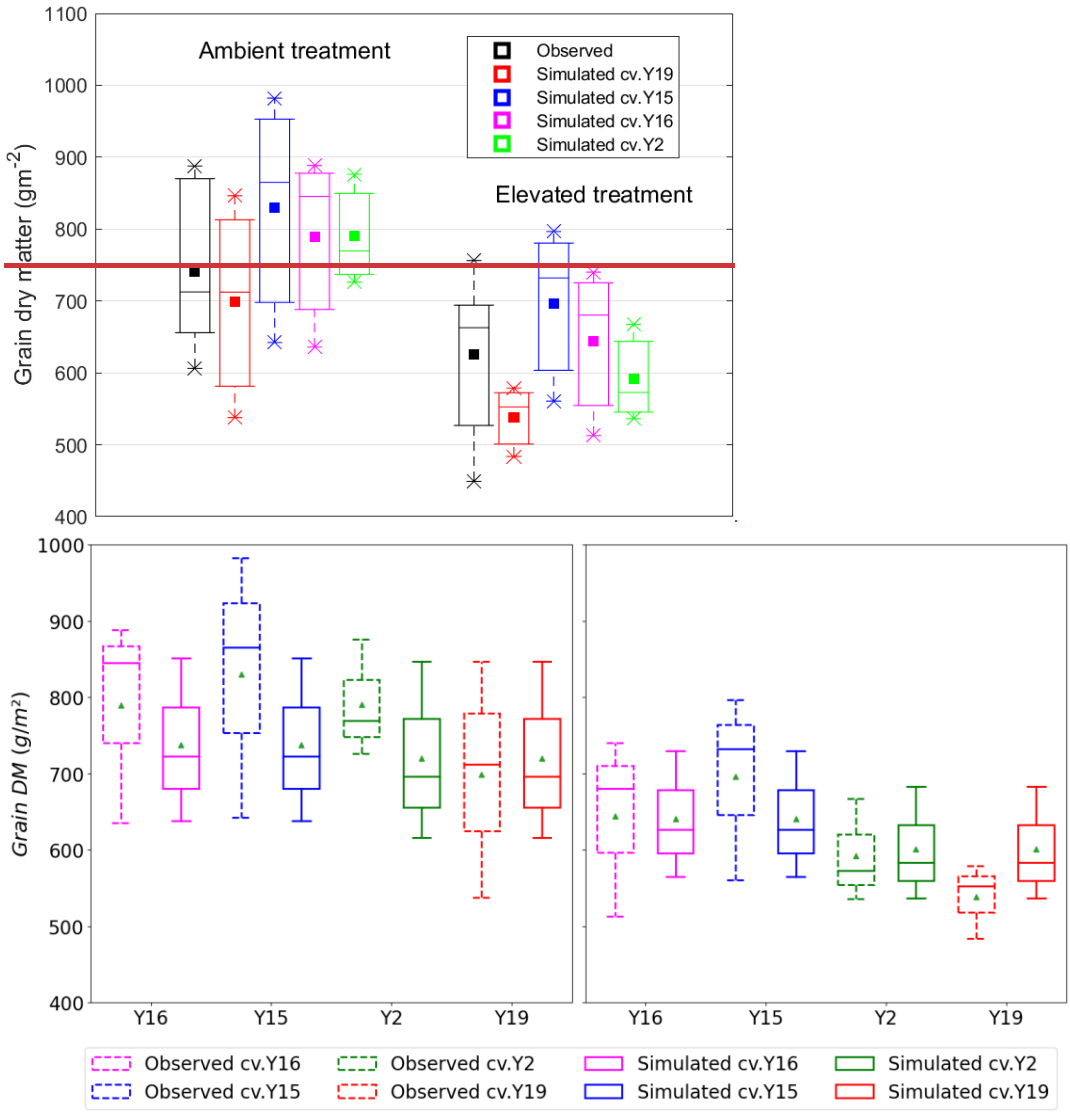

Finally, Fig 9 shows the relationship between modelled *vs* observed $Grain\ DM$ (in g m^{-2}) as a scatter plot, a linear regression through these data gives an R^2 value of 0.68 and RMSE of 76 g m^{-2}, showing the model is able to simulate with reasonable accuracy the differences in absolute yield for different cultivars and for different years. There are some instances of both underestimation and overestimation, however the deviations from the 1:1 line is not excessively large. These model test results compare with an R^2 of 0.92 and an RMSE of 25.49 g m^2 for the training dataset (Y2 cultivar and year 2008, see Figure S3), the stronger agreement between observed and modelled training dataset, as well as the reasonable agreement for the entire dataset would suggest the model is not over-fitted. We find that we tend to underestimate the O_3-induced relative yield loss (RYL) by between -2.76 and 15.34 (observed less modelled RYL) across all years and cultivars.

~~Figure 9 shows the relationship between modelled *vs* observed $Yield_{grain}$ (in g m^{-2}), a linear regression through these data gives an R^2 value of 0.68 and RMSE of 76 g m^{-2} 73, showing the model is able to simulate the differences in absolute yield for different cultivars and for different years reasonably well. There are some instances of both underestimation and overestimation, however he deviations from 1:1 line is are not excessively large. This compares with an R^2 of 0.92 and an RMSE of 25.49 g m^2 for the training dataset (Y2 cultivar and year 2008, see Figure S3), the stronger agreement between observed and modelled training dataset, as well as the reasonable agreement for the entire dataset would suggest the model is not over-fitted. The data points for 2007~~

~~overestimated the $Yield_{grain}$ for the E-O_3 treatments i.e. underestimating the yield loss, this was due to the O_3 treatment period being substantially shorter for the year 2007 compared to the other years (i.e. 2008 and 2009) by 38 days compared to 92 days.~~

Fig. 9. A scatter plot showing modelled *vs* observed $Grain\ DM$ (in g m^{-2}) for the AA and E O_3 treatments for all 4 cultivars and 3 years of the Xiaoji dataset; these data include those used for evaluation.

~~Fig. 98 A scatter plot showing modelled vs observed $Yield_{grain}$ (in g m^{-2}) for the ambient and elevated ozone treatments for all 4 cultivars and 3 years of the Xiaoji dataset; these data include that used for calibration (i.e. to train that mode; 2008 data for Y2 and Y16 cultivars) and those used for evaluation (i.e. to test that model; 2007 and 2009 data for all cultivars and 2008 data for Y15 and Y19).~~

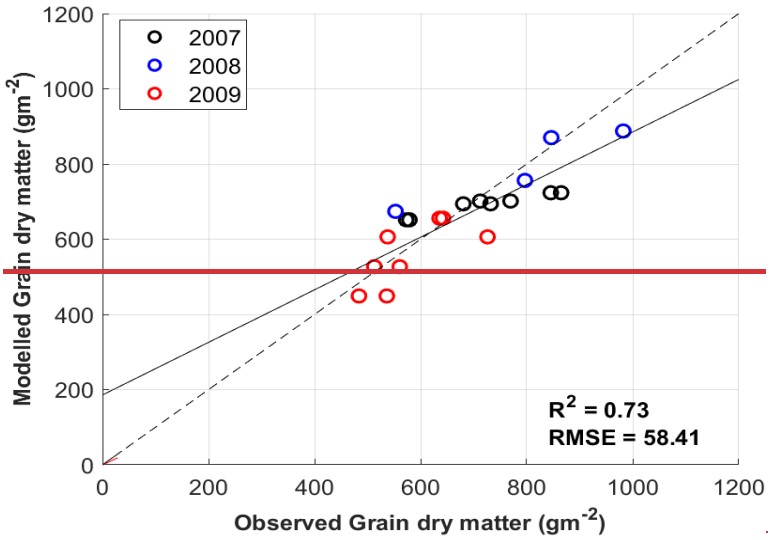

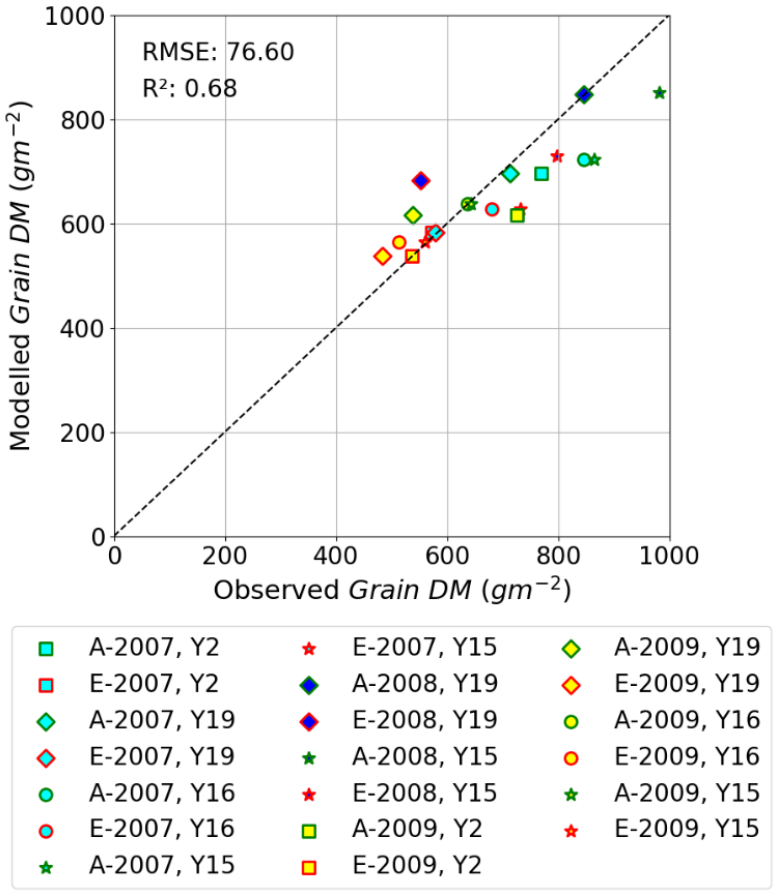

~~We find that we tend to underestimate the O_3-induced relative yield loss (RYL) by between -2.76 and 15.34 (observed less modelled RYL) across all years and cultivars.~~

1256

Discussion

The DO_3SE-Crop model was found capable of simulating O_3 damage to grain yield for O_3-FACE conditions at the experimental site in Xiaoji, China with a good degree of accuracy. Simulated relative yield losses (RYLs) between AA~~ambient~~ and ~~elevated~~E O_3 ~~conditions~~treatments for all years ranged between 11 to 14% and 13 to 19% ~~4-19% and 7-25%~~ for tolerant and sensitive cultivars respectively, these tend to be lower (particularly for the more extreme O_3 induced yield losses of the sensitive cultivars) than the observed values of 13 to 20% and 10 to 35%. Overall, simulations of tolerant and sensitive cultivars underestimated RYLs by 4% and 7% respectively on average across years and cultivars (see data in S6). This would suggest that O_3-induced yield losses can be more reliably modelled for tolerant cultivars, possibly because additional processes causing O_3-induced yield losses in sensitive cultivars are not captured. Such processes might include the effect of O_3 on the allocation of carbon to different plant parts (Feng et al., 2008) or O_3 inducing additional respiratory costs *via* the upregulation of defence mechanisms (Biswas et al., 2008). The model was also able to simulate absolute $Grain\ DM$ reasonably well. Under AA O_3 levels $Grain\ DM$ simulated for all years and cultivars were between 616 and 851 g/m^2 compared to observations of between 537 and 982 g/m^2. There is a tendency to overestimate $Grain\ DM$ under ambient conditions and underestimate $Grain\ DM$ under elevated O_3 which is reflected in the RYL values.

~~However, it should be noted that the model overestimated grain dry matter for the elevated O_3 treatments for the year 2007 (see Fig. 5) due to a shorter exposure period. (Zhu *et al.*, 2011) argued that despite the delayed and shorter O_3 fumigation period in 2007, the elevated O_3 levels were not much less than in other seasons and concluded this was the reason for the same level of O_3 impact on experimental grain yield. However, the accumulated stomatal O_3 flux estimated by the DO_3SE-model was much higher for the elevated O_3 treatment for the years 2008 and 2009 (at ~ 19 mmol O_3 m^{-2}) compared to 2007 (16.3 mmol O_3 m^{-2}), hence the greater modelled impact on the relative grain yield loss (15-18% for 2008 and 2009 versus 4-6% for 2007).~~

Overall, the DO_3SE-Crop model simulation results compare favourably to results made by the MCWLA-Wheat model (Tao et al., 2017) which was also calibrated for the Xiaoji experimental conditions but without distinction between tolerant and sensitive varieties. MCWLA-Wheat simulations of absolute yield varied between ~5700 and 9000 kg/ha (compared to ~5700 to 9800 kg/ha) for ambient and ~4800 to 8000 kg/ha (compared to ~5200 to 8000 kg/ha) for elevated O_3 treatments. A mean relative yield loss of 14% was simulated by the model.

It is useful to set these site-specific estimates of O_3-induced yield losses in the context of yield losses estimated using more traditional, concentration based O_3 risk assessment methods. A seminal paper by Feng et al. (2022) estimated ~~For context~~ mean relative yield losses across East Asia due to ambient O_3 concentrations at 33% (with a mean range of 28 to 37%) according to a mean monitored O_3 concentrations of 30.9 ppm h expressed as AOT40 (six-month accumulated daytime O_3 concentration above a threshold of 40 ppb). The mean difference in AOT40 (accumulated over only 75 days) between the AA and E O_3 treatments at Xiaoji across all years was 7.8 ppm h giving a mean relative yield loss of approximately 10 to 20% depending on year and cultivar. As such, our modelled results in terms of RYLs between AA and E O_3 treatments are consistent with these broader results for East Asia.

Crop phenology plays a crucial role in determining the timing of the ~~entire~~ important O_3 exposure period (i.e., from ~~crop emergence~~ anthesis to maturity), and hence O_3 damage since steady O_3

accumulation (acc_{fst}) occurring from early on in the crop growth period can cause O_3 detoxification mechanisms to be overwhelmed. ~~The~~ Evaluation of the DO$_3$SE-crop phenology model shows the model is able to accurately simulate crop phenology for the three years at Xiaoji (R^2 =0.95 and RMSE =2.5, see Fig. 3). Estimating the correct timing of anthesis is crucial since the period from anthesis to crop maturity is the O_3-sensitive period. During this period, accumulated stomatal O_3 flux (acc_{fst}) will contribute to early and enhanced senescence once the critical threshold ($CLsO3$) is exceeded. This period also coincides with carbon accumulation in the grain (Kohut et al., 1987; Feng et al., 2008) which may be limited by O_3-induced early onset or enhanced senescence. The DO$_3$SE-crop model was developed to accommodate the full range of effects of O_3 on senescence with revised functions, similar to those first developed by Ewert and Porter (2000), able to modify both the O_3 induced onset of senescence as well as the O_3 effect on maturity. This is important since experimental evidence has shown that O_3 can bring forward the maturity date; for example, the flag leaf was found to have senesced 25 days earlier in a high O_3 treatment, compared to a charcoal-filtered treatment (Grandjean and Fuhrer, 1989; Gelang et al., 2000). O_3 was also found to cause differences in the time to maturity of the flag leaf, with Shi et al. (2009) reporting that maturity was brought forward by 8 days under an elevated O_3 treatment (50% higher than ambient). Currently, other crop models with O_3 damage functions (e.g. MLCWLA-Wheat (Tao et al., 2017) and LINTULLCC-2 (Feng et al., 2022) are only able to bring the O_3-induced onset of senescence earlier.

The DO$_3$SE-crop model is also able to simulate differential O_3 uptake in each canopy layer. Fig. 5 shows that the majority of stomatal O_3 uptake occurs in the sunlit layers of the upper canopy. Similar results were found in an experimental study on a productive grassland in Switzerland (Jaggi et al., 2006) who found that different levels of O_3 exposure to canopy components predominantly located in the upper and lower parts of the canopy support a multi-layer approach to modelling O_3 uptake. Therefore, the focus on the upper canopy by flux-based O_3 metrics (e.g. the phytotoxic ozone dose POD_y (UNECE, 2017) seems rational in the absence of multi-layer modelling. Crop models such as LINTULCC-2 (Feng et al., 2022) also focus on estimating stomatal O_3 uptake at the top of the canopy to estimate O_3 induced yield losses. For wheat, such an approach is further supported by the fact that the upper canopy layers consist of the flag leaf, which plays a crucial role in photosynthesis and grain filling (Pleijel et al., 2007). The multi-layer functionality of the DO$_3$SE-Crop model may however become more useful when considering crops that partition assimilated carbon to harvest organs earlier in their growing season such as potato (Okrah et al. 2023).

Our results show that the DO$_3$SE-crop model was able to estimate the seasonal course of leaf A_{net} and g_{O3} daily maxima observed at the Xiaoji site (see Fig. 4a) and when compared to other literature describing leaf physiological variables (Guan et al., 2015; Li et al., 2022). This suggests the coupled $A_{net}g_{sto}$ model is working for Chinese conditions (having previously been applied and evaluated for European O_3 experimental conditions – see Pande et al., 2024). The leaf physiology parameters used in this study (i.e. for Asian conditions and cultivars) are higher than parameters for European studies. For Europe, V_{cmax} values of between 60 and 90 µmol CO_2 m^{-2} s^{-1} were found in the literature (Feng et al., 2022; Pande et.al., 2024, Van Oijen and Ewert, 1999) compared to the observed mean maximum value of 137 µmol CO_2 m^{-2} s^{-1} at Xiaoji which was used in this study. Similarly, European J_{max} values ranged from 160 to 180 µmol CO_2 m^{-2} s^{-1} (Feng et al., 2021, Pande et al. 2024, Van Oijen & Ewert, 1999) compared to the observed Xiaoji mean maximum value of 228 µmol CO_2 m^{-2} s^{-1}. Even though these leaf physiology parameters are higher, absolute yields for these Chinese cultivars are consistent with those found under European conditions. This most likely reflects the importance of other environmental conditions (e.g., high vapour pressure deficits) limiting leaf carbon assimilation. Moreover, the complex interactions between O_3 exposure and the plants' physiological responses also play a crucial role. Ozone significantly affected antioxidative enzymes, thereby limiting overall

photosynthetic efficiency and yield, particularly in O_3-sensitive cultivars, despite their ability to maintain high carboxylation capacity.

Ensuring the seasonal variation in carbon~~C~~ allocation to the different components of the crop (i.e., roots, stem, leaves and harvest organs) is essential for the simulation of crop growth and yield. There are limited data in the literature that provide these variables, so we compare our results to the carbon allocation profiles described for wheat provided in the original JULES Crop model description, recognising this is intended for wheat grown globally. The DO_3SE-Crop model carbon~~C~~ allocation to the stem and roots is comparatively higher than was simulated by JULES Crop (Osborne et al., 2015; see Fig. 6a). However, we can justify the carbon allocation coefficients used for Xiaoji since the DO_3SE-Crop model was able to distribute carbon to different plant components to produce a well-proportioned plant over the course of the growing season, this was determined by the calibration to a number of key crop variables (i.e., ratios of plant respiration, LAI, stem to leaf dry matter, above ground components and grain dry matter). Importantly, the model, was found to simulate the $Grain\ DM$ for the unseen years cultivars under the AA and E O_3 treatments to within 8.7 to 7.9 % of the observed values (R^2 =0.68, 76 g/m² see Fig. 9). ~~Importantly, the model, was found to simulate the grain dry matter for the year 2008 and the cultivar Y16 (tolerant) & Y2(sensitive) under the ambient and elevated O_3 treatment to within 0.08- 2.19% of the observed values (R^2 =0.99, 9.27 g/m² see Fig. S2).~~

The DO_3SE-Crop model, similar to other crop models with O_3 damage functions (i.e. MLCWLA-Wheat (Tao *et al.*, 2017) and LINTULLCC-2 (Feng *et al.*, 2022)) has the capacity to simulate both the instantaneous and long-term O_3 impact on wheat grain yield. The instantaneous O_3 effect on photosynthesis may cause leaf cell damage and decrease the supply of carbohydrate precursors which can significantly decrease g_{O3}, V_{cmax} and leaf chlorophyll content (Farage *et al.*, 1991). Elevated O_3 also leads to generation of reactive oxygen species (ROS) in plant cells which can cause oxidative damage to various cellular components. Rubisco, the enzyme responsible for carbon fixation in the photosynthetic process, can be particularly susceptible to this damage, leading to a reduced carboxylation rate (V_{cmax}). Such an O_3 effect on V_{cmax} reduces net photosynthesis and can also induce early senescence shortening the grain filling period (Triboi and Triboi-Blondel, 2002).

Results from the DO_3SE-crop model found a larger impact on yield due to the long-term O_3 impact causing relative yield loss of between 2 to 36% compared to only 0 to 0.2% resulting from the instantaneous O_3 impact on photosynthesis. Previous studies have also found that the long-term O_3 effect has a larger impact on yield compared to the instantaneous effect of O_3 on photosynthesis (Emberson *et al.*, 2018; Brewster et al., 2024). Senescence is an age-dependent process of degradation and degeneration that allows nutrients to be re-distributed to different plant organs (Lim et al., 2007). Under O_3 stress, this process is often found to occur earlier and more rapidly in leaves as well as at the whole plant or crop canopy scale (Brewster et al., 2024). The causes of this early and accelerated senescence are not completely understood but may be related to O_3 induced enhanced expression of many genes involved in natural senescence (Miller et al., 1999). Elevated O_3 was also found to inhibit sugar export from leaves (Singh Yadav et al., 2020; Feng et al., 2024) which could trigger early onset of leaf senescence.

The DO_3SE-crop model accounts for the impact of O_3 on the Rubisco enzyme by incorporating modified (Ewert and Porter, 2000) functions for instantaneous and long-term O_3 impact on V_{cmax} as an important parameter used to characterize the crop photosynthetic capacity (Ewert and Porter, 2000; Osborne et al., 2019). The DO_3SE-crop model assumes that the O_3 will only accumulate on exceedance of a stomatal O_3 flux threshold of 6 nmol O_3 m^{-2} s^{-1}. The long-term O_3 impact mechanism

of the DO$_3$SE-crop model simulated the effect of senescence on V_{cmax} reasonably well as evidenced by the reduction in leaf chlorophyll content. We used the breakpoint method (Yang et al., 2016; Mariën et al., 2019) to estimate the SOS and EOS using the day of the year and measured chlorophyll content (Fig. S7). It is crucial to accurately model the timing of SOS and EOS correctly as this determines the O_3 effect on the duration of the grain filling period and hence the difference in yield loss due to different O_3 treatments. For example, we modelled a difference of 3 to 5 in SOS, and 6 to 9 days in EOS ~~8 and 3 and 4 and 1 days in SOS &EOS~~ respectively, on average across years for the sensitive and tolerant cultivar respectively.

China's wheat breeding programme has seen more than 1,850 varieties used across China between the 1920s to 2014 leading to increased yields from less than 1 to more than 5 tonnes ha^{-1} (Qin et al., 2015). Here, albeit with an extremely limited dataset, we parameterise the DO$_3$SE-crop model for tolerant and sensitive wheat crop cultivars, since many experimental studies have shown that the response of different cultivars to O_3 stress differs (Biswas et al., 2008). Based on the available data the model seemed able to capture the difference in grain dry matter between these different cultivar groups across different years reasonably well when compared to the observed dataset (R^2 =0.68; see Fig. 8). Such a cultivar sensitivity-based parametrisation can provide additional information on the certainty of regional yield loss estimates given the large number of wheat varieties grown across China. However, when applying the model to a broader region, it would be advisable to calibrate phenology for different agro-ecological zones as the temperature changes across China, impacting the duration of the key phenological stages such as anthesis and maturity (Luo et.al., 2021). Additionally, carbon allocation parameters may need adjustment, as studies have shown changes in dry matter content across different agro-ecological zones (Hussain and Bagash, 2017).

Conclusions

We have shown that the newly developed DO_3SE-Crop model can be calibrated for O_3 tolerant and sensitive wheat varieties for O3-FACE site conditions at Xioaji in China. The model can simulate crop phenology, leaf physiology, crop growth and yield reasonably well across different years. The model is also able to simulate the effect of O_3 stress on grain yield distinguishing the extent of O_3 damage resulting from the same O_3 treatment on cultivars with differing O_3 sensitivities. The DO_3SE-Crop model also has the advantage of simulating O_3 transfer and deposition dynamics within the wheat crop canopy which could in the future improve our understanding of whole canopy O_3 effects for crops with different carbon allocation profiles. The ability of the model to estimate relative yield losses across years also suggests the model is 'fit for purpose' to assess the effects of O_3 under a variety of climate variable and ~~[~~O_3~~]~~ concentration conditions.

Appendix A

A1. DO_3SE-Crop variables

Variable	Unit	Description
T_{eff}	°C days	Effective temperature accumulated between sowing to maturity
DVI	-	Development index
T_{air}	°C	Surface air temperature in degrees Celsius
$T_{air,k}$	degrees Kelvin	Surface air temperature in Kelvin
T_{min}	°C	Daily minimum surface air temperature
T_{max}	°C	Daily maximum surface air temperature
LTT	°C d	Thermal time accumulated by a leaf
V_{dd}	days	Accumulated vernalised days
V	days	Vernalised days
V_d	days	Devernalised days
VF	-	Vernalisation factor
PP	hrs	Photoperiod
PF	-	Photoperiod factor
A_{net}	µmol CO_2 m^{-2} s^{-1}	Net photosynthesis or rate of CO_2 assimilation
A_c	µmol CO_2 m^{-2} s^{-1}	RuBP (ribulose-1,5-bisphosphate) limited A_{net}
A_j	µmol CO_2 m^{-2} s^{-1}	Electron transport limited A_{net}
A_p	µmol CO_2 m^{-2} s^{-1}	TPU (triose phosphate) limited A_{net}
R_d	µmol CO_2 m^{-2} s^{-1}	Dark respiration
f_{PAW}	-	Fraction of plant available water
PAW_t	-	Threshold of PAW, above which g_{sto} is at a maximum as described f_{PAW} function
PAW	m^3/m^3	Plant available water
C_i	µmol/mol	Intercellular CO_2 partial pressure
O_i	mmol/mol	Intercellular O_2 concentrations
Γ^*	µmol/mol	CO_2 compensation point in the absence of respiration
Γ	µmol/mol	CO_2 compensation point
J	µmol CO_2 m^{-2} s^{-1}	electron transport rate
VPD	kPa	Leaf to air vapour pressure deficit
C_z	ppb	O_3 concentration at reference height z
C_h	$nmol/m^3$	O_3 concentration at the crop canopy height
C_{zh}	$nmol/m^3$	O_3 concentration at the top of the crop canopy height
C_{zb}	$nmol/m^3$	O_3 concentration at the bottom of the crop canopy height
f_{st}	nmol O3 m^{-2} s^{-1}	Leaf level stomatal O_3 flux
$accf_{st}$	mmol O3 m^{-2}	Accumulated stomatal O_3 flux
C_l	nmol O_3 m^{-3}	O_3 at the upper surface of the laminar layer of a leaf

$f_{O3,s}(d)$	-	Effect of daily cumulative stomatal O_3 flux on Vc_{max}
$f_{O3,s}(h)$	-	Effect of hourly cumulative stomatal O_3 flux on Vc_{max}
$f_{O3,s}(d-1)$	-	Previous days effect of cumulative stomatal O_3 flux on Vc_{max}
$r_{O3,s}$	-	Incomplete overnight recovery of O_3 affected Vc_{max}
f_{LA}	-	Leaf age related capacity to recover from accumulated stomatal O_3 flux
$fO3_l$	-	Weighted accumulated stomatal O_3 flux that determines the onset of leaf senescence
f_{LS}	-	Accumulated stomatal O_3 flux effect on leaf senescence
tl	°C days	Effective temperature accumulated by a leaf after emergence ($DVI = 0$)
tl_{ep}	-	Effective temperature accumulated by a leaf between full expansion and the onset of leaf senescence
$tl_{ep_{O3}}$	-	Effective temperature accumulated by a leaf between full expansion and the onset of leaf senescence brought forward by O_3
tl_{se}	-	Effective temperature accumulated by a leaf between the onset of leaf senescence and maturity
$tl_{se_{O3}}$	-	Effective temperature accumulated by a leaf between the onset of leaf senescence and maturity brought forward by O_3
g_{CO2}	µmol CO_2 PLA m^{-2} s^{-1}	Stomatal conductance to CO_2
f_{VPD}	-	Relationship between VPD and relative stomatal conductance
c_s	mol CO_2/mol	External CO_2 concentration at the leaf surface
c_a	mmol CO_2/mol	external CO_2 concentration at the upper surface of the leaf boundary layer
g_{bCO2}	mol m^{-2} s^{-1}	Quasi laminar boundary layer conductance to CO_2
C_z	nmol O_3 m^{-3}	O_3 concentration at reference height (z)
C_l	nmol O_3 m^{-3}	O_3 concentration at the upper surface of the laminar layer of a leaf
g_{O3}	mmol O_3 PLA m^{-2} s^{-1}	Stomatal conductance to O_3
$g_{O3_{m/s}}$	m/s	Stomatal conductance to O_3
g_{ext}	m/s	External conductance
r_c	s/m	Leaf surface resistance to O_3
$r_{b,O3}$	s/m	Quasi laminar leaf boundary layer resistance to O_3
r_a	s/m	Atmospheric resistance to O_3
r_{inc}	s/m	In-canopy resistance to O_3
r_{ext}	s/m	External plant cuticle resistance to O_3
r_{sto}	s/m	Stomatal resistance to O_3
u_z	m/s	Wind speed at a reference height z
u_l	m/s	Wind speed at the upper surface of the laminar layer of a leaf
L	m	Cross wind leaf dimension
LAI	m^2 m^{-2}	Leaf Area Index
$PAR_{dir,i}$	W/m^2	Direct PAR in canopy layer i
$PAR_{diff,i}$	W/m^2	Diffuse PAR in canopy layer i
PAR_{total}	W/m^2	Direct and diffuse PAR at the top of the canopy

NPP	kg C m^{-2}	Net primary productivity
GPP	kg C m^{-2}	Gross primary productivity
R_p	kg C m^{-2}	Plant respiration
R_{pm}	kg C m^{-2}	Plant maintenance respiration
R_{pg}	kg C m^{-2}	Plant growth respiration
A_{netc}	kg C m^{-2}	Canopy net photosynthesis
R_{dc}	kg C m^{-2}	Non-water stressed canopy dark respiration
$f_{sw}R_{dc}$	kg C m^{-2}	Water stressed modified canopy dark respiration
C_{root}	kg C m^{-2}	Root C pool
C_{leaf}	kg C m^{-2}	Leaf C pool
C_{stem}	kg C m^{-2}	Stem C pool
C_{resv}	kg C m^{-2}	Reserve C pool
C_{harv}	kg C m^{-2}	Harvest pool
P_{root}	-	Root C pool partition coefficient
P_{leaf}	-	Leaf C pool partition coefficient
P_{stem}	-	Stem C pool partition coefficient
P_{resv}	-	Reserve C pool partition coefficient
P_{harv}	-	Harvest C pool partition coefficient
$C_{leaf,green}$	kg C m^{-2}	Green leaf C
$C_{leaf,brown}$	kg C m^{-2}	Brown leaf C
SLA	m^2 kg^{-1}	Specific Leaf Area
h	m	Crop height
$Yield_{grain}$	g C m^{-2}	Grain yield
k_b'	-	Beam and scattered beam PAR extinction coefficient
k_d'	-	Diffuse and scattered diffuse PAR extinction coefficient
ρ_{cb}	-	Canopy refection coefficient for beam PAR
ρ_{cd}	-	Canopy reflection coefficient for diffuse PAR
β	Radians	Solar elevation angle
δ	Radians	Solar declination angle
$PAR_{dir}\ (LAI)$	$\mu mol\ m{-}2\ s{-}1$	Absorbed beam plus scattered beam PAR per unit leaf area
$PAR_{diff}\ (LAI)$	$\mu mol\ m{-}2\ s{-}1$	Absorbed diffuse plus scattered diffuse PAR per unit leaf area
$PAR\ (LAI)$	$\mu mol\ m^{-2}\ s^{-1}$	Total absorbed PAR per unit leaf area
$I_b\ (LAI)$	$\mu mol\ m^{-2}\ s^{-1}$	Direct PAR per unit ground area
$I_d\ (LAI)$	$\mu mol\ m^{-2}\ s^{-1}$	Diffuse PAR per unit ground area
$I_d\ (0)$	$\mu mol\ m^{-2}\ s^{-1}$	Diffuse PAR per unit ground area at the top of the canopy
$I_b\ (0)$	$\mu mol\ m^{-2}\ s^{-1}$	Beam PAR per unit ground area at the top of the canopy
$I_{bs}\ (LAI)$	$\mu mol\ m^{-2}\ s^{-1}$	Absorbed scattered beam PAR per unit leaf area
$PAR_{bsun}\ (LAI)$	$\mu mol\ m^{-2}\ s^{-1}$	Beam PAR absorbed by sunlit leaves per unit leaf area

$PAR_{sh}\ (LAI)$	$\mu mol\ m^{-2}\ s^{-1}$	Beam PAR absorbed byshaded leaves per unit leaf area
$PAR_{sun}\ (LAI)$	$\mu mol\ m^{-2}\ s^{-1}$	Total PAR absorbed by sunlit leaves per unit leaf area
PAR_{total}	$\mu mol\ m^{-2}\ s^{-1}$	Total absorbed irradiance per unit leaf area
LAI	$m^2 m^{-2}$	Cumulative leaf area index from top of canopy (L=0 at top)
$f1{,}2\ (LAI)$	-	Fraction of leaf area in a leaf-angle class
$LAIsh$	-	Fraction of leaves that are shaded
$LAIsun$	-	Fraction of leaves that are sunlit
σ	-	Leaf scattering coefficient for PAR
α_1	Radians	Angle of beam irradiance to the leaf normal
$sin\beta$	-	Solar elevation angle
$k_b{}'$	-	Beam and scattered beam PAR extinction coefficient
$k_d{}'$	-	Diffuse and scattered diffuse PAR extinction coefficient
σ	-	Leaf scattering coefficient for PAR
α_1	Radians	Angle of beam irradiance to the leaf normal

A2. DO_3SE-Crop parameters for wheat. Highlighted are the parameters (and their associated ranges) which require calibration when applying DO3SE-Crop to varying environmental conditions.

Parameter	**Unit**	**Default Value**	**Description**	**Reference**	**Range**	**Calibrated Parameter Value**
T_b	°C	0	Base temperature	(Tao, Zhang and Zhang, 2012; Osborne *et al.*, 2015)	-0.5-1	-0.25
T_o	°C	20	Optimum temperature	(Tao, Zhang and Zhang, 2012; Osborne *et al.*, 2015)	15-25	17.79
T_m	°C	30	Maximum temperature	(Tao, Zhang and Zhang, 2012; Osborne *et al.*, 2015)	25-40	23.87
TT_{emr}	°C d	100	Thermal time between sowing and emergence	(Lu *et al.*, 2018; Luo *et al.*, 2020)	50-100	220.6
TT_{veg}	°C d	940	Thermal time between emergence and anthesis	Xiaoji experimental dataset	400-940	940
TT_{rep}	°C d	304	Thermal time between anthesis and maturity	(Wang *et al.*, 2013a); Xiaoji experimental dataset	300-650	304
TT_{leaf}	°C d	1000	Total canopy-leaf life span of the crop, covers period from emergence to maturity, distributed over the DVI between 0 and 2	(Lu *et al.*, 2018; Luo *et al.*, 2020)	700-1200	795

T_l	°C d	1400	Total lifespan of the crop, covers the full period from sowing to maturity, corresponding to DVI between -1 to 2	(Ewert and Porter, 2000; Lu *et al.*, 2018; Luo *et al.*, 2020)	1300-1500	Year 2007- 1325, Year 2008- 1400, Year 2009- 1478.
PIV		1.5	Vernalisation coefficient	(Tao, Zhang and Zhang, 2012; Wang *et al.*, 2013)	2.9-4	2.9
PID		40	Photoperiod coefficient	(Wang *et al.*, 2013; Liu *et al.*, 2016; Zhao *et al.*, 2020)	40-57	40
VT_{max}	°C	30	Maximum daily temperature for vernalisation	Zheng et.al, 2015		
VT_{min}	°C	15	Minimum daily temperature for vernalisation	Zheng et.al, 2015		
PAW_t	m^3/m^3	50	Plant available soil water below which stomatal conductance will start to reduce	LRTAP, 2017		
V_{cmax}	µmol CO_2 m^{-2} s^{-1}	90	Maximum carboxylation capacity at 25°C	(Büker *et al.*, 2012)	90-140	137
J_{max}	µmol CO_2 m^{-2} s^{-1}	180	Maximum rate of electron transport at 25°C	(Büker *et al.*, 2012)	180-250	228
K_c	µmol/mol	404.9	Rubisco Michaelis-Menten constants for CO_2	(Medlyn *et al.*, 2002)		
K_0	mmol/mol	278.4	Rubisco Michaelis-Menten constants for O_2	(Medlyn *et al.*, 2002)		
Γ^*	µmol/mol	42.75	CO_2 compensation point in the absence of respiration	(Medlyn *et al.*, 2002)		
a	-	4	Electron requirement for the formation of NADPH	(Sharkey *et al.*, 2007)		
b	-	8	Electron requirement for the formation of ATP	(Sharkey *et al.*, 2007)		
R_{dcoeff}	-	0.015	Leaf dark respiration coefficient	(Clark *et al.*, 2011)	0.010-0.03	0.01
f_{min}	µmol $CO_2/m^2/s$	1000	Minimum daytime stomatal conductance to CO_2	(Ewert and Porter, 2000)		
m	-	7	composite sensitivity slope constant	(Büker *et al.*, 2012)	4-15	5
VPD_0	kPa	2.2	stomatal conductance sensitivity to VPD	UNECE, 2017; Pande et al. 2024		
$\gamma 1$	-	0.027	O_3 short-term damage co-efficient	(Ewert and Porter, 2000)		
$\gamma 2$	(nmol O_3 m^{-2} s^{-1})$^{-1}$	0.0045	O_3 short-term damage co-efficient	(Ewert and Porter, 2000)		
$\gamma 3$	(µmol O_3 m^{-2})$^{-1}$	0.00005	O_3 long-term damage co-efficient	(Ewert and Porter, 2000)	0.00001-0.00009	Tolerant=0.00001 Sensitive=0.00002

$\gamma 4$	-	5	O_3 long-term damage co-efficient determining onset of senescence		5-15	Tolerant=5 Sensitive=15
$\gamma 5$	-	0.8	O_3 long-term damage co-efficient determining maturity		0.5-5	Tolerant=0.8 Sensitive=5
$CLsO3$	mmol O_3 m^{-2}	6.5-20.6,20.5	Critical accumulated stomatal O3 flux that determines the onset of leaf senescence	(Osborne *et al.*, 2019; Feng *et al.*, 2022)	3-21	4.2
r_{ext}	m/s	2500	External leaf cuticular resistance to O_3 uptake	UNECE, 2017		
L	m	0.02	Cross wind leaf dimension for wheat	UNECE, 2017		
P_{st}	Pa	1.013 x 10^5	Standard air pressure at 20^{O}C	UNECE, 2017		
T_{st}	^{o}C	20	Standard temperature	UNECE, 2017		
R	J/mol/K	8.31447	Universal gas constant	UNECE, 2017		
n_e	mol CO_2 m^{-2} s^{-1} kg C (kg N)$^{-1}$	0.0008	Constant relating leaf nitrogen to rubisco carboxylation capacity	(Clark *et al.*, 2011)		
n_0	kg N [kg C]$^{-1}$	0.073	Top canopy leaf N concentration	(Clark *et al.*, 2011)		
kN		0.78	Nitrogen profile co-efficient	(Clark *et al.*, 2011)		
R_{gcoeff}	-	0.25	Plant growth respiration coefficient	(Osborne *et al.*, 2015)	0.15-0.25	0.16
α_{root}	-	18.5	Coefficient for determining partitioning	(Osborne *et al.*, 2015)	16-19	18.4
α_{stem}	-	16.0	Coefficient for determining partitioning	(Osborne *et al.*, 2015)	16-17	16.8
α_{leaf}	-	18.0	Coefficient for determining partitioning	(Osborne *et al.*, 2015)	18-19	18.5
β_{root}	--	-20.0	Coefficient for determining partitioning	(Osborne *et al.*, 2015)	20-21	-20.9
β_{stem}	-	-15.0	Coefficient for determining partitioning	(Osborne *et al.*, 2015)	14-16	-14.5
β_{leaf}	-	-18.5	Coefficient for determining partitioning	(Osborne *et al.*, 2015)	18-19	-18.11
f_c	-	0.5	Carbon fraction of dry matter	(Osborne *et al.*, 2015)		
Υ	m^{-2} kg^{-1}	27.3	Coefficient for determining specific leaf area	(Osborne *et al.*, 2015)	13-28	13.5
δ	-	-0.0507	Coefficient for determining specific leaf area	(Osborne *et al.*, 2015)		
k	-	1.4	allometric coefficient which relates C_{stem} to h	(Osborne *et al.*, 2015)		
τ	-	0.4	allometric coefficient which relates C_{stem} to h	(Osborne *et al.*, 2015)	0.3-0.6	0.4

D_w	-	1/0.84	Conversion factor to allow for grain moisture content	(Mulvaney and Devkota, 2020)		
E_g	-	0.85	Conversion factor for grain to ear ratio	(Nagarajan *et al.*, 1999; Kutman, Yildiz and Cakmak, 2011)	0.7-0.85	0.85
R_{SL}	-	2:1	Stem dry matter to leaf dry matter ratio	(Huang et al., 2022)		
$k_b{}'$	-	0.46/sinβ	Beam and scattered beam PAR extinction coefficient	(Pury and Farquhar,1997)		
$k_d{}'$	-	0.8	Diffuse and scattered diffuse PAR extinction coefficient	(Pury and Farquhar,1997)		
σ	-	0.15	Leaf scattering coefficient for PAR	(Pury and Farquhar,1997)		
α_1	Radians	0.5	Angle of beam irradiance to the leaf normal	(Pury and Farquhar,1997)		

1433

References

Amthor, J. S., Bar-Even, A., Hanson, A. D., Millar, A. H., Stitt, M., Sweetlove, L. J., and Tyerman, S. D.: Engineering strategies to boost crop productivity by cutting respiratory carbon loss, Plant Cell, 31(2), 297–314, https://doi.org/10.1105/tpc.18.00743, 2019.

Betzelberger, A. M., Gillespie, K. M., McGrath, J. M., Koester, R. P., Nelson, R. L., and Ainsworth, E. A.: Ozone exposure response for U.S. soybean cultivars: Linear reductions in photosynthetic potential, biomass, and yield, Plant Physiology, American Society of Plant Biologists, 160(4), 1827–1839, https://doi.org/10.1104/pp.112.205591, 2012.

Biswas, D. K., Xu, H., Li, Y. G., Sun, J. Z., Wang, X. Z., Han, X. G., and Jiang, G. M.: Assessing the genetic relatedness of higher ozone sensitivity of modern wheat to its wild and cultivated progenitors/relatives, Journal of Experimental Botany, 59(4), 951–963, https://doi.org/10.1093/jxb/ern022, 2008.

Brewster, C., Fenner, N., and Hayes, F.: Chronic ozone exposure affects nitrogen remobilization in wheat at key growth stages, Science of The Total Environment, Elsevier B.V., 908(August 2023), 168288, https://doi.org/10.1016/j.scitotenv.2023.168288, 2024.

Brewster, C., Hayes, F., and Fenner, N.: Ozone Tolerance Found in Aegilops tauschii and Primary Synthetic Hexaploid Wheat, Plants, 8(7), 195, https://doi.org/10.3390/plants8070195, 2019.

Campbell, G. S., and Norman, J. M.: An introduction to Environmental Biophysics, Second Edition, Springer, 1998.

Challinor, A. J., Watson, J., Lobell, D. B., Howden, S. M., Smith, D. R., and Chhetri, N.: A meta-analysis of crop yield under climate change and adaptation, Nature Climate Change, 4(4), 287–291, https://doi.org/10.1038/nclimate2153, 2014.

Clark, D. B., Mercado, L. M., Sitch, S., Jones, C. D., Gedney, N., Best, M. J., Pryor, M., Rooney, G. G., Essery, R. L. H., Blyth, E., Boucher, O., Harding, R. J., Huntingford, C., and Cox, P. M.: The Joint UK Land Environment Simulator (JULES), model description – Part 2: Carbon fluxes and vegetation dynamics, Geoscientific Model Development, 4(3), 701–722, https://doi.org/10.5194/gmd-4-701-2011, 2011.

Conibear, L., Butt, E. W., Knote, C., Spracklen, D. V., and Arnold, S. R.: Current and Future Disease Burden From Ambient Ozone Exposure in India, GeoHealth, 2, 334–355, https://doi.org/10.1029/2018GH000168, 2018.

Danielsson, H., Pleijel, H., Gustavsson, P.-E., and Selldén, G.: Ozone uptake modelling and flux-response relationships - An assessment of ozone-induced yield loss in spring wheat, Atmospheric Environment, Pergamon, 37(4), 475–485, https://doi.org/10.1016/S1352-2310(02)00924-X, 2003.

Droutsas, I., Challinor, A. J., Arnold, S. R., Mikkelsen, T. N., and Hansen, E. M. Ø.: A new model of ozone stress in wheat including grain yield loss and plant acclimation to the pollutant, European Journal of Agronomy, 120, 126125, https://doi.org/10.1016/j.eja.2020.126125, 2020.

Emberson, L. D., Ashmore, M. R., Simpson, D., Tuovinen, J.-P., and Cambridge, H. M.: Modelling and mapping ozone deposition in Europe, Water, Air and Soil Pollution, 577–582, 2001.

Emberson, L. D., Ashmore, M. R., Cambridge, H. M., Simpson, D., and Tuovinen, J.-P.: Modelling stomatal ozone flux across Europe, Environmental Pollution, 109(3), 403–413, https://doi.org/10.1016/S0269-7491(00)00043-9, 2000.

Emberson, L. D., Buker, P., Ashmore, M., Mills, G., Pleijel, H., Danielsson, H., Karlsson, G., and Simpson, D.: Ozone effects on crops and consideration in crop models, European Journal of Agronomy, Elsevier, 100(May), 19–34, https://doi.org/10.1016/j.eja.2018.06.002, 2018.

Ewert, F., and Porter, J. R.: Ozone effects on wheat in relation to CO2: Modelling short-term and long-term responses of leaf photosynthesis and leaf duration, Global Change Biology, 6(7), 735–750, https://doi.org/10.1046/j.1365-2486.2000.00351.x, 2000.

Farage, P. K., Long, S. P., Lechner, E. G., and Baker, N. R.: The sequence of change within the photosynthetic apparatus of wheat following short-term exposure to ozone, Plant Physiology, 95(2), 529–535, https://doi.org/10.1104/pp.95.2.529, 1991.

Farquhar, G. D., von Caemmerer, S., and Berry, J. A.: A biochemical model of photosynthetic CO2 assimilation in leaves of C3 species, Planta, 149, 78–90, https://doi.org/10.1007/BF00386231, 1980.

Feng, Y., Uddling, J., Feng, Z., Pleijel, H., and Karlsson, P. E.: Identifying and modelling key physiological traits that confer tolerance or sensitivity to ozone in winter wheat, Environmental Pollution, Elsevier Ltd, 304(April), 119251, https://doi.org/10.1016/j.envpol.2022.119251, 2022.

Feng, Y., Pleijel, H., Uddling, J., and Feng, Z.: Alteration of carbon and nitrogen allocation in winter wheat under elevated ozone, Plant Science, Elsevier, 338, 111924, https://doi.org/10.1016/j.plantsci.2023.111924, 2024.

Feng, Z., Wang, S., Szantoi, Z., Chen, Z., Wang, X., and Guo, W.: Differential responses in two varieties of winter wheat to elevated ozone concentration under fully open-air field conditions, Global Change Biology, 17(1), 580–591, https://doi.org/10.1111/j.1365-2486.2010.02184.x, 2011.

Feng, Z., Kobayashi, K., Ainsworth, E. A., Zhu, Y., and Wang, X.: A stomatal ozone flux-response relationship to assess ozone-induced yield loss of winter wheat in subtropical China, Environmental Pollution, Elsevier Ltd, 164, 16–23, https://doi.org/10.1016/j.envpol.2012.01.014, 2012.

Feng, Z., Wang, S., Feng, Y., Pleijel, H., and Zhu, J.: Differential effects of ozone on photosynthesis of winter wheat among cultivars depend on antioxidative enzymes rather than stomatal conductance, The Science of the Total Environment, 572, 404–411, https://doi.org/10.1016/j.scitotenv.2016.08.083, 2016.

Feng, Z., Pleijel, H., Uddling, J., Ahmadi, H., and Zhu, J.: Comparison of crop yield sensitivity to ozone between open-top chamber and free-air experiments, Global Change Biology, 24(6), 2231–2238, https://doi.org/10.1111/gcb.14077, 2018.

Feng, Z., Wang, X., Pleijel, H., Zhu, J., Kobayashi, K., Feng, Y., and Calatayud, V.: Emerging challenges of ozone impacts on Asian plants: Actions are needed to protect ecosystem health, Environmental Pollution, 304, 119251, https://doi.org/10.1080/20964129.2021.1911602, 2021.

Feng, Z., Kobayashi, K., and Ainsworth, E. A.: Impact of elevated ozone concentration on growth, physiology, and yield of wheat (Triticum aestivum L.): A meta-analysis, Global Change Biology, 14(11), 2696–2708, https://doi.org/10.1111/j.1365-2486.2008.01673.x, 2008.

Feng, Z., Xu, Y., Kobayashi, K., and Zhu, J.: Ozone pollution threatens the production of major staple crops in East Asia, Nature Food, 3, 47–56, https://doi.org/10.1038/s43016-021-00422-6, 2022.

Gelang, J., Pleijel, H., Sild, E., Danielsson, H., Younis, S., Selldén, G., and Wallin, G.: Rate and duration of grain filling in relation to flag leaf senescence and grain yield in spring wheat (Triticum aestivum)

exposed to different concentrations of ozone, Physiologia Plantarum, 110(3), 366–375, https://doi.org/10.1111/j.1399-3054.2000.1100311.x, 2000.

Graham, A. M., Stevenson, D. S., Zoogman, P., Sander, S. P., and Geddes, J. A.: Impact on air quality and health due to the Saddleworth Moor fire in northern England, Environmental Research Letters, 15(7), 074001, https://doi.org/10.1088/1748-9326/ab8496, 2020.

Graham, A. M., Geddes, J. A., Stevenson, D. S., and Arnold, S. R.: Impact of the 2019/2020 Australian Megafires on Air Quality and Health, GeoHealth, 5(10), e2021GH000454, https://doi.org/10.1029/2021GH000454, 2021.

Grandjean, A., and Fuhrer, J.: Growth and leaf senescence in spring wheat (Triticum aestivum) grown at different ozone concentrations in open-top field chambers, Environmental Pollution, 59, 299–314, 1989.

Guan, X. K., He, M., Sun, C., Zhao, T., and Wang, Y.: Effect of Drought on the Gas Exchange, Chlorophyll Fluorescence and Yield of Six Different-Era Spring Wheat Cultivars, Journal of Agronomy and Crop Science, 201(4), 253–266, https://doi.org/10.1111/jac.12103, 2015.

Guarin, J. R., Kassie, B., Mashaheet, A. M., Burkey, K., and Asseng, S.: Modeling the effects of tropospheric ozone on wheat growth and yield, European Journal of Agronomy, 105, 13–23, https://doi.org/10.1016/j.eja.2019.03.001, 2019.

Guarin, J. R., Jägermeyr, J., Ainsworth, E. A., Oliveira, F. A. A., Asseng, S., Boote, K., Elliott, J., Emberson, L., Foster, I., Hoogenboom, G., Kelly, D., Ruane, A. C., and Sharps, K.: Modeling the effects of tropospheric ozone on the growth and yield of global staple crops with DSSAT v4.8.0, Geoscientific Model Development, 17, 2547–2567, https://doi.org/10.5194/gmd-17-2547-2024, 2024.

Huang, H., Yang, G., Zhang, C., Feng, J., Xu, B., and Yin, Y.: A dataset of winter wheat aboveground biomass in China during 2007–2015 based on data assimilation, Scientific Data, Springer US, 9(1), 1–11, https://doi.org/10.1038/s41597-022-01305-6, 2022.

Hussain, A., and Bangash, R.: Human development and economic growth nexus: The role of the agricultural and industrial sector in Pakistan, The Pakistan Development Review, 56(2), 163–187, https://www.jstor.org/stable/26875191, 2017.

Jaggi, M., Fuhrer, J., Rosset, R., and Neftel, A.: Environmental control of profiles of ozone concentration in a grassland canopy, Atmospheric Environment, 40(28), 5496–5507, https://doi.org/10.1016/j.atmosenv.2006.01.025, 2006.

Jones, H. G.: Plants and microclimate: A quantitative approach to environmental plant physiology, Cambridge University Press, 1992.

Kohut, R. J., Amundson, R. G., and Laurence, J. A.: Effects of ozone and sulfur dioxide on yield of winter wheat, Phytopathology, 77(1), 71–74, https://doi.org/10.1094/Phyto-77-71, 1987.

Konduri, V. S., Tao, H., Osman, H. H., Anapalli, S., and Sui, R.: Data Science for Weather Impacts on Crop Yield, Frontiers in Sustainable Food Systems, 4(May), 52, https://doi.org/10.3389/fsufs.2020.00052, 2020.

Lee, J. D., Drysdale, W. S., Finch, D. P., Wilde, S. E., and Palmer, P. I.: UK surface NO2 levels dropped by 42% during the COVID-19 lockdown: Impact on surface O3, Atmospheric Chemistry and Physics, 20(24), 15743–15759, https://doi.org/10.5194/acp-20-15743-2020, 2020.

Leung, F., Mercado, L. M., Pugh, T. A. M., Lambert, F. H., and Clark, D. B.: Calibrating soybean parameters in JULES 5.0 from the US-Ne2/3 FLUXNET sites and the SoyFACE-O3 experiment, Geoscientific Model Development, 13(12), 6201–6213, https://doi.org/10.5194/gmd-13-6201-2020, 2020.

IPCC: Climate Change 2021: The Physical Science Basis. Contribution of Working Group I to the Sixth Assessment Report of the Intergovernmental Panel on Climate Change, Cambridge University Press, https://doi.org/10.1017/9781009157896, 2021

Leuning, R.: Modeling stomatal behavior and photosynthesis of Eucalyptus grandis, Australian Journal of Plant Physiology, 17(2), 159–175, 1990.

Leuning, R.: A critical appraisal of combined stomatal models for C3 plants, Plant, Cell & Environment, 18(4), 339–355, 1995. Available at: http://www.unc.edu/courses/2010spring/geog/595/001/www/Leuning95b-PCE.pdf.

Li, A., Zhou, Q., and Xu, Q.: Prospects for ozone pollution control in China: An epidemiological perspective, Environmental Pollution, 285, 117670, https://doi.org/10.1016/j.envpol.2021.117670, 2021.

Li, D., Chang, D., Zou, H., Sun, L., Zhang, C., and Wang, Y.: Surface ozone impacts on major crop production in China from 2010 to 2017, Atmospheric Chemistry and Physics, 22(4), 2625–2638, https://doi.org/10.5194/acp-22-2625-2022, 2022.

Li, K., Jacob, D. J., Shen, L., Lu, X., De Smedt, I., and Liao, H.: Anthropogenic and meteorological influences on surface ozone in the China during the COVID-19 lockdown, Atmospheric Chemistry and Physics, 20(20), 11423–11433, https://doi.org/10.5194/acp-20-11423-2020, 2020.

Lin, M., Horowitz, L. W., Payton, R., Fiore, A. M., Tonnesen, G., and Mao, J.: US surface ozone trends and extremes from 1980 to 2014: Quantifying the roles of rising Asian emissions, domestic controls, wildfires, and climate, Atmospheric Chemistry and Physics, 17(4), 2943–2970, https://doi.org/10.5194/acp-17-2943-2017, 2017.

Lim, P. O., Kim, H. J., and Nam, H. G.: Leaf senescence, Annu. Rev. Plant Biol., 58, 115–136, https://doi.org/10.1146/annurev.arplant.57.032905.105316, 2007.

Liu, S., Tao, F., and Shi, W.: Crop yield responses to climate change in the Huang-Huai-Hai Plain of China, Agricultural Water Management, 97(8), 1195–1209, https://doi.org/10.1016/j.agwat.2010.03.001, 2010.

Liu, Z., Liu, J., Fan, Q., Zhong, J., Liu, H., and Li, D.: Tropospheric ozone changes and ozone sensitivity from the present day to the future under shared socio-economic pathways, Atmospheric Chemistry and Physics, 22(2), 1209–1227, https://doi.org/10.5194/acp-22-1209-2022, 2022.

Malhi, G. S., Kaur, M., and Kaushik, P.: Impact of Climate Change on Agriculture and Its Mitigation Strategies: A Review, Sustainability, 13(3), 1318, https://doi.org/10.3390/su13031318, 2021.

Mariën, B., Maes, S. L., Perring, M. P., Depauw, L., Blondeel, H., De Frenne, P., and Verheyen, K.: Detecting the onset of autumn leaf senescence in deciduous forest trees of the temperate zone, New Phytologist, 224(1), 166–176, https://doi.org/10.1111/nph.15991, 2019.

Masutomi, Y.: The appropriate analytical solution for coupled leaf photosynthesis and stomatal conductance models for C3 plants, Ecological Modelling, 481, 110306, https://doi.org/10.1016/j.ecolmodel.2023.110306, 2023.

Medlyn, B. E., Loustau, D., and Delzon, S.: Temperature response of parameters of a biochemically based model of photosynthesis. II. A review of experimental data, Plant, Cell and Environment, 25(9), 1167–1179, https://doi.org/10.1046/j.1365-3040.2002.00891.x, 2002.

Miller, J. D., Arteca, R. N., and Pell, E. J.: Senescence-Associated Gene Expression during Ozone-Induced Leaf Senescence in Arabidopsis, Plant Physiology, 120(4), 1015, https://doi.org/10.1104/pp.120.4.1015, 1999.

Muhie, S. H.: Novel approaches and practices to sustainable agriculture, Journal of Agriculture and Food Research, 10, 100446, https://doi.org/10.1016/j.jafr.2022.100446, 2022.

Mulvaney, M. J., and Devkota, P. J.: Adjusting Crop Yield to a Standard Moisture Content, EDIS, University of Florida George A Smathers Libraries, 2020(3), https://doi.org/10.32473/edis-ag442-2020, 2020.

Nguyen, T. H., Vu, T. K., Shcherbak, I., Smith, P., Ma, S., Yan, X., and Wang, Y.: Assessing the spatio-temporal tropospheric ozone and drought impacts on leaf growth and grain yield of wheat across Europe through crop modeling and remote sensing data, European Journal of Agronomy, 153, 127052, https://doi.org/10.1016/j.eja.2023.127052, 2024.

LRTAP: Mapping critical levels for vegetation, chapter III of manual on methodologies and criteria for modelling and mapping critical loads and levels and air pollution effects, risks and trends, UNECE Convention on Long-range Transboundary Air Pollution, 2017

Van Oijen, M., and Ewert, F.: The effects of climatic variation in Europe on the yield response of spring wheat cv. Minaret to elevated CO2 and O3: an analysis of open-top chamber experiments by means of two crop growth simulation models, European Journal of Agronomy, 10(3–4), 249–264, https://doi.org/10.1016/s1161-0301(99)00014-3, 1999.

Osborne, S., Doherty, R., Arnold, S. R., Karney, C., and Mills, G.: New insights into leaf physiological responses to ozone for use in crop Modelling, Plants, 8(4), 84, https://doi.org/10.3390/plants8040084, 2019.

Osborne, T., Jones, C. D., Levy, P., and Huntingford, C.: JULES-crop: A parametrisation of crops in the Joint UK Land Environment Simulator, Geoscientific Model Development, 8(4), 1139–1155, https://doi.org/10.5194/gmd-8-1139-2015, 2015.

Pande, P., Hayes, F., Bland, S., Booth, N., Pleijel, H., and Emberson, L. D.: Ozone dose-response relationships for wheat can be derived using photosynthetic-based stomatal conductance models, *Agricultural and Forest Meteorology*, 356, 110150, https://doi.org/10.1016/j.agrformet.2024.110150, 2024

Pleijel, H., Danielsson, H., Gelang, J., Sild, E., and Selldén, G.: Ozone risk assessment for agricultural crops in Europe: Further development of stomatal flux and flux–response relationships for European wheat and potato, Atmospheric Environment, 41(14), 3022–3040, https://doi.org/10.1016/j.atmosenv.2006.12.002, 2007.

Pury, D. G. G., and Farquhar, G. D.: Simple scaling of photosynthesis from leaves to canopies without the errors of big-leaf models, Functional Plant Biology, 24(5), 537–557, https://doi.org/10.1071/pp97030, 1997.

Qin, X., Zhang, L., Li, W., and Xie, Y.: Wheat yield improvements in China: Past trends and future directions, Field Crops Research, 177, 117–124, https://doi.org/10.1016/j.fcr.2015.03.013, 2015.

Schauberger, B., Rolinski, S., Müller, C., Schütze, N., Kersebaum, K. C., and Pugh, T. A. M.: Global historical soybean and wheat yield loss estimates from ozone pollution considering water and temperature as modifying effects, Agricultural and Forest Meteorology, 265, 1–15, https://doi.org/10.1016/j.agrformet.2018.11.004, 2019.

Sharkey, T. D., Bernacchi, C. J., Farquhar, G. D., and Singsaas, E. L.: Fitting photosynthetic carbon dioxide response curves for C3 leaves, Plant, Cell and Environment, 30(9), 1035–1040, https://doi.org/10.1111/j.1365-3040.2007.01710.x, 2007.

Sillmann, J., Lenton, T. M., Levermann, A., and Leipprand, A.: Combined impacts of climate and air pollution on human health and agricultural productivity, Environmental Research Letters, 16(9), 074001, https://doi.org/10.1088/1748-9326/ac1df8, 2021.

Simpson, D., Benedictow, A., Berge, H., Bergström, R., Emberson, L. D., Fagerli, H., Flechard, C. R., Hayman, G., Gauss, M., Jonson, J. E., Jenkin, M. E., Nyíri, Á., Richter, C., Semeena, V. S., Tsyro, S., Tuovinen, J.-P., Valdebenito, Á., and Wind, P.: The EMEP MSC-W chemical transport model – Technical description, Atmospheric Chemistry and Physics, 12(16), 7825–7865, https://doi.org/10.5194/acp-12-7825-2012, 2012.

Singh Yadav, D., Yadav, D. S., Kumari, N., Pathak, H., and Singh, J.: Responses of an old and a modern Indian wheat cultivar to future O3 levels: Physiological, yield and grain quality parameters, Environmental Pollution, 263, 113939, https://doi.org/10.1016/j.envpol.2020.113939, 2020.

Sitch, S., Cox, P. M., Collins, W. J., and Huntingford, C.: Indirect radiative forcing of climate change through ozone effects on the land-carbon sink, Nature, 448(7155), 791–795, https://doi.org/10.1038/nature06059, 2007.

Tao, F., Yin, Y., Qian, Z., Guo, J., Zhang, Z., and Liang, M.: Effects of climate change, CO2 and O3 on wheat productivity in Eastern China, singly and in combination, Atmospheric Environment, 153, 182–193, https://doi.org/10.1016/j.atmosenv.2017.01.032, 2017.

Thomson, A. M., Calvin, K. V., Smith, S. J., Kyle, G. P., Volke, A., Patel, P., DelGrosso, S. J., and Chini, L. P.: RCP4.5: a pathway for stabilization of radiative forcing by 2100, Climatic Change, 109(1–2), 77–94, https://doi.org/10.1007/s10584-011-0151-4, 2011.

Triboi, E., and Triboi-Blondel, A. M.: Productivity and grain or seed composition: A new approach to an old problem - Invited paper, European Journal of Agronomy, 16(3), 163–186, https://doi.org/10.1016/S1161-0301(01)00146-0, 2002.

Wang, Q. J.: Using genetic algorithms to optimise model parameters, Environmental Modelling and Software, 12(1), 27–34, https://doi.org/10.1016/S1364-8152(96)00030-8, 1997.

Yang, L., Liu, S., Tsoka, S., and Papageorgiou, L. G.: Mathematical programming for piecewise linear regression analysis, Expert Systems with Applications, 44, 156–167, https://doi.org/10.1016/j.eswa.2015.08.034, 2016.

Zhang, X., Sun, Y., Wang, X., Tong, H., and Gao, Y.: First long-term surface ozone variations at an agricultural site in the North China Plain: Evolution under changing meteorology and emissions, Science of The Total Environment, 860, 160520, https://doi.org/10.1016/j.scitotenv.2022.160520, 2023.

Zheng, B., Caldwell, P. M., Martre, P., and Asseng, S.: The APSIM-Wheat Module (7.5 R3008), APSIM Initiative, 44 pp, 2015. Available at: https://www.apsim.info/documentation/model-documentation/crop-module-documentation/wheat/.

Zhu, X., Wang, L., Zhang, Y., Ma, H., Zhao, L., Feng, Z., and Guo, W.: Effects of elevated ozone concentration on yield of four Chinese cultivars of winter wheat under fully open-air field conditions, Global Change Biology, 17(8), 2697–2706, https://doi.org/10.1111/j.1365-2486.2011.02400.x, 2011.

Amthor, J. S. *et al.* (2019) 'Engineering strategies to boost crop productivity by cutting respiratory carbon loss', *Plant Cell*, 31(2), pp. 297–314. doi: 10.1105/tpc.18.00743.

Betzelberger, A. M. *et al.* (2012) 'Ozone exposure response for U.S. soybean cultivars: Linear reductions in photosynthetic potential, biomass, and yield', *Plant Physiology*. American Society of Plant Biologists, 160(4), pp. 1827–1839. doi: 10.1104/pp.112.205591.

Biswas, D. K. *et al.* (2008) 'Assessing the genetic relatedness of higher ozone sensitivity of modern wheat to its wild and cultivated progenitors/relatives', *Journal of experimental botany*. J Exp Bot, 59(4), pp. 951–963. doi: 10.1093/JXB/ERN022.

Brewster, C., Fenner, N. and Hayes, F. (2024) 'Chronic ozone exposure affects nitrogen remobilization in wheat at key growth stages', *Science of The Total Environment*. Elsevier B.V., 908(August 2023), p. 168288. doi: 10.1016/j.scitotenv.2023.168288.

Brewster, C., Hayes, F. and Fenner, N. (2019) 'Ozone Tolerance Found in Aegilops tauschii and Primary Synthetic Hexaploid Wheat', *Plants 2019, Vol. 8, Page 195*. Multidisciplinary Digital Publishing Institute, 8(7), p. 195. doi: 10.3390/PLANTS8070195.

Campbell, G.S., Norman, J. M. (1998) *An introduction to Environmental Biophysics*. Second. Springer.

Challinor, A. J. *et al.* (2014) 'A meta-analysis of crop yield under climate change and adaptation', *Nature Climate Change*, 4(4), pp. 287–291. doi: 10.1038/nclimate2153.

Clark, D. B. *et al.* (2011) 'The Joint UK Land Environment Simulator (JULES), model description – Part 2: Carbon fluxes and vegetation dynamics', *Geoscientific Model Development*, 4(3), pp. 701–722. doi: 10.5194/gmd-4-701-2011.

Danielsson, H. *et al.* (2003) 'Ozone uptake modelling and flux-response relationships - An assessment of ozone-induced yield loss in spring wheat', *Atmospheric Environment*. Pergamon, 37(4), pp. 475–485. doi: 10.1016/S1352-2310(02)00924-X.

Emberson, L.D., Ashmore, M.R., Simpson, D., Tuovinen, J. P. and Cambridge, H. M. (2001) 'Modelling and mapping ozone deposition in Europe', *Water, Air and Soil Pollution*, pp. 577–582.

Emberson, L. D. *et al.* (2000) 'Modelling stomatal ozone flux across Europe', *Environmental Pollution*, 109(3), pp. 403–413. doi: 10.1016/S0269-7491(00)00043-9.

Emberson, L. D. *et al.* (2018) 'Ozone effects on crops and consideration in crop models', *European Journal of Agronomy*. Elsevier, 100(May), pp. 19–34. doi: 10.1016/j.eja.2018.06.002.

Ewert, F. and Porter, J. R. (2000) 'Ozone effects on wheat in relation to CO2: Modelling short-term and long-term responses of leaf photosynthesis and leaf duration', *Global Change Biology*, 6(7), pp. 735–750. doi: 10.1046/j.1365-2486.2000.00351.x.

Farage, P. K. *et al.* (1991) 'The sequence of change within the photosynthetic apparatus of wheat following short-term exposure to ozone', *Plant Physiology*, 95(2), pp. 529–535. doi: 10.1104/pp.95.2.529.

Farquhar, G.D., von Caemmerer, S., Berry, J. A. (1980) 'A biochemical model of photosynthetic CO2 assimilation in leaves of C3 species', *Planta*, 149, pp. 78–90.

Farquhar, G. D., Caemmerer, S. and Berry, J. A. (1980) 'A biochemical model of photosynthetic CO_2 assimilation in leaves of C_3 species', *Planta*, 149(1), pp. 78–90. Available at: http://dx.doi.org/10.1007/BF00386231.

Feng, Y. *et al.* (2022) 'Identifying and modelling key physiological traits that confer tolerance or sensitivity to ozone in winter wheat', *Environmental Pollution*. Elsevier Ltd, 304(April), p. 119251. doi: 10.1016/j.envpol.2022.119251.

Feng, Y. *et al.* (2024) 'Alteration of carbon and nitrogen allocation in winter wheat under elevated ozone', *Plant Science*. Elsevier, 338, p. 111924. doi: 10.1016/J.PLANTSCI.2023.111924.

Feng, Z. *et al.* (2011) 'Differential responses in two varieties of winter wheat to elevated ozone concentration under fully open-air field conditions', *Global Change Biology*, 17(1), pp. 580–591. doi: 10.1111/J.1365-2486.2010.02184.X.

Feng, Z. *et al.* (2012) 'A stomatal ozone flux-response relationship to assess ozone-induced yield loss of winter wheat in subtropical China', *Environmental Pollution*. Elsevier Ltd, 164, pp. 16–23. doi: 10.1016/j.envpol.2012.01.014.

Feng, Z. *et al.* (2016) 'Differential effects of ozone on photosynthesis of winter wheat among cultivars depend on antioxidative enzymes rather than stomatal conductance', *The Science of the total environment*. Sci Total Environ, 572, pp. 404–411. doi: 10.1016/J.SCITOTENV.2016.08.083.

Feng, Z. *et al.* (2018) 'Comparison of crop yield sensitivity to ozone between open-top chamber and free-air experiments', *Global Change Biology*. Blackwell Publishing Ltd, 24(6), pp. 2231–2238. doi: 10.1111/gcb.14077.

Feng, Z. *et al.* (2021) 'Emerging challenges of ozone impacts on asian plants: actions are needed to protect ecosystem health'. doi: 10.1080/20964129.2021.1911602.

Feng, Z., Kobayashi, K. and Ainsworth, E. A. (2008) 'Impact of elevated ozone concentration on growth, physiology, and yield of wheat (Triticum aestivum L.): A meta-analysis', *Global Change Biology*, 14(11), pp. 2696–2708. doi: 10.1111/j.1365-2486.2008.01673.x.

Gelang, J. *et al.* (2000) 'Rate and duration of grain filling in relation to flag leaf senescence and grain yield in spring wheat (Triticum aestivum) exposed to different concentrations of ozone', *Physiologia Plantarum*, 110(3), pp. 366–375. doi: 10.1111/J.1399-3054.2000.1100311.X.

Graham, A. M. *et al.* (2020) 'Impact on air quality and health due to the Saddleworth Moor fire in northern England', *Environmental Research Letters*, 15(7). doi: 10.1088/1748-9326/ab8496.

Graham, A. M. *et al.* (2021) 'Impact of the 2019/2020 Australian Megafires on Air Quality and Health', *GeoHealth*, 5(10), pp. 1–17. doi: 10.1029/2021GH000454.

Grandjean, A. and Fuhrer Grandjean, J. (1989) *Growth and leaf senescence in spring wheat (Triticum aestivum) grown at different ozone concentrations in open-top field chambers*.

Guan, X. K. *et al.* (2015) 'Effect of Drought on the Gas Exchange, Chlorophyll Fluorescence and Yield of Six Different-Era Spring Wheat Cultivars', *Journal of Agronomy and Crop Science*, 201(4), pp. 253–266. doi: 10.1111/jac.12103.

Huang, H. *et al.* (2022) 'A dataset of winter wheat aboveground biomass in China during 2007–2015 based on data assimilation', *Scientific Data*. Springer US, 9(1), pp. 1–11. doi: 10.1038/s41597-022-01305-6.

Jaggi, M. *et al.* (2006) 'Environmental control of profiles of ozone concentration in a grassland canopy', *Atmospheric Environment*, 40(28), pp. 5496–5507. doi: 10.1016/j.atmosenv.2006.01.025.

Jones, H. G. (1992) *Plants and microclimate: A quamntitative approach to environmental plant physiology*. Cambridge University Press.

Kohut, R. J., Amundson, R. G. and Laurence, J. A. (1987) 'Effects of ozone and sulfur dioxide on yield of winter wheat', *Phytopathology*, 77(1), pp. 71–74. doi: 10.1094/Phyto-77-71.

Konduri, V. S. *et al.* (2020) 'Data Science for Weather Impacts on Crop Yield', *Frontiers in Sustainable Food Systems*, 4(May). doi: 10.3389/fsufs.2020.00052.

Lee, J. D. *et al.* (2020) 'UK surface NO2 levels dropped by 42 % during the COVID-19 lockdown: Impact on surface O3', *Atmospheric Chemistry and Physics*, 20(24), pp. 15743–15759. doi: 10.5194/acp-20-15743-2020.

Leung, F. *et al.* (2020) 'Calibrating soybean parameters in JULES 5.0 from the US-Ne2/3 FLUXNET sites and the SoyFACE-O3 experiment', *Geoscientific Model Development*. Copernicus GmbH, 13(12), pp. 6201–6213. doi: 10.5194/GMD-13-6201-2020.

Leuning, R. (1990) 'MODELING STOMATAL BEHAVIOR AND PHOTOSYNTHESIS OF EUCALYPTUS-GRANDIS', *AUSTRALIAN JOURNAL OF PLANT PHYSIOLOGY*, 17(2), pp. 159–175.

Leuning, R. (1995) 'A critical appraisal of combine stomatal model C3 plants', *Plant, Cell & Environment*, 18, pp. 339–355. Available at: http://www.unc.edu/courses/2010spring/geog/595/001/www/Leuning95b-PCE.pdf%0Apapers2://publication/uuid/B8B998AB-EB42-4E09-A609-B192084D13EE.

Li, A., Zhou, Q. and Xu, Q. (2021) 'Prospects for ozone pollution control in China: An epidemiological perspective', *Environmental Pollution*. Elsevier Ltd, 285. doi: 10.1016/J.ENVPOL.2021.117670.

Li, D. *et al.* (2022) 'Surface ozone impacts on major crop production in China from 2010 to 2017', *Atmospheric Chemistry and Physics*, 22(4), pp. 2625–2638. doi: 10.5194/acp-22-2625-2022.

Li, K. *et al.* (2020) 'anthropogenic and meteorological influences', *Atmos. Chem. Phys*, 20, pp. 11423–11433. doi: 10.5194/acp-20-11423-2020.

Lin, M. *et al.* (2017) 'US surface ozone trends and extremes from 1980 to 2014: Quantifying the roles of rising Asian emissions, domestic controls, wildfires, and climate', *Atmospheric Chemistry and Physics*, 17(4), pp. 2943–2970. doi: 10.5194/acp-17-2943-2017.

Liu, S. *et al.* (2010) 'Crop yield responses to climate change in the Huang-Huai-Hai Plain of China', *Agricultural Water Management*. Elsevier, 97(8), pp. 1195–1209. doi: 10.1016/J.AGWAT.2010.03.001.

Liu, Z. *et al.* (2022) 'Tropospheric ozone changes and ozone sensitivity from the present day to the future under shared socio-economic pathways', *Atmospheric Chemistry and Physics*. Copernicus GmbH, 22(2), pp. 1209–1227. doi: 10.5194/ACP-22-1209-2022.

Malhi, G. S., Kaur, M. and Kaushik, P. (2021) 'Impact of Climate Change on Agriculture and Its Mitigation Strategies: A Review', *Sustainability 2021, Vol. 13, Page 1318*. Multidisciplinary Digital Publishing Institute, 13(3), p. 1318. doi: 10.3390/SU13031318.

Mariën, B. *et al.* (2019) 'Detecting the onset of autumn leaf senescence in deciduous forest trees of the temperate zone', *New Phytologist*. John Wiley & Sons, Ltd, 224(1), pp. 166–176. doi: 10.1111/NPH.15991.

Masutomi, Y. (2023) 'The appropriate analytical solution for coupled leaf photosynthesis and

stomatal conductance models for C3 plants', *Ecological Modelling*. Elsevier B.V., 481(January), p. 110306. doi: 10.1016/j.ecolmodel.2023.110306.

Medlyn, B. E. *et al.* (2002) 'Temperature response of parameters of a biochemically based model of photosynthesis. II. A review of experimental data', *Plant, Cell and Environment*, 25(9), pp. 1167–1179. doi: 10.1046/j.1365-3040.2002.00891.x.

Miller, J. D., Arteca, R. N. and Pell, E. J. (1999) 'Senescence-Associated Gene Expression during Ozone-Induced Leaf Senescence in Arabidopsis', *Plant Physiology*. Oxford University Press, 120(4), p. 1015. doi: 10.1104/PP.120.4.1015.

Muhie, S. H. (2022) 'Novel approaches and practices to sustainable agriculture', *Journal of Agriculture and Food Research*. Elsevier B.V., 10(August), p. 100446. doi: 10.1016/j.jafr.2022.100446.

Mulvaney, M. J. and Devkota, P. J. (2020) 'Adjusting Crop Yield to a Standard Moisture Content', *EDIS*. University of Florida George A Smathers Libraries, 2020(3). doi: 10.32473/EDIS-AG442-2020.

Nguyen, T. H. *et al.* (2024) 'Assessing the spatio-temporal tropospheric ozone and drought impacts on leaf growth and grain yield of wheat across Europe through crop modeling and remote sensing data', *European Journal of Agronomy*. Elsevier, 153, p. 127052. doi: 10.1016/J.EJA.2023.127052.

Van Oijen, M. and Ewert, F. (1999) 'The effects of climatic variation in Europe on the yield response of spring wheat cv. Minaret to elevated CO2 and O3: an analysis of open-top chamber experiments by means of two crop growth simulation models', *European Journal of Agronomy*. Elsevier, 10(3–4), pp. 249–264. doi: 10.1016/S1161-0301(99)00014-3.

Osborne, S. *et al.* (2019) 'New insights into leaf physiological responses to ozone for use in crop Modelling', *Plants*, 8(4). doi: 10.3390/plants8040084.

Osborne, T. *et al.* (2015) 'JULES-crop: A parametrisation of crops in the Joint UK Land Environment Simulator', *Geoscientific Model Development*, 8(4), pp. 1139–1155. doi: 10.5194/gmd-8-1139-2015.

Pleijel, H. *et al.* (2007) 'Ozone risk assessment for agricultural crops in Europe: Further development of stomatal flux and flux–response relationships for European wheat and potato', *Atmospheric Environment*. Pergamon, 41(14), pp. 3022–3040. doi: 10.1016/J.ATMOSENV.2006.12.002.

Pury, D. G. G. D. E. and Earquhar, G. D. (1997) 'Simple scaling of photosynthesis from leaves to canopies without the errors of big-leaf models', pp. 537–557.

Qin, X. *et al.* (2015) 'Wheat yield improvements in China: Past trends and future directions', *Field Crops Research*. Elsevier B.V., 177, pp. 117–124. doi: 10.1016/j.fcr.2015.03.013.

Schauberger, B. *et al.* (2019) 'Global historical soybean and wheat yield loss estimates from ozone pollution considering water and temperature as modifying effects', *Agricultural and Forest Meteorology*, 265(October 2018), pp. 1–15. doi: 10.1016/j.agrformet.2018.11.004.

Sharkey, T. D. *et al.* (2007) 'Fitting photosynthetic carbon dioxide response curves for C3 leaves', *Plant, Cell and Environment*, 30(9), pp. 1035–1040. doi: 10.1111/j.1365-3040.2007.01710.x.

Sillmann, J. *et al.* (2021) 'Combined impacts of climate and air pollution on human health and agricultural productivity', *Environmental Research Letters*, 16(9). doi: 10.1088/1748-9326/ac1df8.

Simpson, D. *et al.* (2012) 'The EMEP MSC-W chemical transport model – Technical description', *Atmospheric Chemistry and Physics*, 12(16), pp. 7825–7865. doi: 10.5194/acp-12-7825-2012.

Singh Yadav, D. *et al.* (2020) 'Responses of an old and a modern Indian wheat cultivar to future O 3 level: Physiological, yield and grain quality parameters *'. doi: 10.1016/j.envpol.2020.113939.

Sitch, S. *et al.* (2007) 'Indirect radiative forcing of climate change through ozone effects on the land-carbon sink', 448. doi: 10.1038/nature06059.

Tao, F. *et al.* (2017) 'Effects of climate change, CO2 and O3 on wheat productivity in Eastern China, singly and in combination', *Atmospheric Environment*. Elsevier Ltd, 153, pp. 182–193. doi: 10.1016/j.atmosenv.2017.01.032.

Thomson, A. M. *et al.* (no date) 'RCP4.5: a pathway for stabilization of radiative forcing by 2100'. doi: 10.1007/s10584-011-0151-4.

Triboi, E. and Triboi-Blondel, A. M. (2002) 'Productivity and grain or seed composition: A new approach to an old problem - Invited paper', *European Journal of Agronomy*, 16(3), pp. 163–186. doi: 10.1016/S1161-0301(01)00146-0.

Wang, Q. J. (1997) 'Using genetic algorithms to optimise model parameters', *Environmental Modelling and Software*. Elsevier Ltd, 12(1), pp. 27–34. doi: 10.1016/S1364-8152(96)00030-8.

Yang, L. *et al.* (no date) 'Mathematical Programming for Piecewise Linear Regression Analysis'.

Zhang, X. *et al.* (2023) 'First long-term surface ozone variations at an agricultural site in the North China Plain: Evolution under changing meteorology and emissions', *Science of The Total Environment*. Elsevier, 860, p. 160520. doi: 10.1016/J.SCITOTENV.2022.160520.

Zheng, B. *et al.* (2015) 'The APSIM-Wheat Module (7.5 R3008)', p. 44. Available at: https://www.apsim.info/documentation/model-documentation/crop-module-documentation/wheat/.

Zhu, X. *et al.* (2011) 'Effects of elevated ozone concentration on yield of four Chinese cultivars of winter wheat under fully open-air field conditions', *Global Change Biology*. John Wiley & Sons, Ltd, 17(8), pp. 2697–2706. doi: 10.1111/J.1365-2486.2011.02400.X.

Amthor, J. S. *et al.* (2019) 'Engineering strategies to boost crop productivity by cutting respiratory carbon loss', *Plant Cell*, 31(2), pp. 297–314. doi: 10.1105/tpc.18.00743.

Betzelberger, A. M. *et al.* (2012) 'Ozone exposure response for U.S. soybean cultivars: Linear reductions in photosynthetic potential, biomass, and yield', *Plant Physiology*. American Society of Plant Biologists, 160(4), pp. 1827–1839. doi: 10.1104/pp.112.205591.

Biswas, D. K. *et al.* (2008) 'Assessing the genetic relatedness of higher ozone sensitivity of modern wheat to its wild and cultivated progenitors/relatives', *Journal of experimental botany*. J Exp Bot, 59(4), pp. 951–963. doi: 10.1093/JXB/ERN022.

Brewster, C., Fenner, N. and Hayes, F. (2024) 'Chronic ozone exposure affects nitrogen remobilization in wheat at key growth stages', *Science of The Total Environment*. Elsevier B.V., 908(August 2023), p. 168288. doi: 10.1016/j.scitotenv.2023.168288.

Brewster, C., Hayes, F. and Fenner, N. (2019) 'Ozone Tolerance Found in Aegilops tauschii and Primary Synthetic Hexaploid Wheat', *Plants 2019, Vol. 8, Page 195*. Multidisciplinary Digital Publishing Institute, 8(7), p. 195. doi: 10.3390/PLANTS8070195.

Campbell, G.S., Norman, J. M. (1998) *An introduction to Environmental Biophysics*. Second. Springer.

Challinor, A. J. *et al.* (2014) 'A meta-analysis of crop yield under climate change and adaptation', *Nature Climate Change*, 4(4), pp. 287–291. doi: 10.1038/nclimate2153.

Clark, D. B. *et al.* (2011) 'The Joint UK Land Environment Simulator (JULES), model description – Part

2: Carbon fluxes and vegetation dynamics', *Geoscientific Model Development*, 4(3), pp. 701–722. doi: 10.5194/gmd-4-701-2011.

Danielsson, H. *et al.* (2003) 'Ozone uptake modelling and flux-response relationships - An assessment of ozone-induced yield loss in spring wheat', *Atmospheric Environment*. Pergamon, 37(4), pp. 475–485. doi: 10.1016/S1352-2310(02)00924-X.

Emberson, L.D., Ashmore, M.R., Simpson, D., Tuovinen, J.-P. and Cambridge, H. M. (2001) 'Modelling and mapping ozone deposition in Europe', *Water, Air and Soil Pollution*, pp. 577–582.

Emberson, L. D. *et al.* (2000) 'Modelling stomatal ozone flux across Europe', *Environmental Pollution*, 109(3), pp. 403–413. doi: 10.1016/S0269-7491(00)00043-9.

Emberson, L. D. *et al.* (2018) 'Ozone effects on crops and consideration in crop models', *European Journal of Agronomy*. Elsevier, 100(May), pp. 19–34. doi: 10.1016/j.eja.2018.06.002.

Ewert, F. and Porter, J. R. (2000) 'Ozone effects on wheat in relation to CO2: Modelling short-term and long-term responses of leaf photosynthesis and leaf duration', *Global Change Biology*, 6(7), pp. 735–750. doi: 10.1046/j.1365-2486.2000.00351.x.

Farage, P. K. *et al.* (1991) 'The sequence of change within the photosynthetic apparatus of wheat following short-term exposure to ozone', *Plant Physiology*, 95(2), pp. 529–535. doi: 10.1104/pp.95.2.529.

Farquhar, G.D., von Caemmerer, S., Berry, J. A. (1980) 'A biochemical model of photosynthetic CO2 assimilation in leaves of C3 species', *Planta*, 149, pp. 78–90.

Farquhar, G. D., Caemmerer, S. and Berry, J. A. (1980) 'A biochemical model of photosynthetic CO_2 assimilation in leaves of C_3 species', *Planta*, 149(1), pp. 78-90–90. Available at: http://dx.doi.org/10.1007/BF00386231.

Feng, Y. *et al.* (2022) 'Identifying and modelling key physiological traits that confer tolerance or sensitivity to ozone in winter wheat', *Environmental Pollution*. Elsevier Ltd, 304(April), p. 119251. doi: 10.1016/j.envpol.2022.119251.

Feng, Y. *et al.* (2024) 'Alteration of carbon and nitrogen allocation in winter wheat under elevated ozone', *Plant Science*. Elsevier, 338, p. 111924. doi: 10.1016/J.PLANTSCI.2023.111924.

Feng, Z. *et al.* (2011) 'Differential responses in two varieties of winter wheat to elevated ozone concentration under fully open-air field conditions', *Global Change Biology*, 17(1), pp. 580–591. doi: 10.1111/J.1365-2486.2010.02184.X.

Feng, Z. *et al.* (2012) 'A stomatal ozone flux-response relationship to assess ozone-induced yield loss of winter wheat in subtropical China', *Environmental Pollution*. Elsevier Ltd, 164, pp. 16–23. doi: 10.1016/j.envpol.2012.01.014.

Feng, Z. *et al.* (2016) 'Differential effects of ozone on photosynthesis of winter wheat among cultivars depend on antioxidative enzymes rather than stomatal conductance', *The Science of the total environment*. Sci Total Environ, 572, pp. 404–411. doi: 10.1016/J.SCITOTENV.2016.08.083.

Feng, Z. *et al.* (2018) 'Comparison of crop yield sensitivity to ozone between open-top chamber and free-air experiments', *Global Change Biology*. Blackwell Publishing Ltd, 24(6), pp. 2231–2238. doi: 10.1111/gcb.14077.

Feng, Z. *et al.* (2021) 'Emerging challenges of ozone impacts on asian plants: actions are needed to protect ecosystem health'. doi: 10.1080/20964129.2021.1911602.

Feng, Z., Kobayashi, K. and Ainsworth, E. A. (2008) 'Impact of elevated ozone concentration on

growth, physiology, and yield of wheat (Triticum aestivum L.): A meta-analysis', *Global Change Biology*, 14(11), pp. 2696–2708. doi: 10.1111/j.1365-2486.2008.01673.x.

Gelang, J. *et al.* (2000) 'Rate and duration of grain filling in relation to flag leaf senescence and grain yield in spring wheat (Triticum aestivum) exposed to different concentrations of ozone', *Physiologia Plantarum*, 110(3), pp. 366–375. doi: 10.1111/J.1399-3054.2000.1100311.X.

Graham, A. M. *et al.* (2020) 'Impact on air quality and health due to the Saddleworth Moor fire in northern England', *Environmental Research Letters*, 15(7). doi: 10.1088/1748-9326/ab8496.

Graham, A. M. *et al.* (2021) 'Impact of the 2019/2020 Australian Megafires on Air Quality and Health', *GeoHealth*, 5(10), pp. 1–17. doi: 10.1029/2021GH000454.

Grandjean, A. and Fuhrer Grandjean, J. (1989) *Growth and leaf senescence in spring wheat (Triticum aestivum) grown at different ozone concentrations in open-top field chambers*.

Guan, X. K. *et al.* (2015) 'Effect of Drought on the Gas Exchange, Chlorophyll Fluorescence and Yield of Six Different-Era Spring Wheat Cultivars', *Journal of Agronomy and Crop Science*, 201(4), pp. 253–266. doi: 10.1111/jac.12103.

Huang, H. *et al.* (2022) 'A dataset of winter wheat aboveground biomass in China during 2007–2015 based on data assimilation', *Scientific Data*. Springer US, 9(1), pp. 1–11. doi: 10.1038/s41597-022-01305-6.

Jaggi, M. *et al.* (2006) 'Environmental control of profiles of ozone concentration in a grassland canopy', *Atmospheric Environment*, 40(28), pp. 5496–5507. doi: 10.1016/j.atmosenv.2006.01.025.

Jones, H. G. (1992) *Plants and microclimate: A quamntitative approach to environmental plant physiology*. Cambridge University Press.

Kohut, R. J., Amundson, R. G. and Laurence, J. A. (1987) 'Effects of ozone and sulfur dioxide on yield of winter wheat', *Phytopathology*, 77(1), pp. 71–74. doi: 10.1094/Phyto-77-71.

Konduri, V. S. *et al.* (2020) 'Data Science for Weather Impacts on Crop Yield', *Frontiers in Sustainable Food Systems*, 4(May). doi: 10.3389/fsufs.2020.00052.

Lee, J. D. *et al.* (2020) 'UK surface NO2 levels dropped by 42 % during the COVID-19 lockdown: Impact on surface O3', *Atmospheric Chemistry and Physics*, 20(24), pp. 15743–15759. doi: 10.5194/acp-20-15743-2020.

Leung, F. *et al.* (2020) 'Calibrating soybean parameters in JULES 5.0 from the US-Ne2/3 FLUXNET sites and the SoyFACE-O3 experiment', *Geoscientific Model Development*. Copernicus GmbH, 13(12), pp. 6201–6213. doi: 10.5194/GMD-13-6201-2020.

Leuning, R. (1990) 'MODELING STOMATAL BEHAVIOR AND PHOTOSYNTHESIS OF EUCALYPTUS-GRANDIS', *AUSTRALIAN JOURNAL OF PLANT PHYSIOLOGY*, 17(2), pp. 159–175.

Leuning, R. (1995) 'A critical appraisal of combine stomatal model C3 plants', *Plant, Cell & Environment*, 18, pp. 339–355. Available at: http://www.unc.edu/courses/2010spring/geog/595/001/www/Leuning95b-PCE.pdf%0Apapers2://publication/uuid/B8B998AB-EB42-4E09-A609-B192084D13EE.

Li, A., Zhou, Q. and Xu, Q. (2021) 'Prospects for ozone pollution control in China: An epidemiological perspective', *Environmental Pollution*. Elsevier Ltd, 285. doi: 10.1016/J.ENVPOL.2021.117670.

Li, D. *et al.* (2022) 'Surface ozone impacts on major crop production in China from 2010 to 2017', *Atmospheric Chemistry and Physics*, 22(4), pp. 2625–2638. doi: 10.5194/acp-22-2625-2022.

Li, K. *et al.* (2020) 'anthropogenic and meteorological influences', *Atmos. Chem. Phys*, 20, pp. 11423–11433. doi: 10.5194/acp-20-11423-2020.

Lin, M. *et al.* (2017) 'US surface ozone trends and extremes from 1980 to 2014: Quantifying the roles of rising Asian emissions, domestic controls, wildfires, and climate', *Atmospheric Chemistry and Physics*, 17(4), pp. 2943–2970. doi: 10.5194/acp-17-2943-2017.

Liu, S. *et al.* (2010) 'Crop yield responses to climate change in the Huang-Huai-Hai Plain of China', *Agricultural Water Management*. Elsevier, 97(8), pp. 1195–1209. doi: 10.1016/J.AGWAT.2010.03.001.

Liu, Z. *et al.* (2022) 'Tropospheric ozone changes and ozone sensitivity from the present day to the future under shared socio-economic pathways', *Atmospheric Chemistry and Physics*. Copernicus GmbH, 22(2), pp. 1209–1227. doi: 10.5194/ACP-22-1209-2022.

Malhi, G. S., Kaur, M. and Kaushik, P. (2021) 'Impact of Climate Change on Agriculture and Its Mitigation Strategies: A Review', *Sustainability 2021, Vol. 13, Page 1318*. Multidisciplinary Digital Publishing Institute, 13(3), p. 1318. doi: 10.3390/SU13031318.

Mariën, B. *et al.* (2019) 'Detecting the onset of autumn leaf senescence in deciduous forest trees of the temperate zone', *New Phytologist*. John Wiley & Sons, Ltd, 224(1), pp. 166–176. doi: 10.1111/NPH.15991.

Masutomi, Y. (2023) 'The appropriate analytical solution for coupled leaf photosynthesis and stomatal conductance models for C3 plants', *Ecological Modelling*. Elsevier B.V., 481(January), p. 110306. doi: 10.1016/j.ecolmodel.2023.110306.

Medlyn, B. E. *et al.* (2002) 'Temperature response of parameters of a biochemically based model of photosynthesis. II. A review of experimental data', *Plant, Cell and Environment*, 25(9), pp. 1167–1179. doi: 10.1046/j.1365-3040.2002.00891.x.

Miller, J. D., Arteca, R. N. and Pell, E. J. (1999) 'Senescence-Associated Gene Expression during Ozone-Induced Leaf Senescence in Arabidopsis', *Plant Physiology*. Oxford University Press, 120(4), p. 1015. doi: 10.1104/PP.120.4.1015.

Muhie, S. H. (2022) 'Novel approaches and practices to sustainable agriculture', *Journal of Agriculture and Food Research*. Elsevier B.V., 10(August), p. 100446. doi: 10.1016/j.jafr.2022.100446.

Mulvaney, M. J. and Devkota, P. J. (2020) 'Adjusting Crop Yield to a Standard Moisture Content', *EDIS*. University of Florida George A Smathers Libraries, 2020(3). doi: 10.32473/EDIS-AG442-2020.

Nguyen, T. H. *et al.* (2024) 'Assessing the spatio-temporal tropospheric ozone and drought impacts on leaf growth and grain yield of wheat across Europe through crop modeling and remote sensing data', *European Journal of Agronomy*. Elsevier, 153, p. 127052. doi: 10.1016/J.EJA.2023.127052.

Van Oijen, M. and Ewert, F. (1999) 'The effects of climatic variation in Europe on the yield response of spring wheat cv. Minaret to elevated CO2 and O3: an analysis of open-top chamber experiments by means of two crop growth simulation models', *European Journal of Agronomy*. Elsevier, 10(3–4), pp. 249–264. doi: 10.1016/S1161-0301(99)00014-3.

Osborne, S. *et al.* (2019) 'New insights into leaf physiological responses to ozone for use in crop Modelling', *Plants*, 8(4). doi: 10.3390/plants8040084.

Osborne, T. *et al.* (2015) 'JULES-crop: A parametrisation of crops in the Joint UK Land Environment Simulator', *Geoscientific Model Development*, 8(4), pp. 1139–1155. doi: 10.5194/gmd-8-1139-2015.

Pleijel, H. *et al.* (2007) 'Ozone risk assessment for agricultural crops in Europe: Further development of stomatal flux and flux–response relationships for European wheat and potato', *Atmospheric*

Environment. Pergamon, 41(14), pp. 3022–3040. doi: 10.1016/J.ATMOSENV.2006.12.002.

Pury, D. G. G. D. E. and Earquhar, G. D. (1997) 'Simple scaling of photosynthesis from leaves to canopies without the errors of big-leaf models', pp. 537–557.

Qin, X. *et al.* (2015) 'Wheat yield improvements in China: Past trends and future directions', *Field Crops Research*. Elsevier B.V., 177, pp. 117–124. doi: 10.1016/j.fcr.2015.03.013.

Schauberger, B. *et al.* (2019) 'Global historical soybean and wheat yield loss estimates from ozone pollution considering water and temperature as modifying effects', *Agricultural and Forest Meteorology*, 265(October 2018), pp. 1–15. doi: 10.1016/j.agrformet.2018.11.004.

Sharkey, T. D. *et al.* (2007) 'Fitting photosynthetic carbon dioxide response curves for C3 leaves', *Plant, Cell and Environment*, 30(9), pp. 1035–1040. doi: 10.1111/j.1365-3040.2007.01710.x.

Sillmann, J. *et al.* (2021) 'Combined impacts of climate and air pollution on human health and agricultural productivity', *Environmental Research Letters*, 16(9). doi: 10.1088/1748-9326/ac1df8.

Simpson, D. *et al.* (2012) 'The EMEP MSC-W chemical transport model – Technical description', *Atmospheric Chemistry and Physics*, 12(16), pp. 7825–7865. doi: 10.5194/acp-12-7825-2012.

Singh Yadav, D. *et al.* (2020) 'Responses of an old and a modern Indian wheat cultivar to future O 3 level: Physiological, yield and grain quality parameters *'. doi: 10.1016/j.envpol.2020.113939.

Sitch, S. *et al.* (2007) 'Indirect radiative forcing of climate change through ozone effects on the land-carbon sink', 448. doi: 10.1038/nature06059.

Tao, F. *et al.* (2017) 'Effects of climate change, CO2 and O3 on wheat productivity in Eastern China, singly and in combination', *Atmospheric Environment*. Elsevier Ltd, 153, pp. 182–193. doi: 10.1016/j.atmosenv.2017.01.032.

Thomson, A. M. *et al.* (no date) 'RCP4.5: a pathway for stabilization of radiative forcing by 2100'. doi: 10.1007/s10584-011-0151-4.

Triboi, E. and Triboi-Blondel, A. M. (2002) 'Productivity and grain or seed composition: A new approach to an old problem - Invited paper', *European Journal of Agronomy*, 16(3), pp. 163–186. doi: 10.1016/S1161-0301(01)00146-0.

Wang, Q. J. (1997) 'Using genetic algorithms to optimise model parameters', *Environmental Modelling and Software*. Elsevier Ltd, 12(1), pp. 27–34. doi: 10.1016/S1364-8152(96)00030-8.

Yang, L. *et al.* (no date) 'Mathematical Programming for Piecewise Linear Regression Analysis'.

Zhang, X. *et al.* (2023) 'First long-term surface ozone variations at an agricultural site in the North China Plain: Evolution under changing meteorology and emissions', *Science of The Total Environment*. Elsevier, 860, p. 160520. doi: 10.1016/J.SCITOTENV.2022.160520.

Zheng, B. *et al.* (2015) 'The APSIM-Wheat Module (7.5 R3008)', p. 44. Available at: https://www.apsim.info/documentation/model-documentation/crop-module-documentation/wheat/.

Zhu, X. *et al.* (2011) 'Effects of elevated ozone concentration on yield of four Chinese cultivars of winter wheat under fully open-air field conditions', *Global Change Biology*. John Wiley & Sons, Ltd, 17(8), pp. 2697–2706. doi: 10.1111/J.1365-2486.2011.02400.X.

Acknowledgments

We acknowledge the financial support of the Science and Technology Facilities Council (STFC) Research Grant (ST/V002481/1) for the "Pollution and Climate Smart Agriculture in China (PaCSAC)" project which supported initial development of the DO3SE-Crop model. Support from the Royal Society through the International Exchanges 2021 Cost Share (NSFC) grant (IEC\NSFC\211154) facilitated the UK-China collaboration to parameterise the DO3SE-Crop model within the project "Understanding the role of air pollution and climate on staple crop yields and nutrition in China". We also received support from STFC Research Grant (ST/Y005317/1) under the EO4AgroClimate programme for the project "Towards a digital twin of cropping systems based on ingestion of EO into process-based crop models" which helped refine the DO3SE-Crop model for a broader set of country applications.